

*CR-137969*

## Princeton University

---

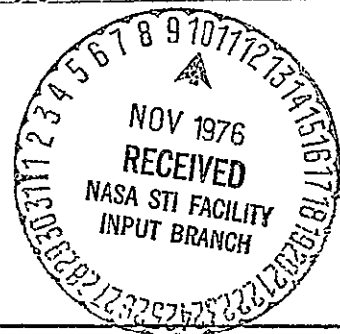
---



(NASA-CR-137969) : AN EXPERIMENTAL STUDY OF  
THE 'NONLINEAR' STIFFNESS OF A ROTOR BLADE  
UNDERGOING FLAP, LAG AND TWIST DEFORMATIONS  
(Princeton Univ., N.J.), 79 p HC A05/MF A01.

N77-10009

Unclassified  
CSCL 01A G3/02 08057



---

Department of  
Aerospace and  
Mechanical Sciences

---

CR- 137969

AN ADDENDUM  
to  
AMS Report No. 1194  
entitled

AN EXPERIMENTAL STUDY OF THE NONLINEAR  
STIFFNESS OF A ROTOR BLADE UNDERGOING  
FLAP, LAG AND TWIST DEFORMATIONS

by  
E. H. Dowell  
and  
J. J. Traybar

AMS Report No. 1257

December 1975

Prepared for  
U. S. Army Air Mobility Research Development Laboratory  
AMES Research Center  
Contract NAS 2-7615

## FOREWORD

This Addendum to AMS Technical Report Number 1194 was prepared by the Aeroelasticity and Flight Mechanics Laboratories of the Department of Aerospace and Mechanical Sciences, Princeton University, Princeton, New Jersey under contract number NAS 2-7615 with NASA-Ames Research Center. It was funded by and under the technical direction of the U. S. Army Air Mobility Research and Development Laboratory, Ames Directorate, Ames Research Center at Moffett Field, California and was monitored and administered by Dr. Dewey H. Hodges of that Directorate.

The analysis and work covered in this Addendum was performed by Professor E. H. Dowell, Principal Investigator and Mr. Joseph J. Traybar, of the Research Staff of Princeton University.

For internal control, the Aerospace and Mechanical Sciences Department has designed this work as AMS Technical Report Number 1257. It is an Addendum to the principal final technical report designated AMS Report Number 1194 dated January 1975.

## ABSTRACT

This is an Addendum to an experimental study of the large deformation of a cantilevered beam under a gravity tip load. It adds higher quality and new data on the static twist and bending deflections of the beam. The experimental data are compared with a recently developed non-linear structural theory. Agreement is good for deflections that are small compared to the beam span and have systematic deviations for larger deflections.

## TABLE OF CONTENTS

	<u>Page</u>
ABSTRACT.....	ii
LIST OF SYMBOLS.....	iv
INTRODUCTION.....	1
EXPERIMENTAL APPARATUS AND PROCEDURE.....	3
EXPERIMENTAL RESULTS AND COMPARISON WITH THEORY.....	8
REFERENCES.....	10
FIGURES.....	11

## LIST OF SYMBOLS

P	applied tip load, lb
r	distance along span (radius or length) of blade, in
R	span (radius or length) of aluminum spar blade, in
V	bending deflection of beam in lag (chordwise) direction (body-fixed axis system), in
W	bending deflection of beam in flap direction (body-fixed axis system), in
X	bending deflection of beam in lateral (sidewise) direction with applied tip load (space-fixed axis system), in
$x^0$ DISTANCE	bending deflection reference distance in lateral sense and measured when $P = 0$ , in
$x'$ DISTANCE	bending deflection reference distance in lateral sense and measured $P \neq 0$ , in
Z	bending deflection of beam in vertical direction with applied tip load (space-fixed axis system), in
$z^0$ DISTANCE	bending deflection reference distance in vertical sense and measured when $P = 0$ , in
$z'$ DISTANCE	bending deflection reference distance in vertical sense and measured when $P \neq 0$ , in
$\theta$	initial blade pitch angle setting, deg
$\phi$	twist of blade in loaded condition, $P \neq 0$ , deg
$\phi_0$	twist of blade in unloaded condition, $P = 0$ , deg
$\delta$	blade twist (incremental) and equal to $\phi - \phi_0$ , deg
r/R	radial station along blade spar, N. D.

## INTRODUCTION

This Addendum to AMS Technical Report Number 1194 entitled "An Experimental Study of the Nonlinear Stiffness of a Rotor Blade Undergoing Flap, Lag and Twist Deformation", contains new, additional information and data on the section concerned with large deflections of a beam due to static loading at the tip.

These additional experiments were conducted to improve the quality and quantity of previous data, provide new data for blade twist (as well as flap and lag bending deflections) and also provide data for distribution of bending deflections and twist at four blade spanwise stations (including the blade tip).

In Princeton University AMS Report Number 1194 (Reference 1), an experimental study of the large deformation of a blade spar represented by a simple cantilevered beam under a gravity tip load was made. Hodges and Dowell have formulated a nonlinear theory of hingeless rotor blade dynamics (References 2 and 3) which indicates that the primary nonlinear effect is due to a nonlinear stiffness arising from mutual interaction among elastic flap, lag and twist. Reference 1 devised a simple experiment to measure the predicted effect and made a quantitative comparison of the experimental results with the results obtained by using the theoretical model.

The experiment used a rectangular cross-section, uniform aluminum beam under a static point load at the tip. In that previous work, measurements of the static deflections in the flapping and lagging degrees-of-freedom due to various tip loads (for several initial blade pitch angle settings) were recorded. These were rather simple measurements based on a "mapping"

of the blade tip movement projected on graph paper (Figure 2.1 of Reference 1). Due to the inherent limited accuracy of this measurement system twist angle data points contained sufficient scatter that it was difficult to infer any suitable results. However, measurements of blade tip deflections under various tip loads appeared satisfactory.

The intent of the work reported in this Addendum is to improve the quality and quantity of the static data, provide new data on blade twist as well as additional flap and lag bending deflection information, and finally to provide data for the blade spanwise distribution (at four selected blade spanwise stations) of bending deflections and blade twist for the various initial pitch angle settings and tip loads on the aluminum spar blade.

## EXPERIMENTAL APPARATUS AND PROCEDURE

As detailed in Reference 1 and depicted in Figure 2.1 of that work, a blade spar was simulated by a uniform rectangular cross-section beam fabricated from 7075 type aluminum. Of the several beams utilized in the Reference 1 experiments, beam number 2 was chosen for the studies in this Addendum. Its dimensions are:

Beam #2: Length (Radius) 20", Width 1/2", Thickness 1/8".

This beam was mounted in a specially fabricated "end-fixture" that insured positive support and clamping. The blade end-fixture was inserted into a precision, milling-machine type, indexing-chuck that provided both a secure, stable mount and the accurate, repeatable angular settings required for the experiments. This same indexing-chuck was used in Reference 1; however, in the experiments conducted here and reported in this Addendum, different measurement setups and apparatus were used to improve accuracy and repeatability of the data. In the previous work, a simple "mapping" of the projected end points of the beam was traced on graph paper as the loads were applied. The two coordinates of the static deflection were simply measured with a scale, recorded and plotted.

In this series of experiments, a different experimental procedure was implemented. The indexing-chuck was used as in Reference 1 but this time it was setup using a "flat-table". The chuck was bolted down and shimmed accordingly so that its axis of rotation, the pitch axis, (coaxial with the centroid or elastic axis of a straight, weightless beam) was precisely parallel to the flat-table surface. The 20 inch aluminum beam was clamped into the indexing chuck. A survey of the beam (through 360°

of pitch rotation and deflected only by its own weight) using a dial-type caliper measuring scale (capable of measuring to three or four decimal places) mounted on the flat surface revealed an essentially "straight" beam. Only a very small curvature was noted near the tip and was probably caused by internal stresses due to machining. Therefore, the combination of the precision indexing-chuck, the flat-table, and the caliper scale provided an increased accuracy (compared to the previous method of mapping) in measuring the Z coordinate (vertical movement) of static deflection when the various tip weights were applied.

For the lateral or X coordinate (sidewise movement) of static deflection, a grid was affixed to the flat-table and lateral movement of the beam reference points was "tracked" with a flat-table fixture that provided an accurate vertical projection to the grid on the flat-table. Using this technique, the sidewise movement of the various beam reference points were accurately "traced" as each different tip weight was applied. Then the X coordinate was measured with a scale placed on the grid and the lateral deflection for each case was recorded.

The previous problems associated with moving the graph paper measuring plane (due to beam foreshortening) with each applied load (as was necessary in the earlier experiments) were entirely circumvented using the new procedures.

Although there is no doubt that the increase in measuring accuracy of the Z deflection was improved substantially from  $\pm .1"$  to  $\pm .001"$  over the old method, it is reasonable to assume that the measuring accuracy of the X deflection was improved to a lesser degree from  $\pm .1"$  to  $\pm .01"$  over the

old system. Nevertheless, it appears that the measuring repeatability and increased accuracy does provide usable data that permits one to infer blade twist angles not only at the tip but at several stations along the span of the blade. It is admitted that the determination of blade twist angle, because of the small incremental angles involved, is an exceedingly difficult measurement to acquire unless one utilizes certain expensive, sophisticated electronic amplification techniques or reflecting mirror light/beam devices and procedures. Since use of the above mentioned equipment was beyond the scope of this present work, some attempt was made to improve the twist angle measurement data in this study by attaching lightweight reference rods at each of the four selected spanwise stations (Figure 3B). This improved the reference points on the beam and aided the measurements of twist angle data at the spanwise stations. These lightweight reference rods were quite stiff and were made from 5/32" diameter, thin wall (0.012"), aluminum tubing. Sharpened end points were inserted into the ends of the tubes in order to provide an accurate reference point. The exact length of the rods was 6.000"  $\pm$  0.001" and each weighed about 1.6 grams. They were attached to the sides of the beam by epoxy and were located at each spanwise station including the blade tip.

The notation, axis systems, geometry and radial station locations are shown in Figures 1, 2 and 3. The initial blade pitch angle setting  $\theta$ , was pre-set and locked and known calibrated weights were applied at the blade tip. The static deflections X and Z, (measured in a space-fixed-axis system, always parallel and perpendicular to the flat-table

surface) were determined at each station. The Z deflection measurements were made using the points at the ends of reference rods. With the aid of magnifying eye glasses and the dial caliper scales, the vertical displacement or height of both ends of the reference rods above the flat surface was carefully measured and the Z movement of the elastic axis points with applied load were calculated accordingly.

The X deflection measurements were made by tracing the movement of the reference rod tips on the graph paper on the flat surface (by dropping perpendiculars to that surface). The X movement of the elastic axis points were then calculated. The X and Z deflection data as well as V and W data (transformed from the X-Z space-fixed axes to the V-W body-fixed axes) are shown in Table I for all stations and weights applied. The initial blade pitch angle setting,  $\theta$ , was varied from  $0^\circ$  to  $\pm 90^\circ$  using  $\pm 15^\circ$  increments. Some data are shown for  $\theta = 180^\circ$ . Positive and negative pitch angle settings were utilized to assess data repeatability and symmetry. The blade twist angle,  $\psi$ , (the measured incremental twist of the beam at each pitch angle,  $\theta$ ) is that caused by the addition of a tip load (with the initial condition that the measured angle of the blade when the load P is zero pounds -- defines the initial twist of the blade as zero degrees for that pitch angle). Therefore, when the loads are applied, the blade twist angle values listed in the Table are the incremental angles to those measured when no loads were applied,  $P = 0$  lb.

Because of the known length of the reference rods and the measured X-Z deflection data, the twist angle,  $\psi$ , may be calculated to different accuracies by either the arc tan or arc cos depending on initial pitch angle. The results of both calculations are shown in the Table. The

information listed in the Table is presented graphically in the included Figures.

The formulae used to calculate  $V$ ,  $W$ ,  $\phi$  are

$$V = Z \cos \theta - X \sin \theta$$

$$W = Z \sin \theta + X \cos \theta$$

$$\phi' = \phi - \phi_0 \quad (\phi = \phi_0 \text{ when } P = 0 \text{ lb})$$

where

$$\phi_0 = \text{arc tan} \frac{\frac{X^0}{Z^0} \text{DISTANCE}}{6.0} \quad (P = 0 \text{ lb})$$

or

$$\phi_0 = \text{arc cos} \frac{\frac{Z^0}{6.0} \text{DISTANCE}}{6.0} \quad (P = 0 \text{ lb})$$

and

$$\phi = \text{arc tan} \frac{\frac{X^1}{Z^1} \text{DISTANCE}}{6.0} \quad (P \neq 0 \text{ lb})$$

or

$$\phi = \text{arc cos} \frac{\frac{Z^1}{6.0} \text{DISTANCE}}{6.0} \quad (P \neq 0 \text{ lb})$$

See Figure 3C for illustration of above quantities.

## EXPERIMENTAL RESULTS AND COMPARISON WITH THEORY

Measurements of flap and lag bending deflection at the beam (free end) tip,  $W_{TIP}$  and  $V_{TIP}$ , as well as twist,  $\hat{\phi}_{TIP}$ , have been obtained for  $\theta = 0^\circ \rightarrow 90^\circ$  and for  $P = 0$  to 4 pounds maximum.  $\hat{\phi}$  is the angle determined by the projection of the elastic axis and leading edge of the cross-section at the beam tip on a plane perpendicular to the undeformed cross-section. Intermediate values of  $W$ ,  $V$  and  $\hat{\phi}$  along the beam span were also obtained. These data are presented in Figures 4-10 along with their theoretical counterparts where available.

The most sensitive indicator of the difference between the linear and nonlinear theoretical models is the twist as it is identically zero in the linear model. All theoretical results discussed below are for the nonlinear theoretical model. In Figs. 5-3, 6-3, 7-3, 8-3, 9-3, results for static tip twist are presented for various loading angles,  $\theta$ , as a function of the magnitude of the load,  $P$ . For  $\theta = 0^\circ$  and  $90^\circ$  theory predicts no twist and, within the accuracy of the experimental measurement, there was none. There is reasonable agreement for any  $\theta$  and sufficiently small  $P$  (and hence  $\hat{\phi}$ ). As  $\theta$  increases, the range of  $P$  for which there is reasonable agreement becomes smaller. This is thought to be associated with the larger static flapwise deflections (for a given  $P$ ) as  $\theta \rightarrow 90^\circ$ . In the Hodges-Dowell theory, terms of the order of the square of the flap deflection,  $W$ , divided by beam radius,  $R$ , are neglected with respect to unity (Reference 1).

A cross-plot of the data in terms of  $\hat{\phi}$  versus  $\theta$  for various  $P$  is given in Figure 11. In Figures 12 and 13, the flap and lag tip deflections

are plotted in the same format. As mentioned above, for large  $P$ , say  $P \geq 3$ , and  $\theta \rightarrow 90^\circ$ , the flap deflections are such that  $(W/R)^2$  is no longer negligible compared to unity. Where the theoretical curves are terminated the theoretical solution procedure failed to converge or there was a change in sign of  $\hat{\phi}$  or  $V_{TIP}$  indicating a jump from one equilibrium configuration to another. Again these are associated with large  $(W/R)^2$  and the theoretical results under such conditions cannot be regarded as reliable. Multi-mode calculations were carried out using the method described in Reference 3 to insure numerical convergence.

It is particularly interesting that both theory and experiment show that  $V_{TIP}$  increases for small  $\theta$  at  $P = 3^{\#}$ , (see Figure 13). Such detailed agreement with respect to an unexpected result is a pleasant surprise.

The theoretical results described in this report were obtained by Dr. Dewey H. Hodges.

#### REFERENCES

1. Dowell, E.H., and Traybar, J.J., "An Experimental Study of the Non-linear Stiffness of a Rotor Blade Undergoing Flap, Lag and Twist Deformations", Princeton University AMS Report No. 1194, January 1975.
2. Hedges, D.H. and Dowell, E.H., "Nonlinear Equations of Motion for the Elastic Bending and Torsion of Twisted Non-Uniform Rotor Blades", NASA TN D-7818, December 1974.
3. Hedges, D.H. and Ormiston, R.A., "Stability of Elastic Bending and Torsion of Uniform Cantilevered Rotor Blades in Hover", AIAA Paper No. 73-405, March 1973.

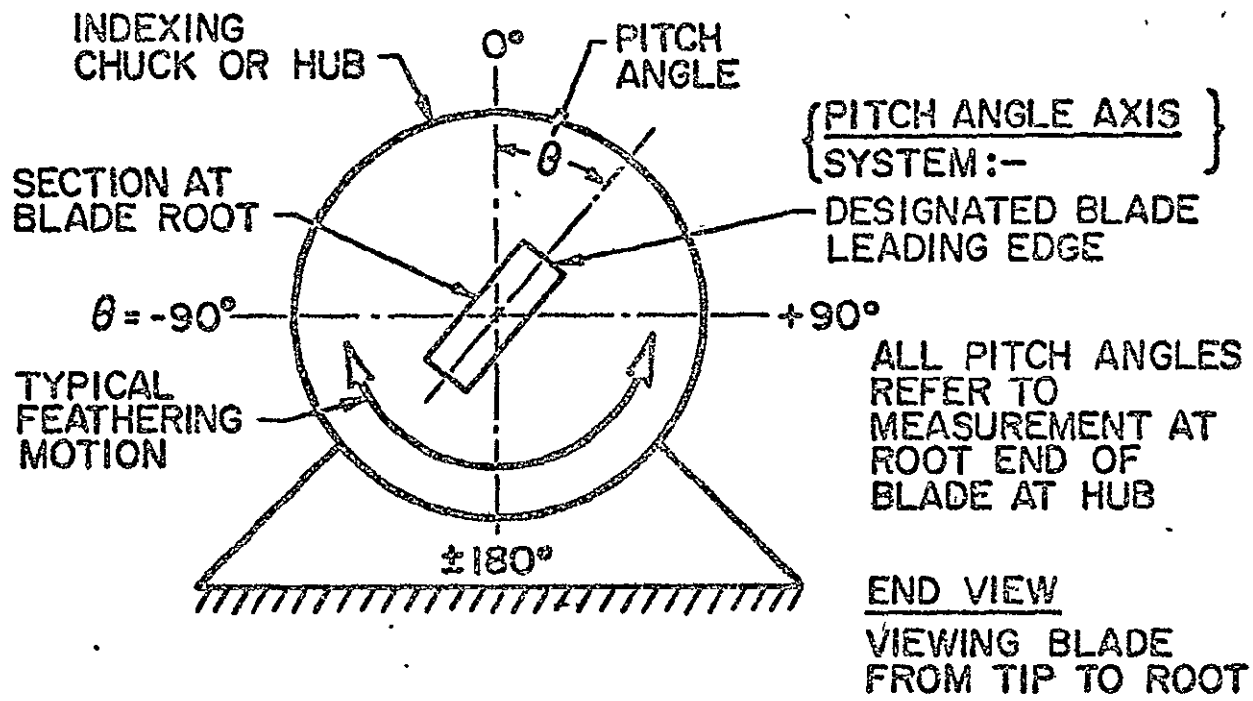


FIGURE 1 GENERAL NOTATION.

X - Z SPACE-FIXED AXIS SYSTEM

V - W BODY-FIXED AXIS SYSTEM

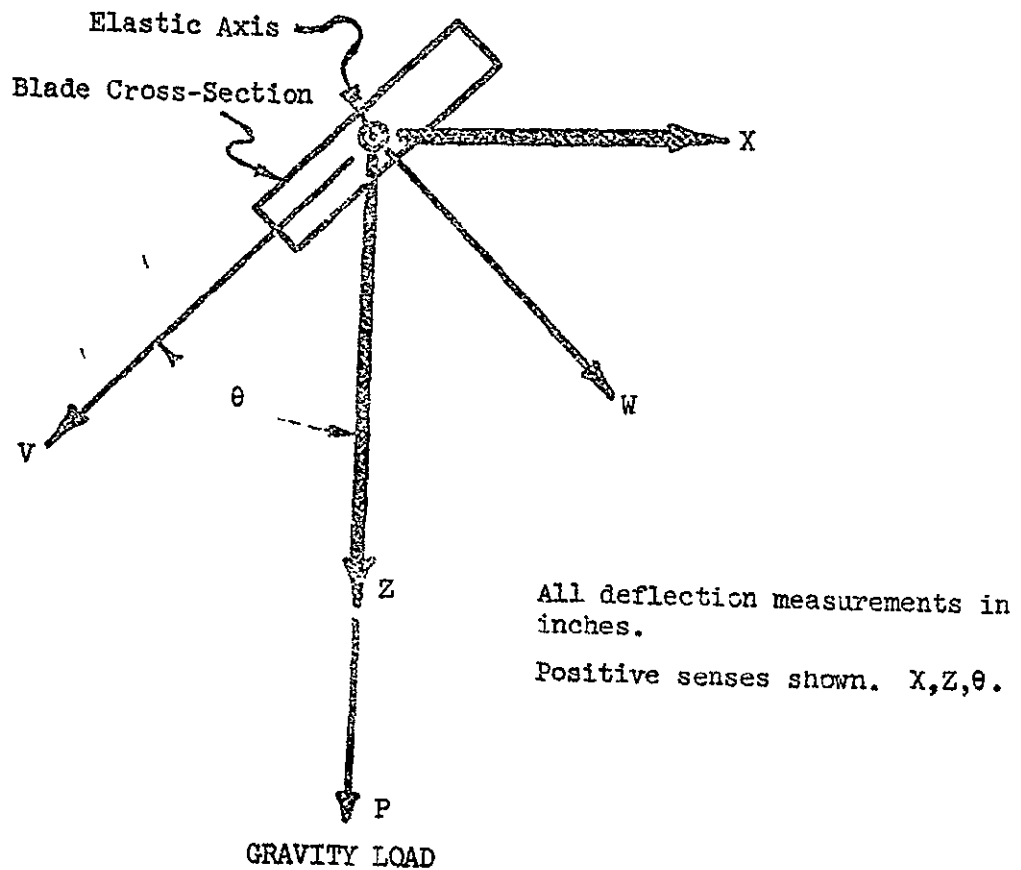


FIGURE 2 AXIS SYSTEMS.

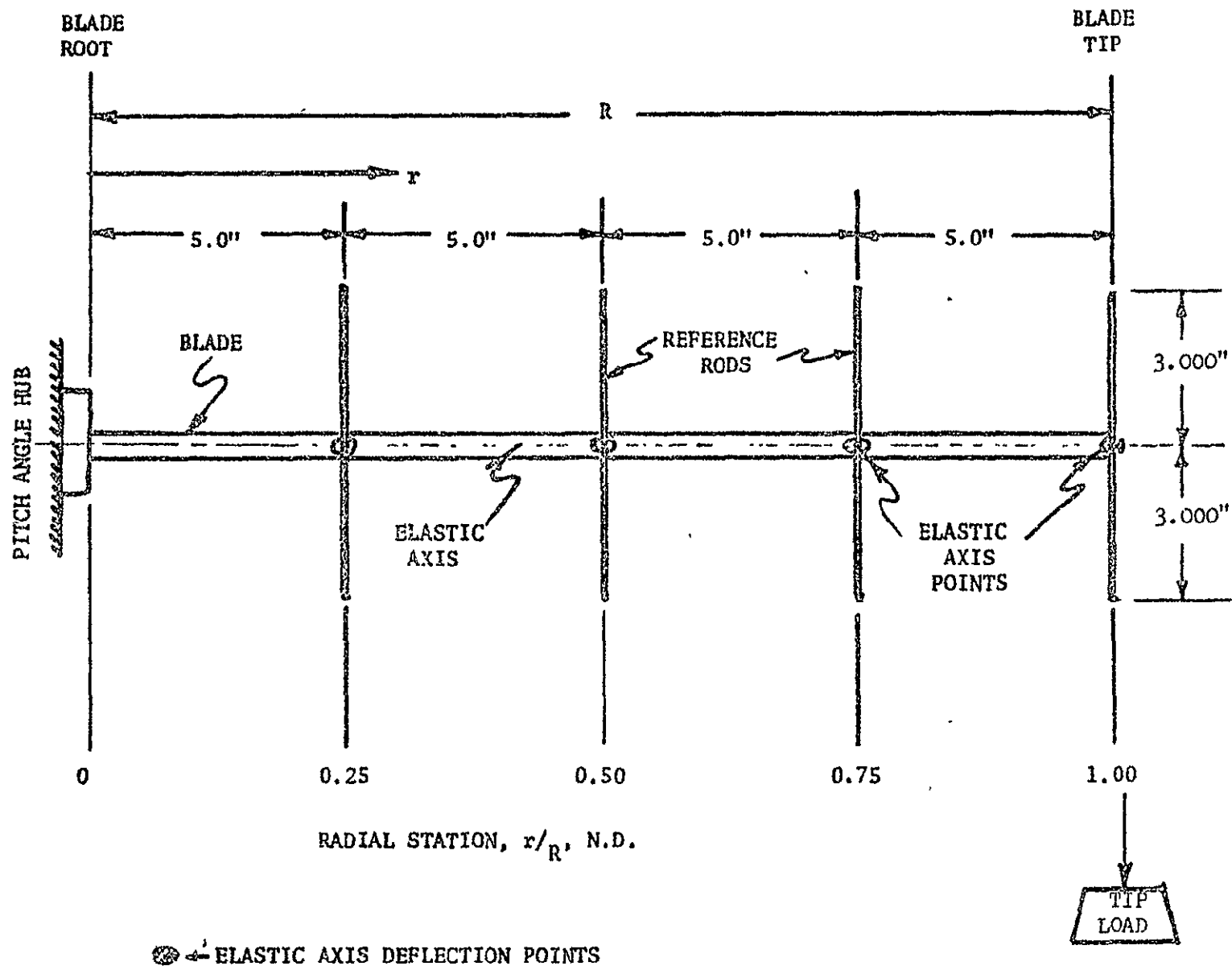


FIGURE 3A BLADE SCHEMATIC SHOWING REFERENCE RODS AND RADIAL STATION LOCATIONS

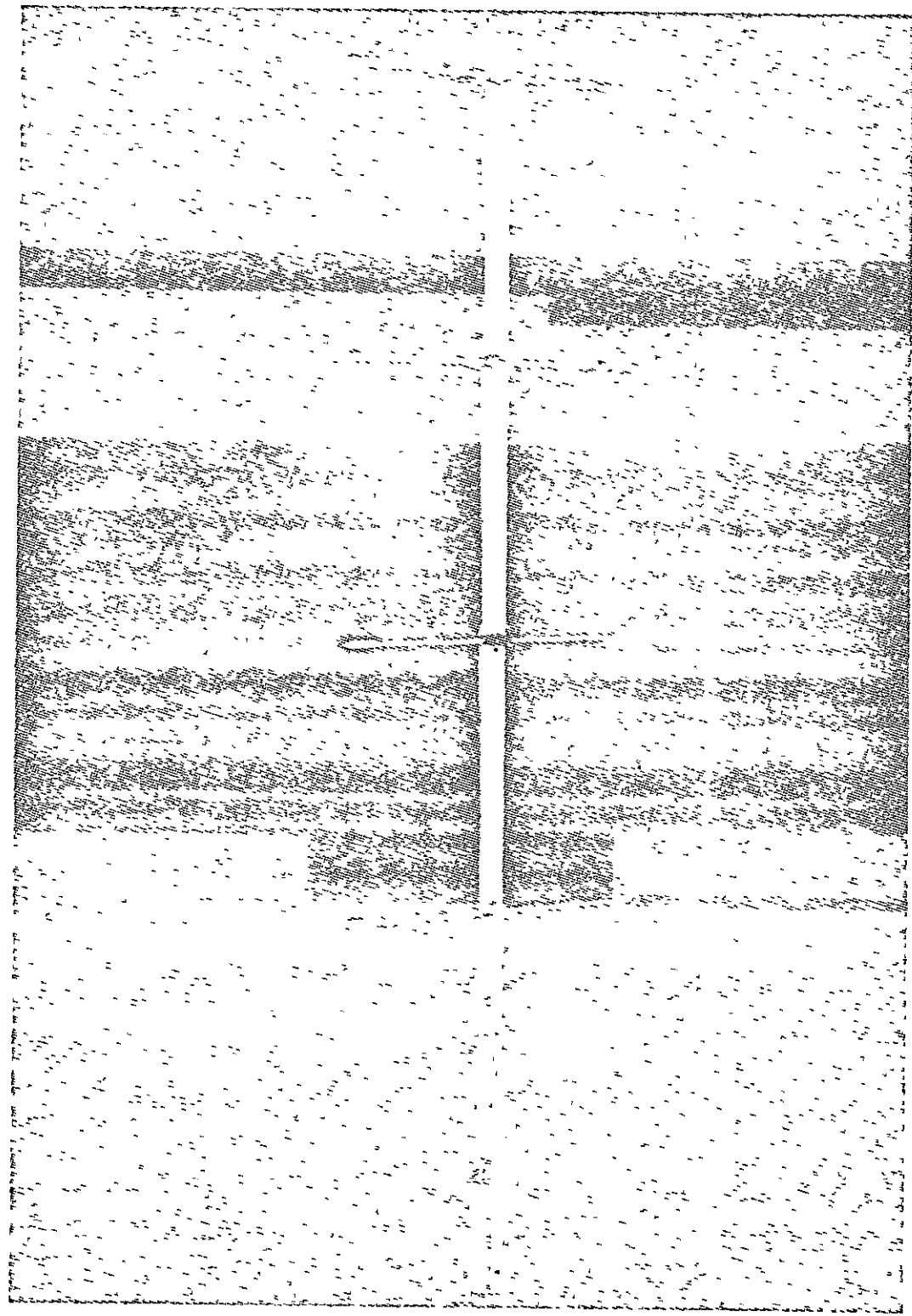


FIGURE 3B PHOTOGRAPH OF BEAM NUMBER TWO SHOWING REFERENCE RODS ATTACHED AT FOUR SPANWISE STATIONS.

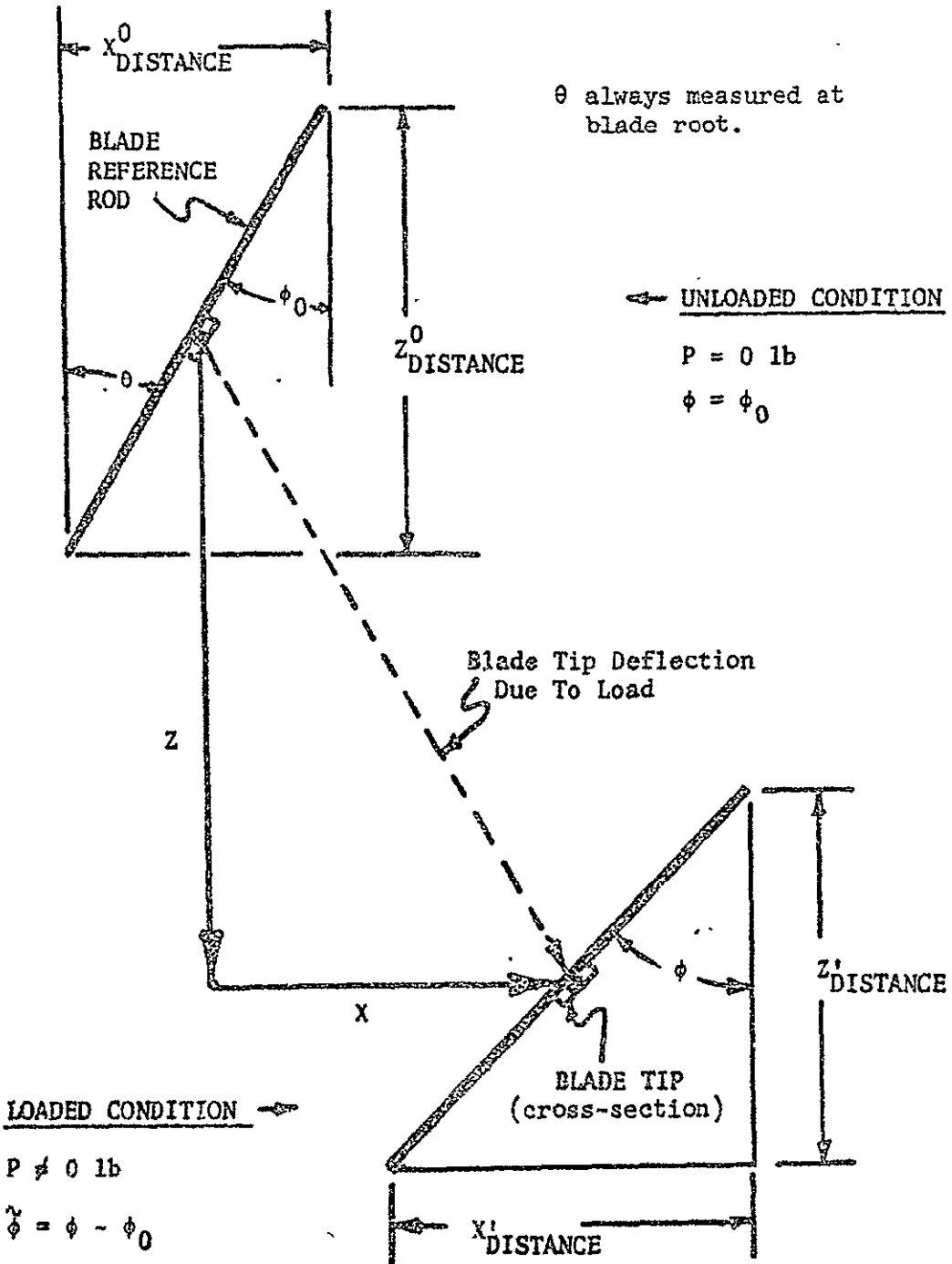


FIGURE 3C END VIEW SHOWING TYPICAL MEASURED QUANTITIES AND NOTATION  
AT BLADE TIP.

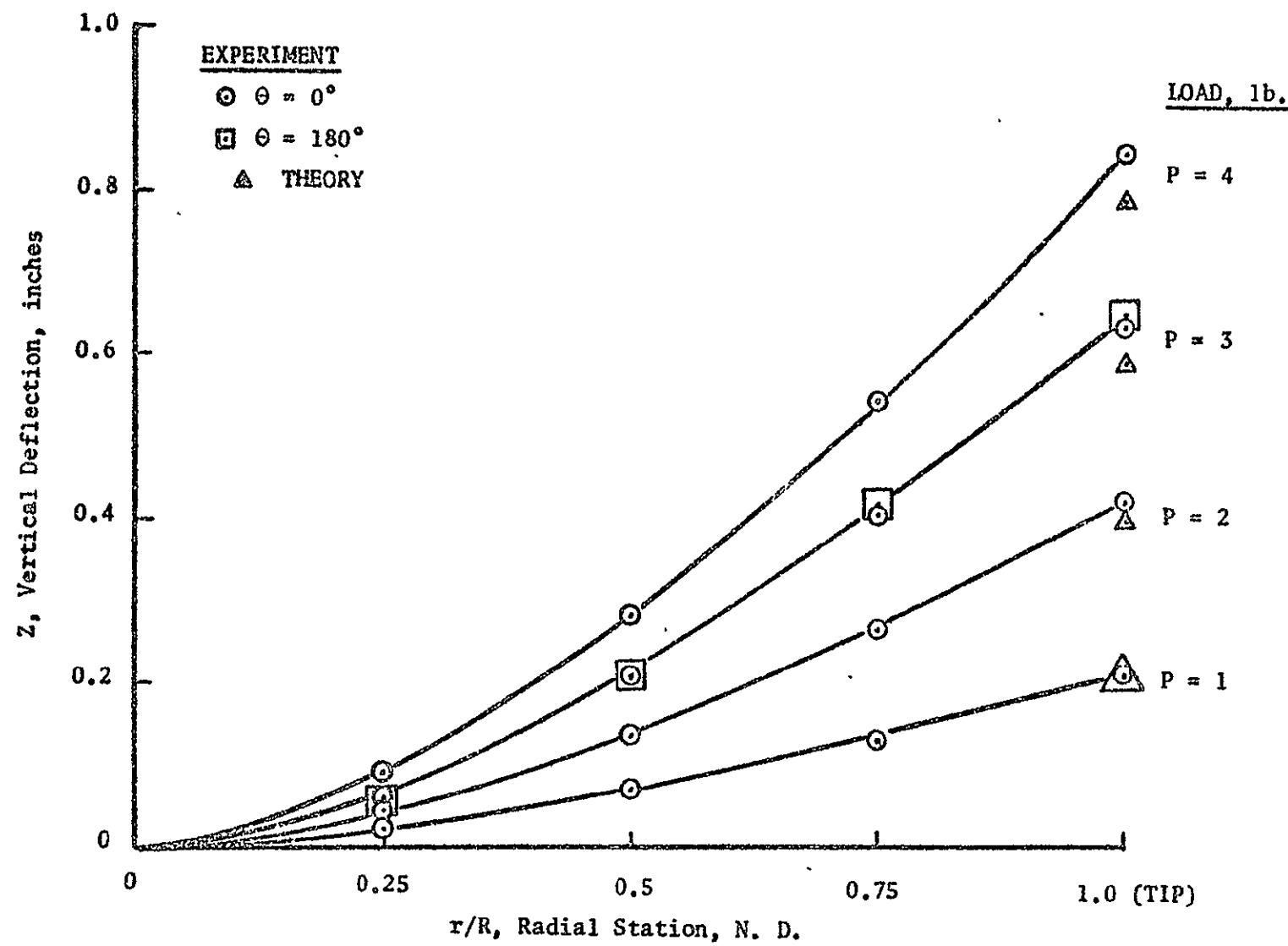


Figure 4. Vertical Deflection versus Radial Station,  $\theta = 0^\circ, 180^\circ$

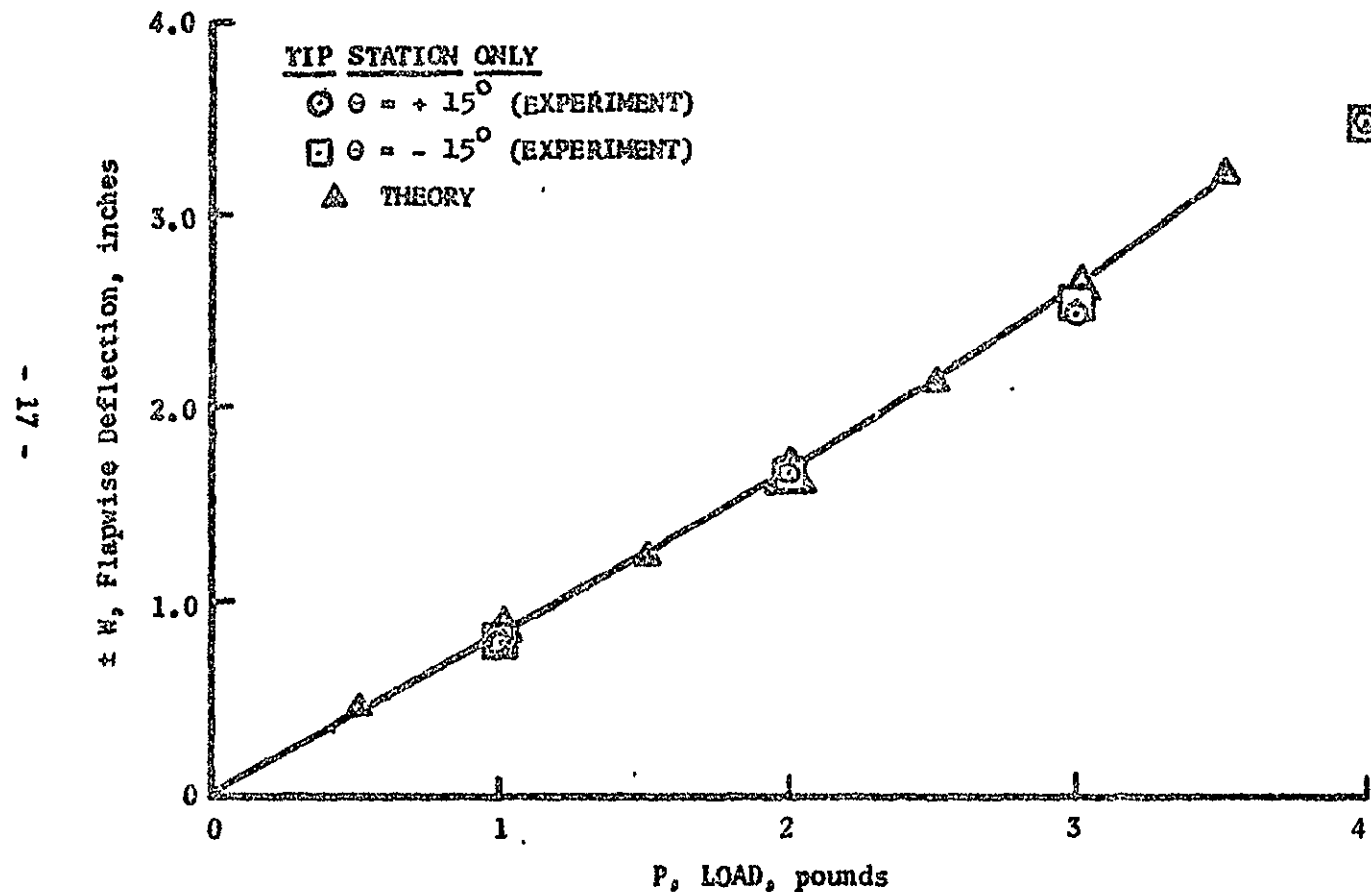


Figure 5-1. Flapwise Deflection versus Load,  $\theta = \pm 15^\circ$

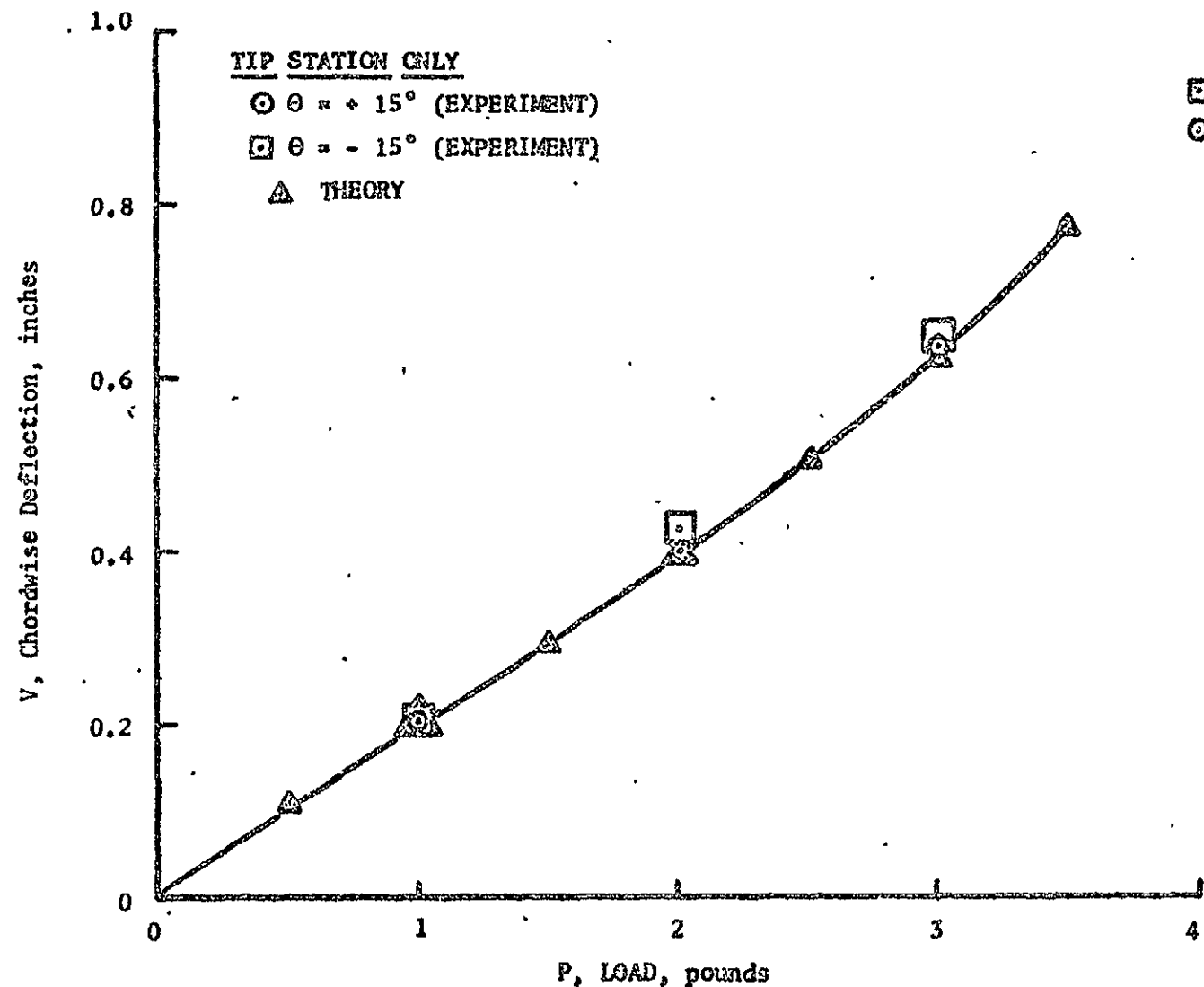


Figure 5-2. Chordwise Deflection versus Load,  $\theta = \pm 15^\circ$

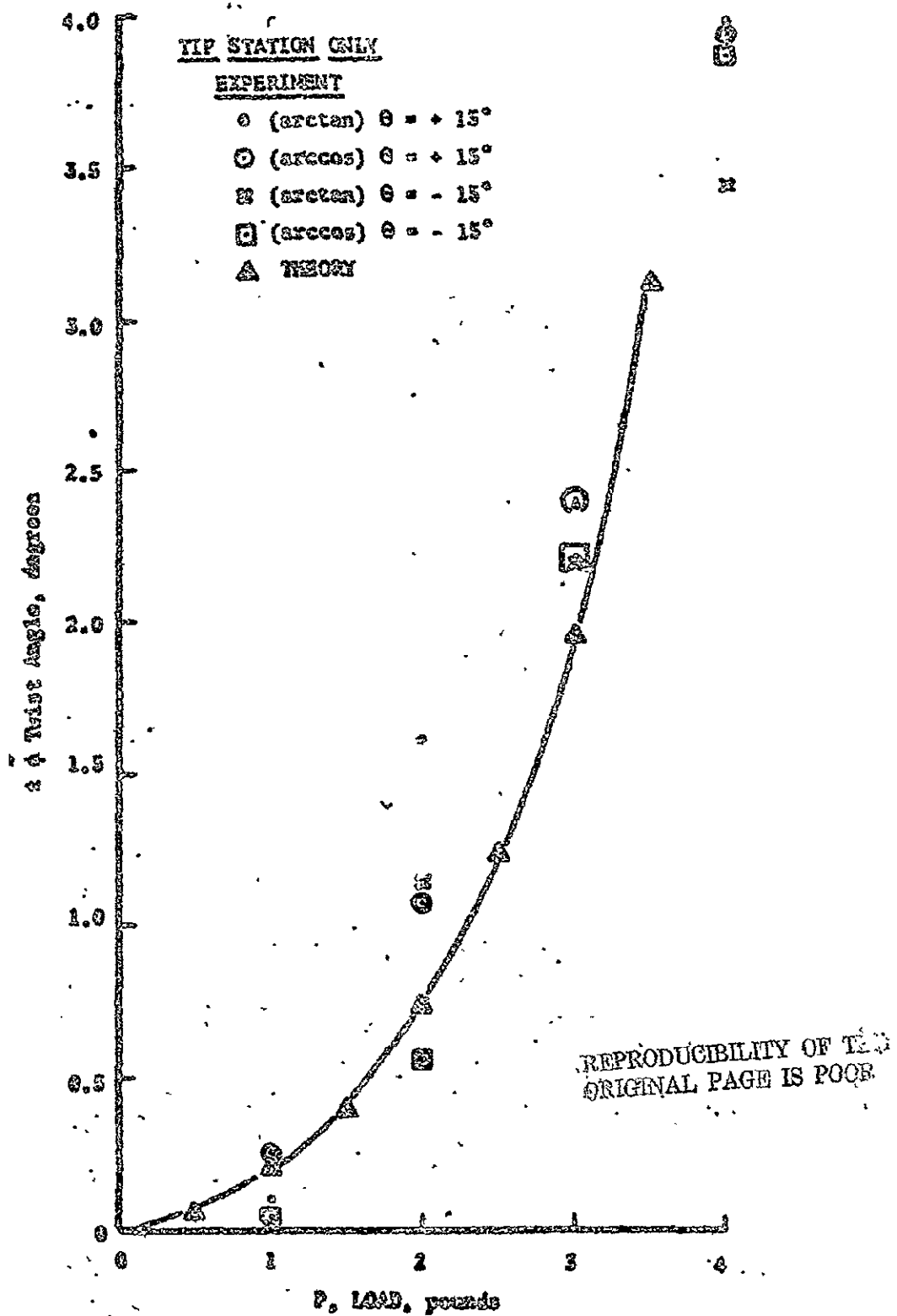


Figure 5-3. Twist Angle versus Load,  $\theta = \pm 15^\circ$

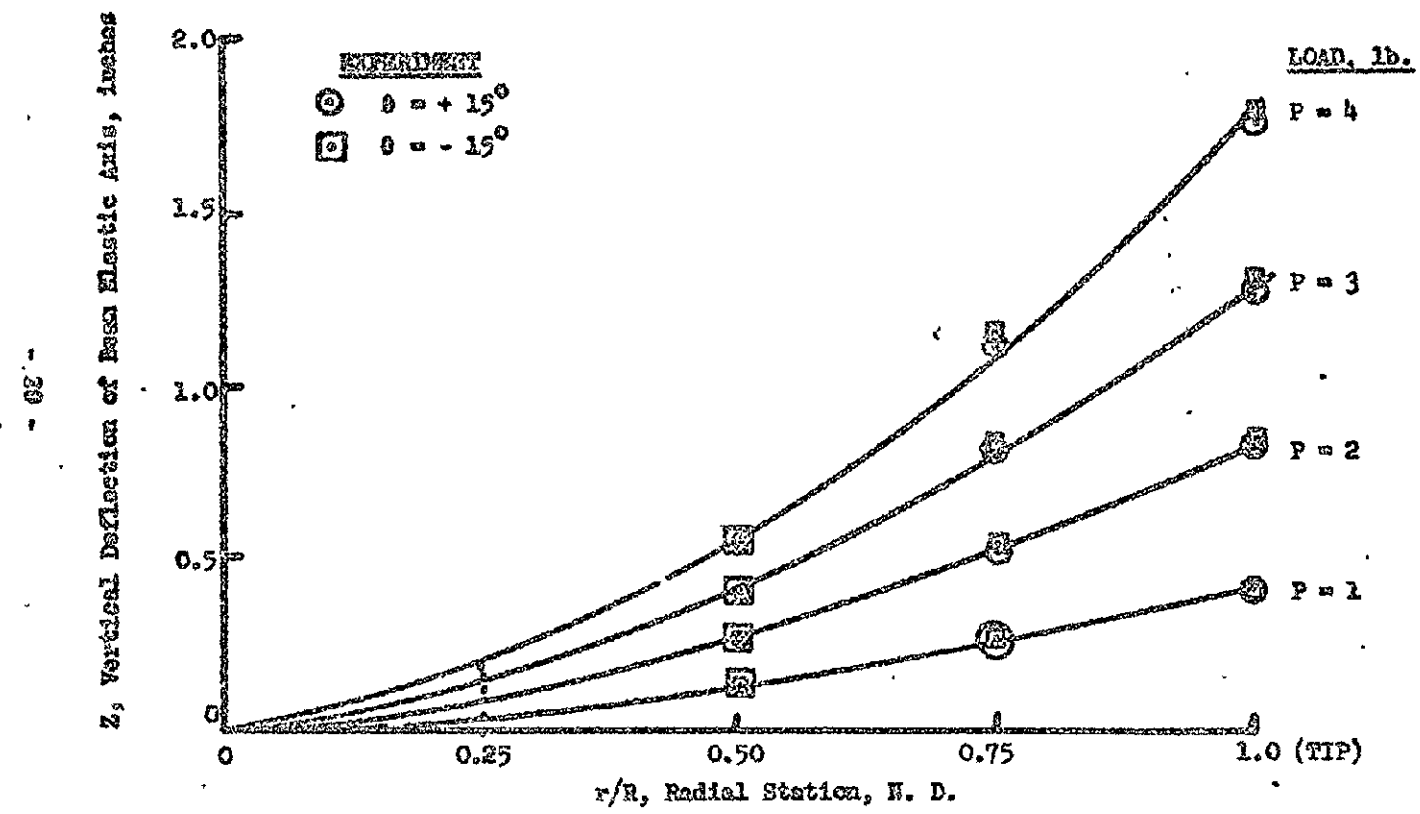


Figure 5-4. Vertical Deflection of Beam Elastic Axis versus Radial Station,  $\theta = \pm 15^\circ$

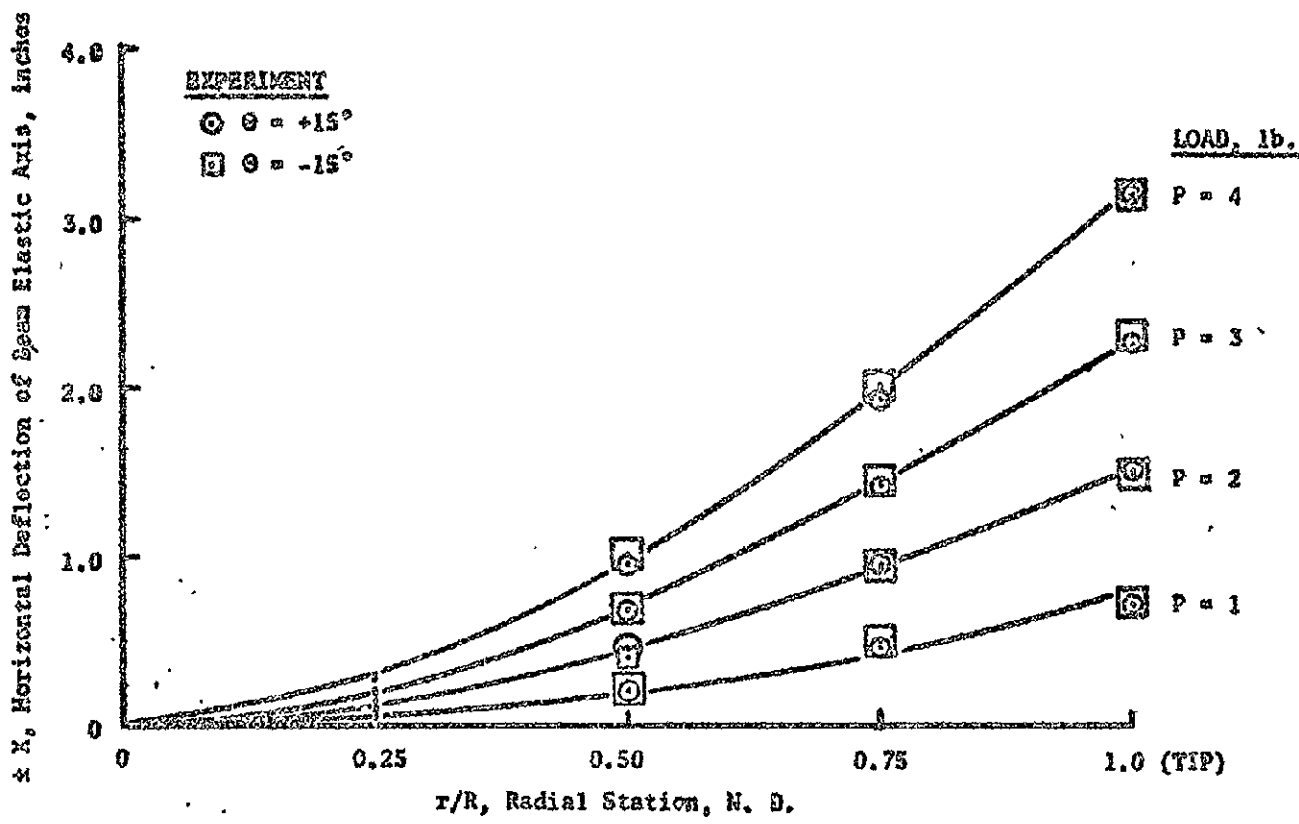


Figure 5-5. Horizontal Deflection of Beam Elastic Axis versus Radial Stations,  $\theta = \pm 15^\circ$

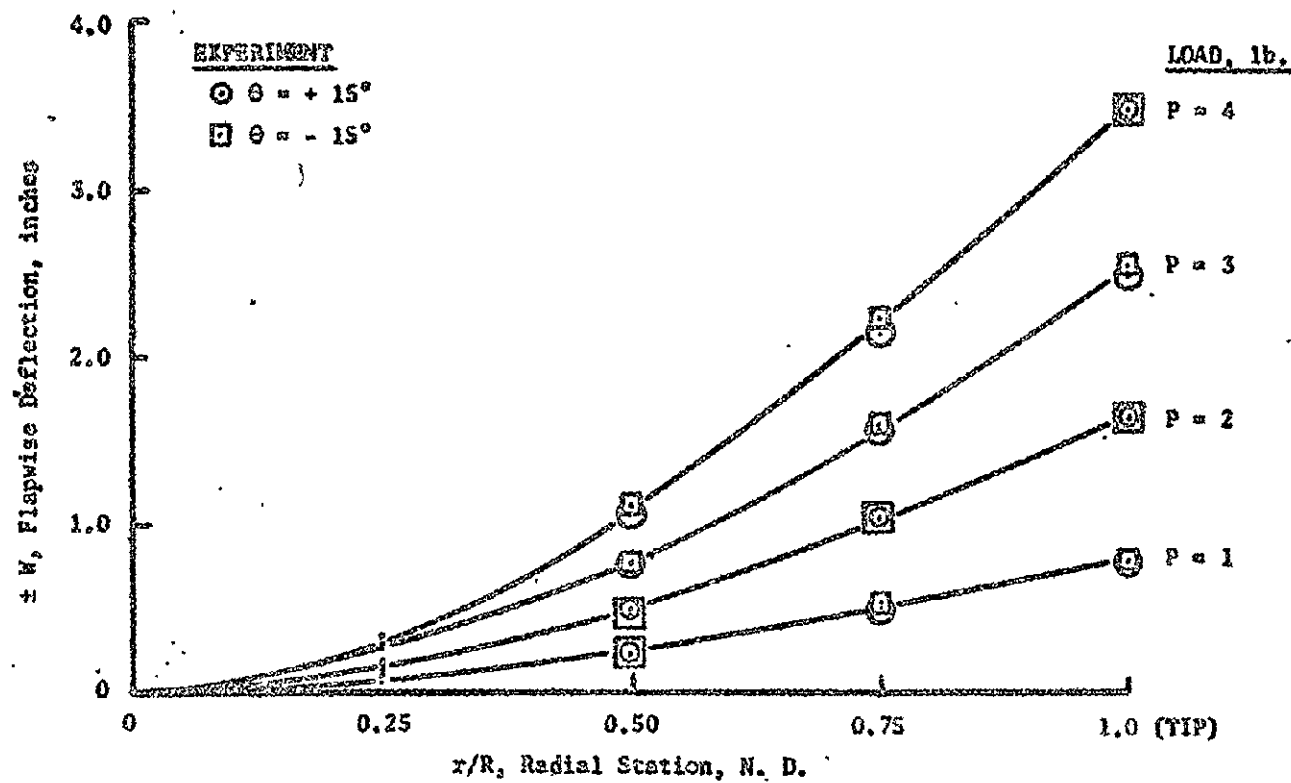


Figure 5-6. Playwise Deflection versus Radial Station,  $\theta = \pm 15^\circ$

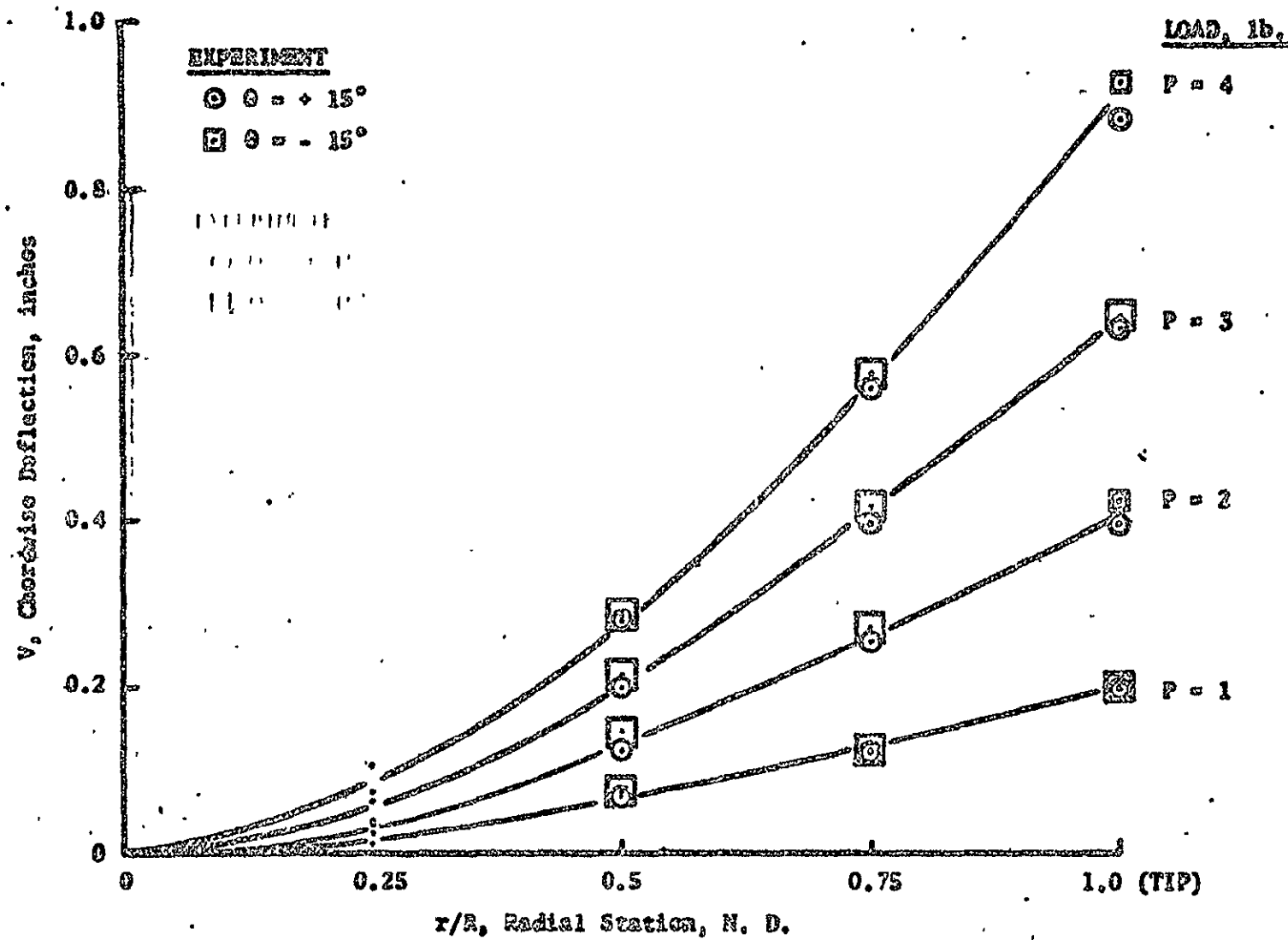


Figure 5-7. Chordwise Deflection versus Radial Station,  $\theta = \pm 15^\circ$

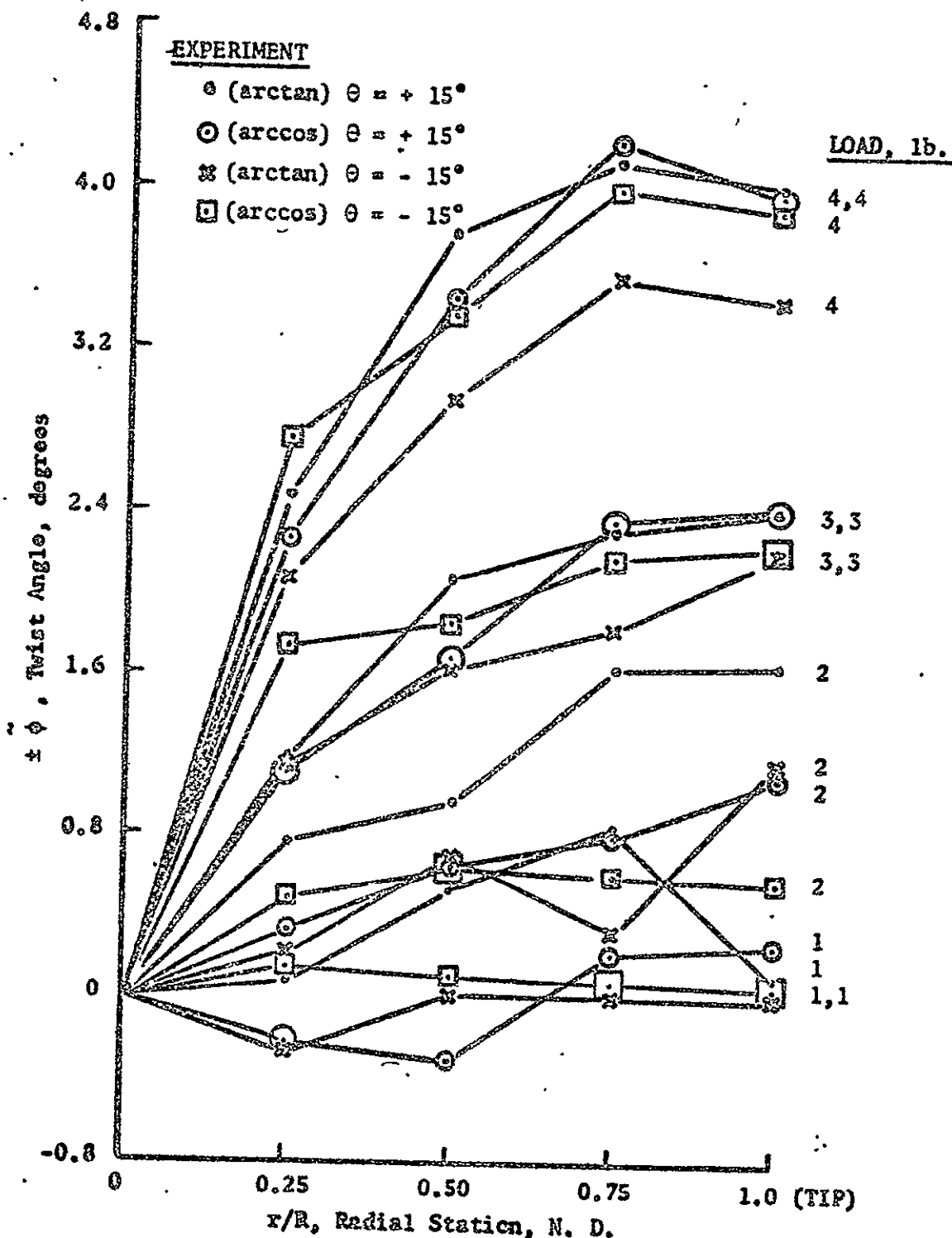


Figure 5-8. Blade Twist Angle versus Radial Station,  $\theta = \pm 15^\circ$

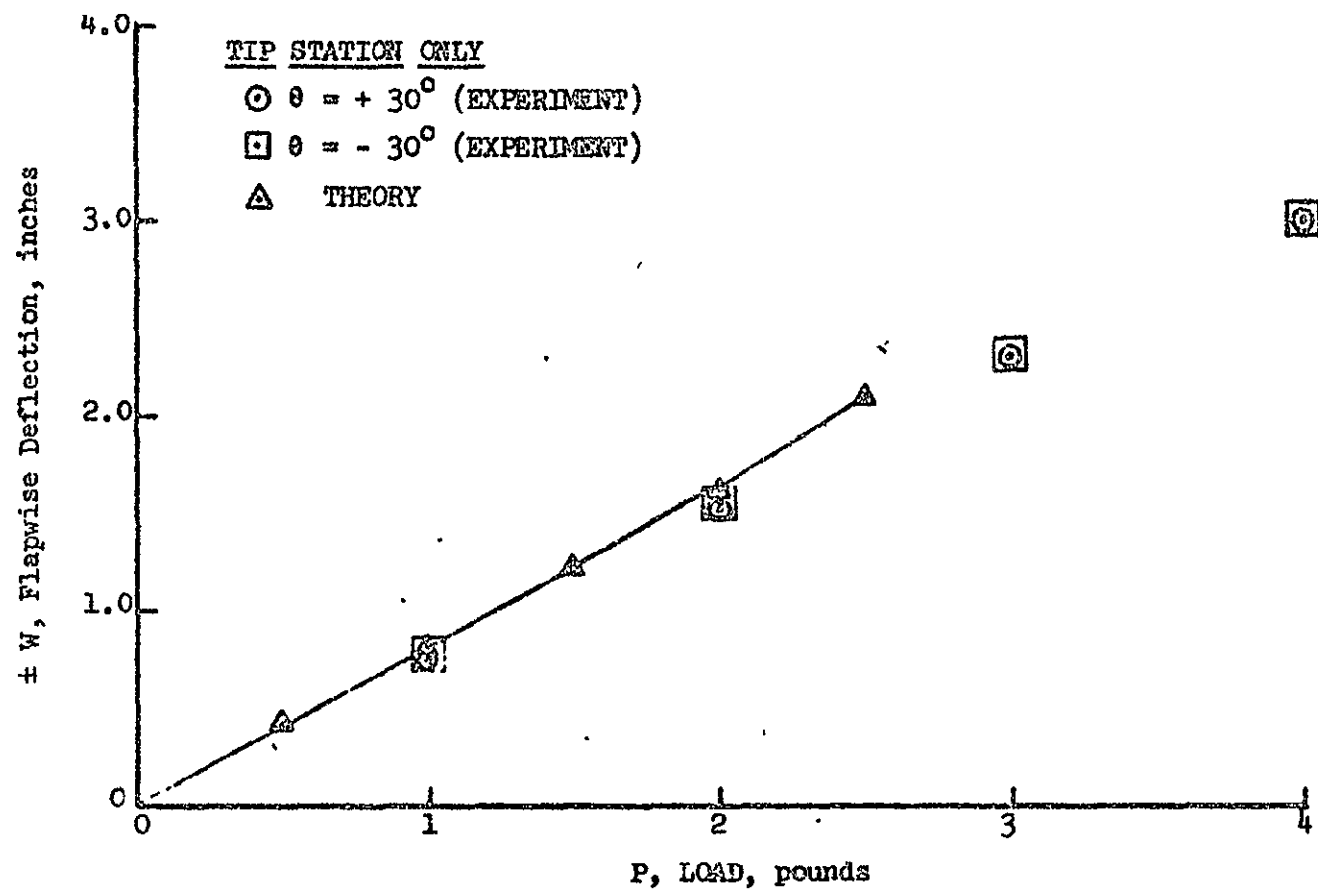


Figure 6-1. Flapwise Deflection Versus Load,  $\theta = \pm 30^\circ$ .

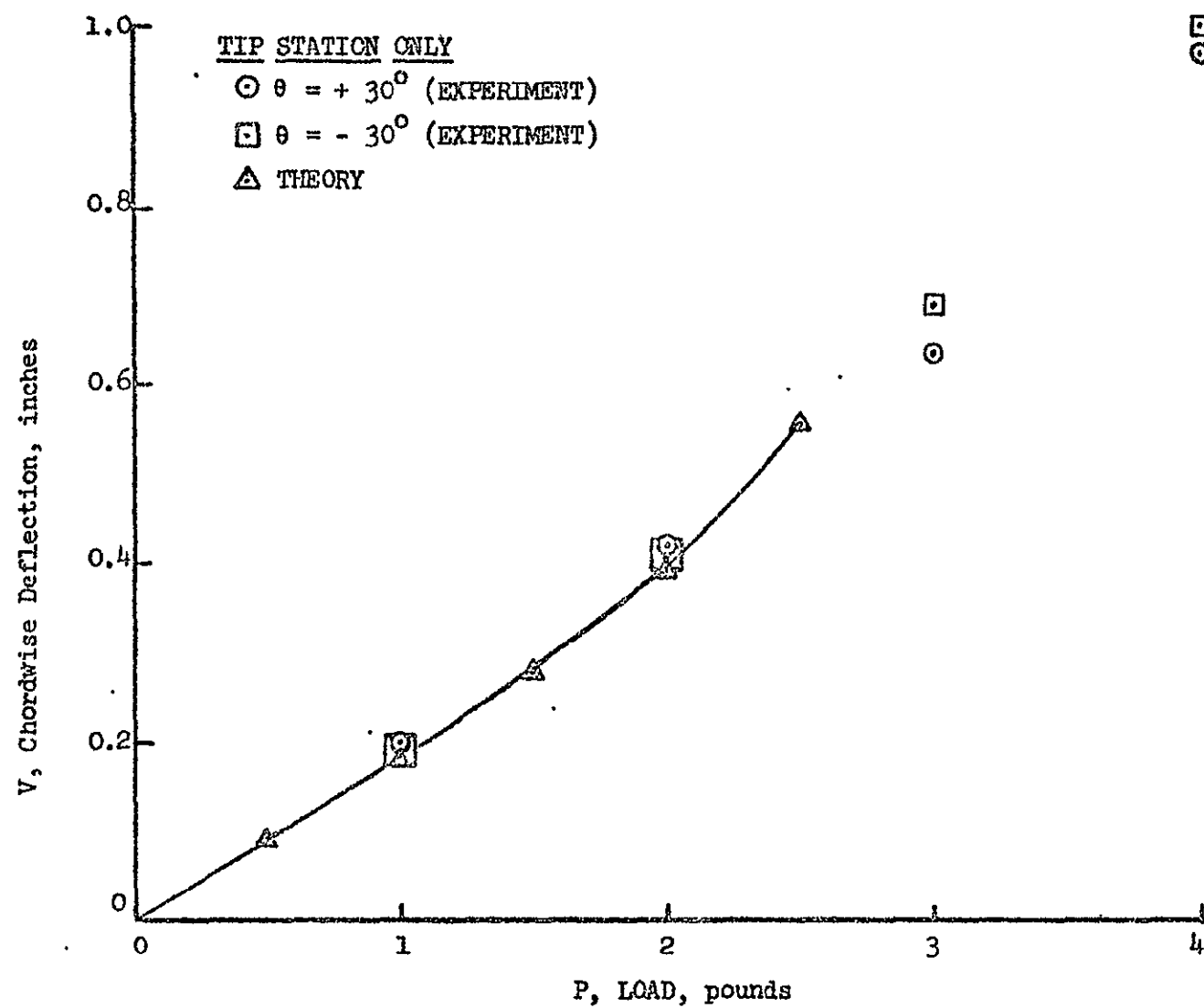


Figure 6-2. Chordwise Deflection versus Load,  $\theta = \pm 30^\circ$

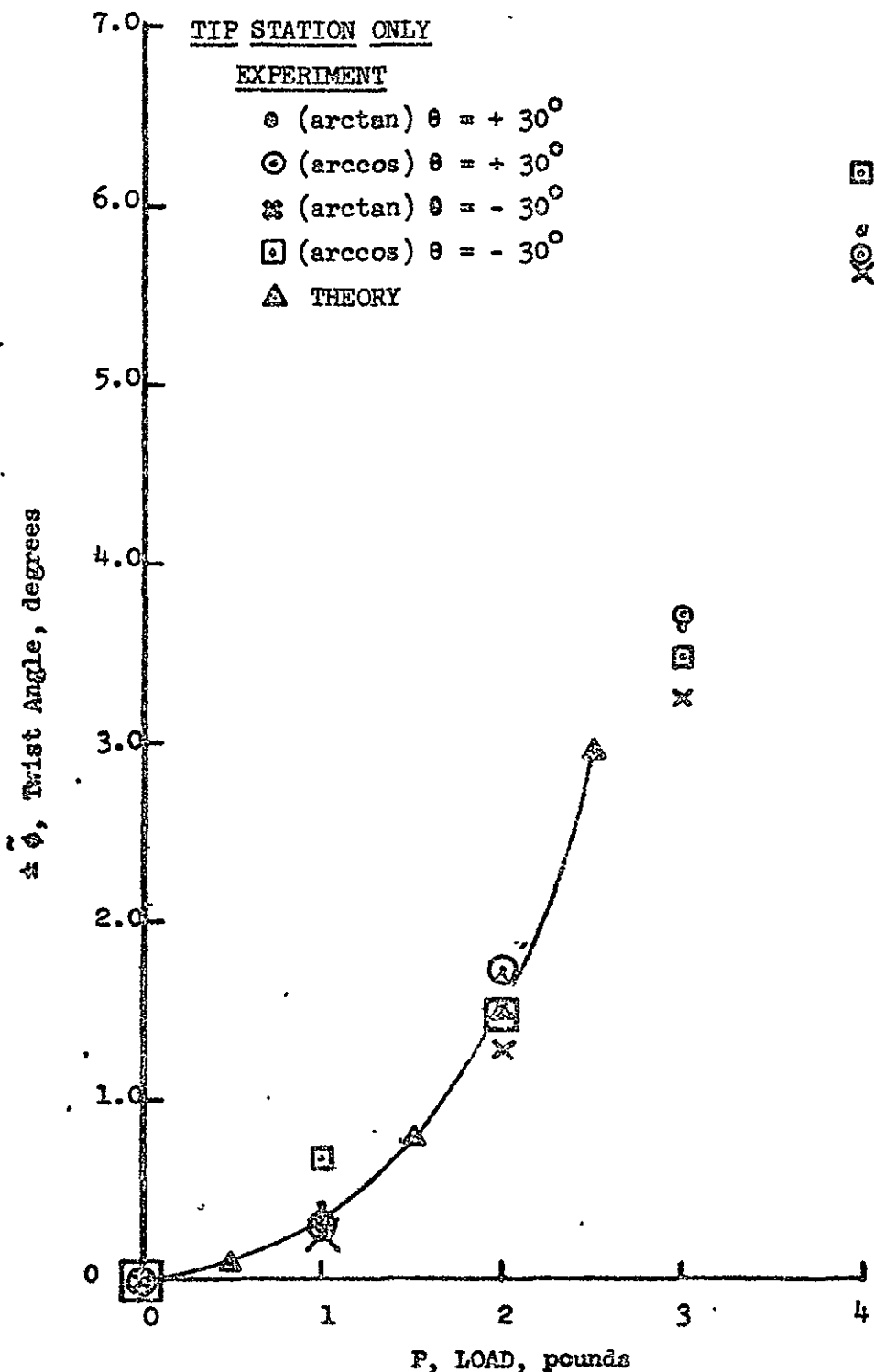


Figure 6-3. Twist Angle versus Load,  $\theta = \pm 30^\circ$ .

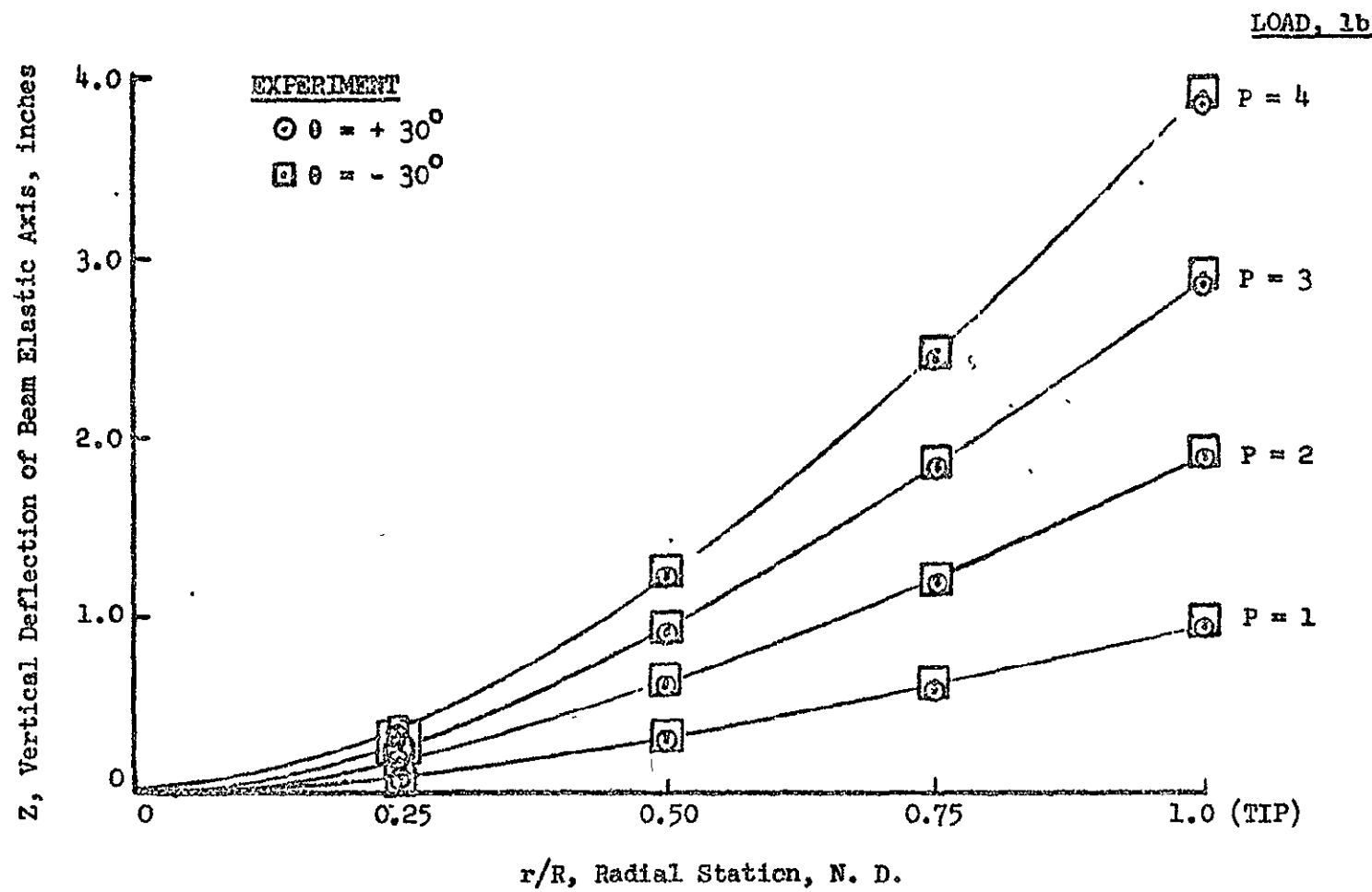


Figure 6-4. Vertical Deflection of Beam Elastic Axis versus Radial Station,  $\theta = \pm 30^\circ$ .

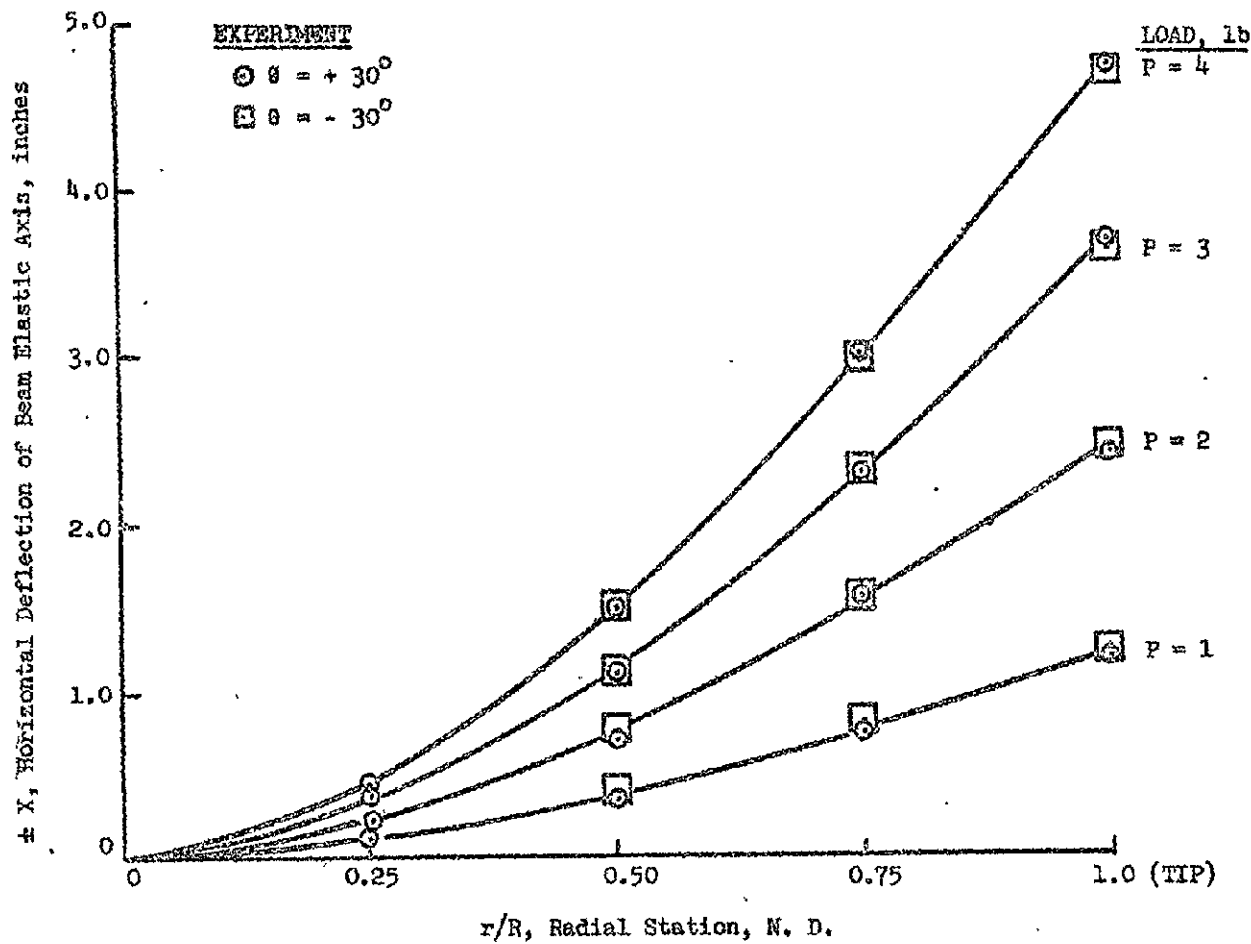


Figure 6-5. Horizontal Deflection of Beam Elastic Axis versus Radial Station,  $\theta = \pm 30^\circ$ .

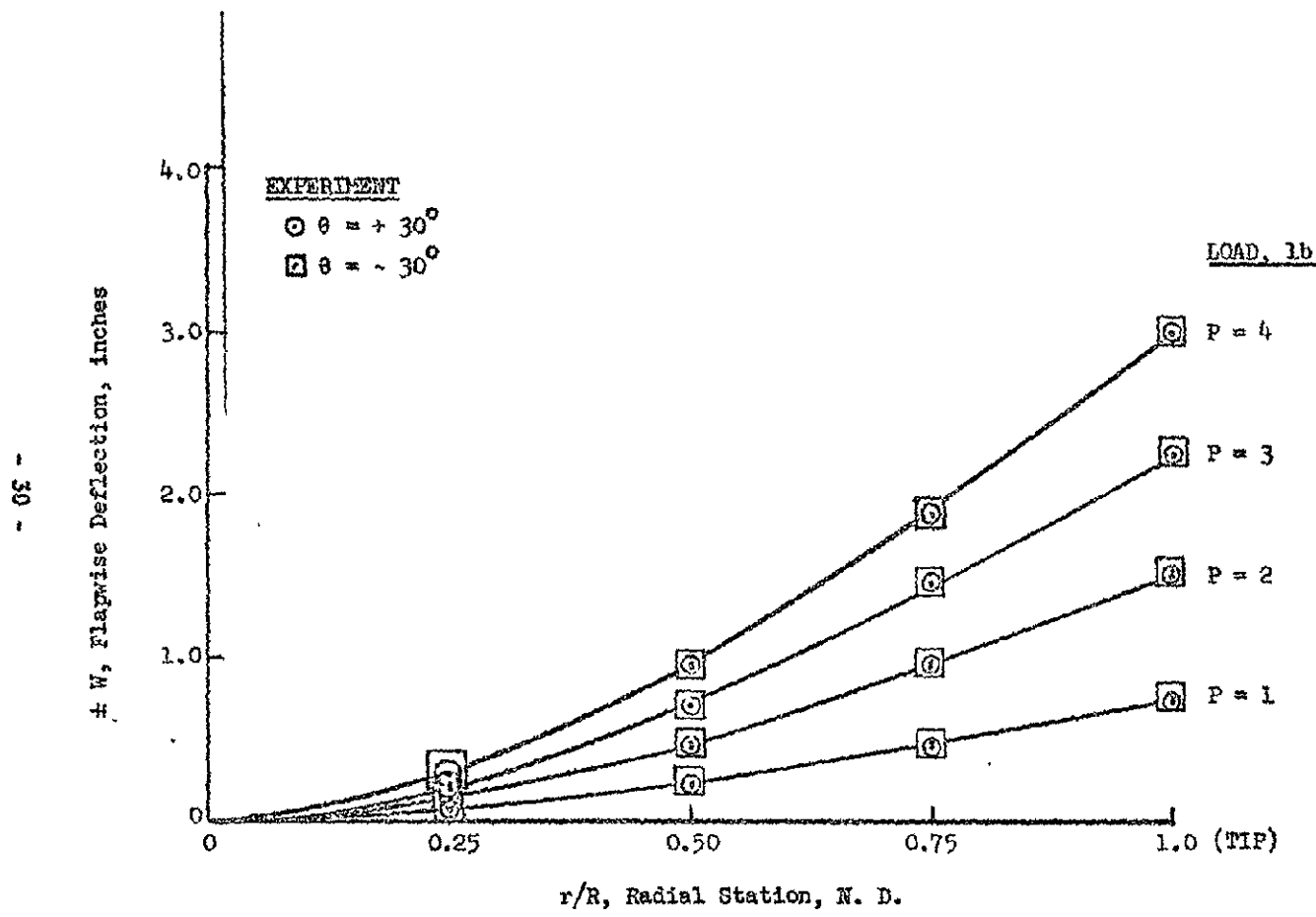


Figure 6-6. Flapwise Deflection versus Radial Station,  $\theta = \pm 30^\circ$ .

- 15 -

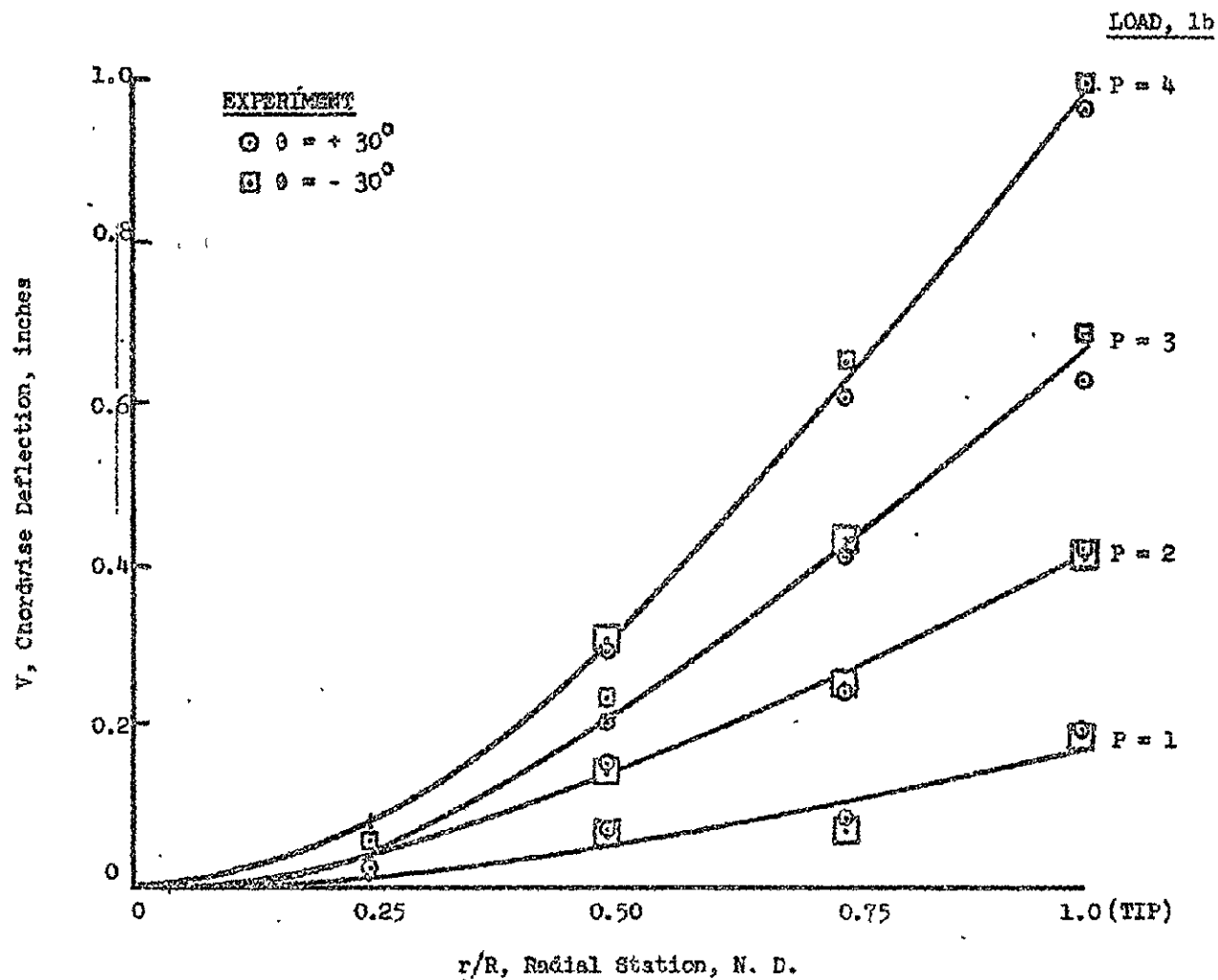


Figure 6-7. Chordwise Deflection versus Radial Station,  $\theta = \pm 30^\circ$ .

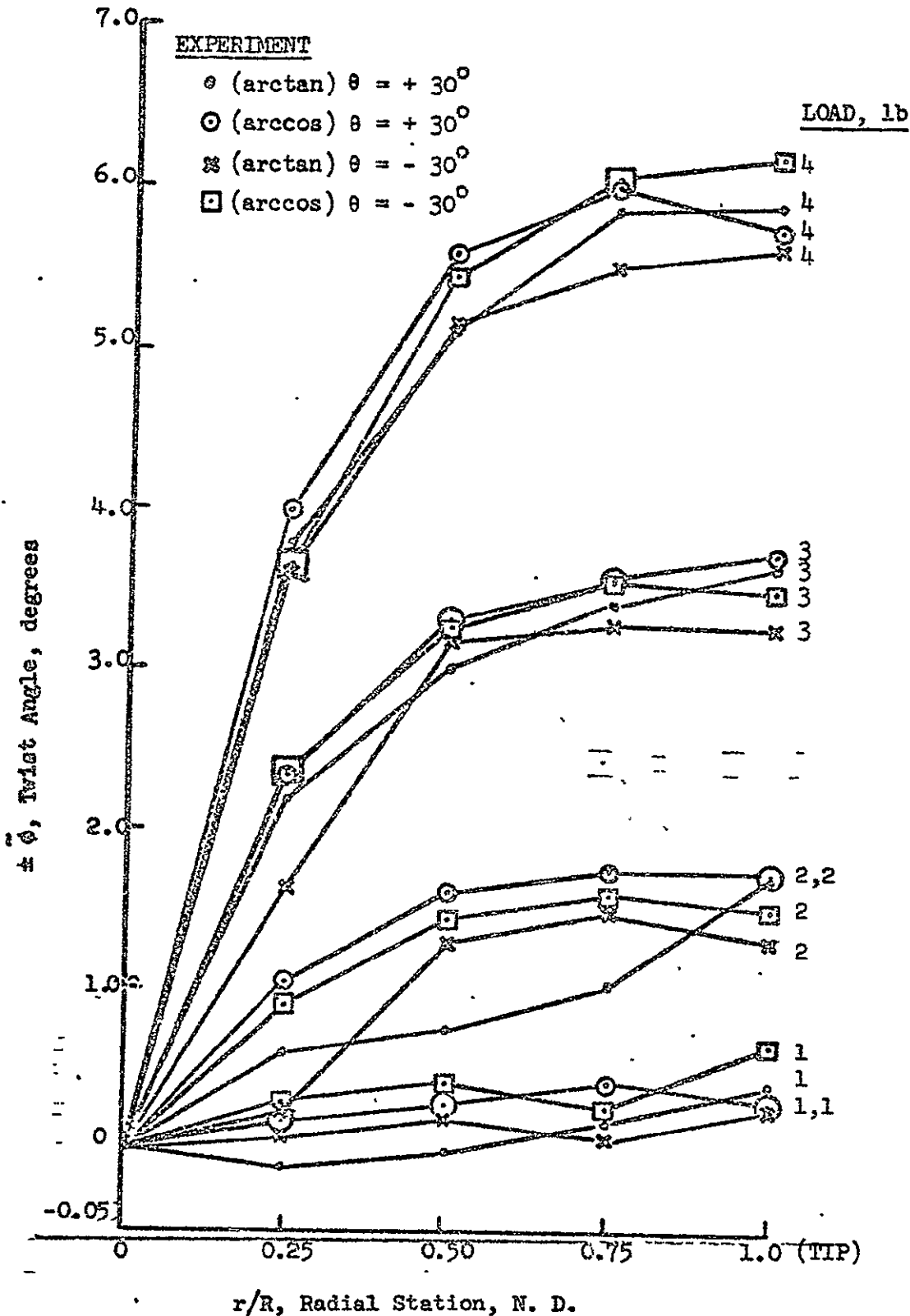


Figure 6-8. Blade Twist Angle versus Radial Station,  
 $\theta = \pm 30^\circ$ .

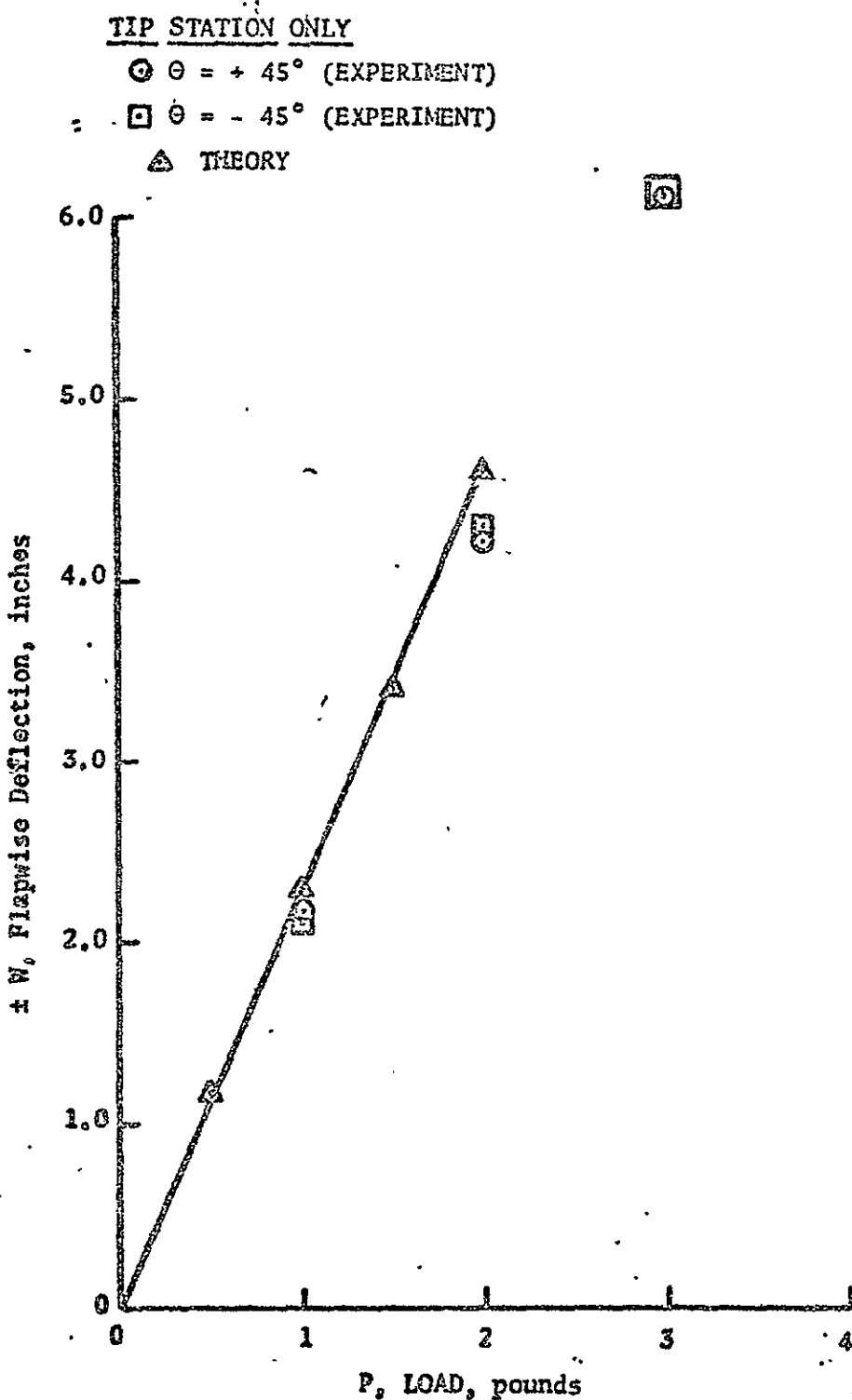


Figure 7-1. Flapwise Deflection versus Load,  $\theta = \pm 45^\circ$

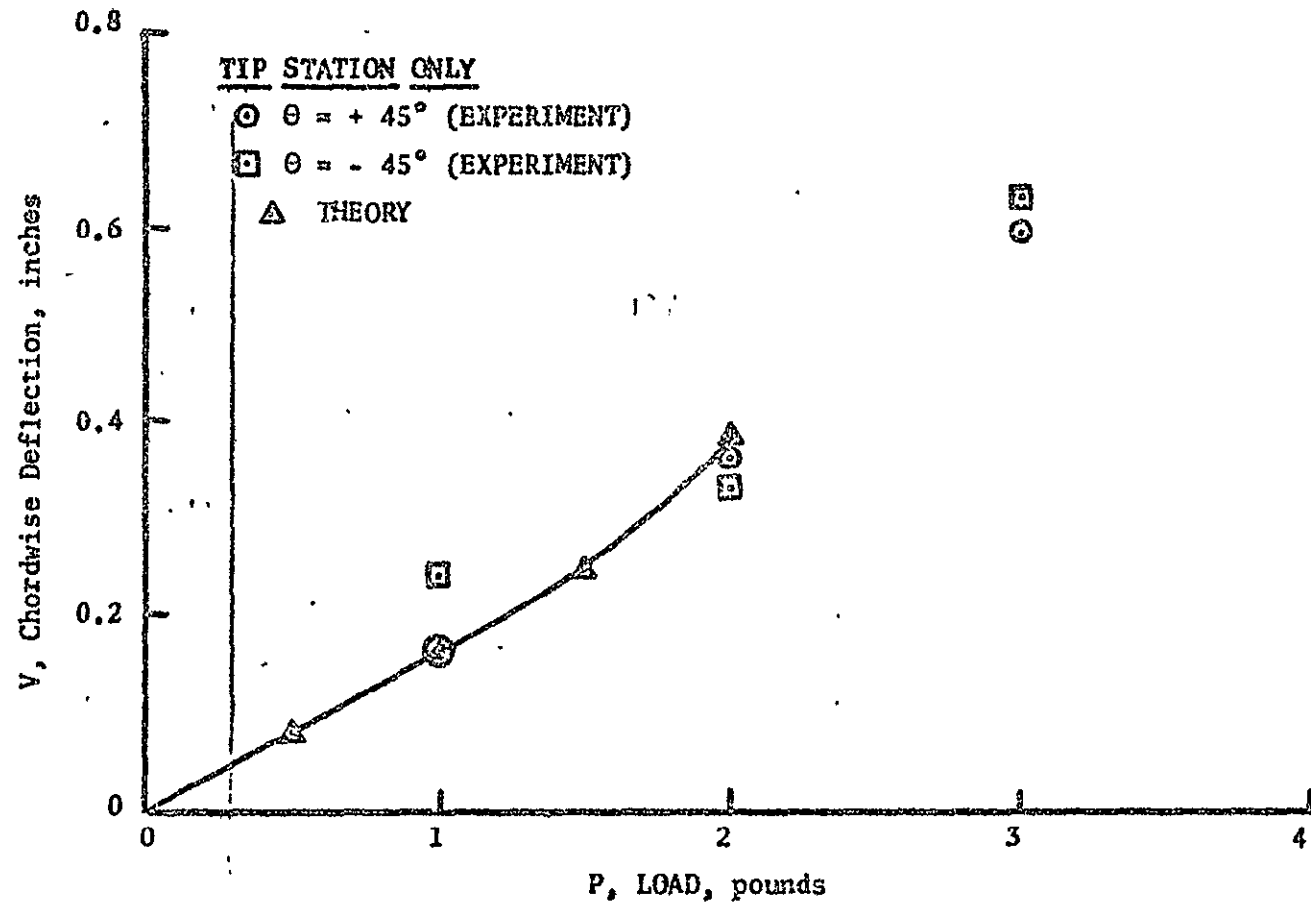


Figure 7-2. Chordwise Deflection versus Load,  $\theta = \pm 45^\circ$

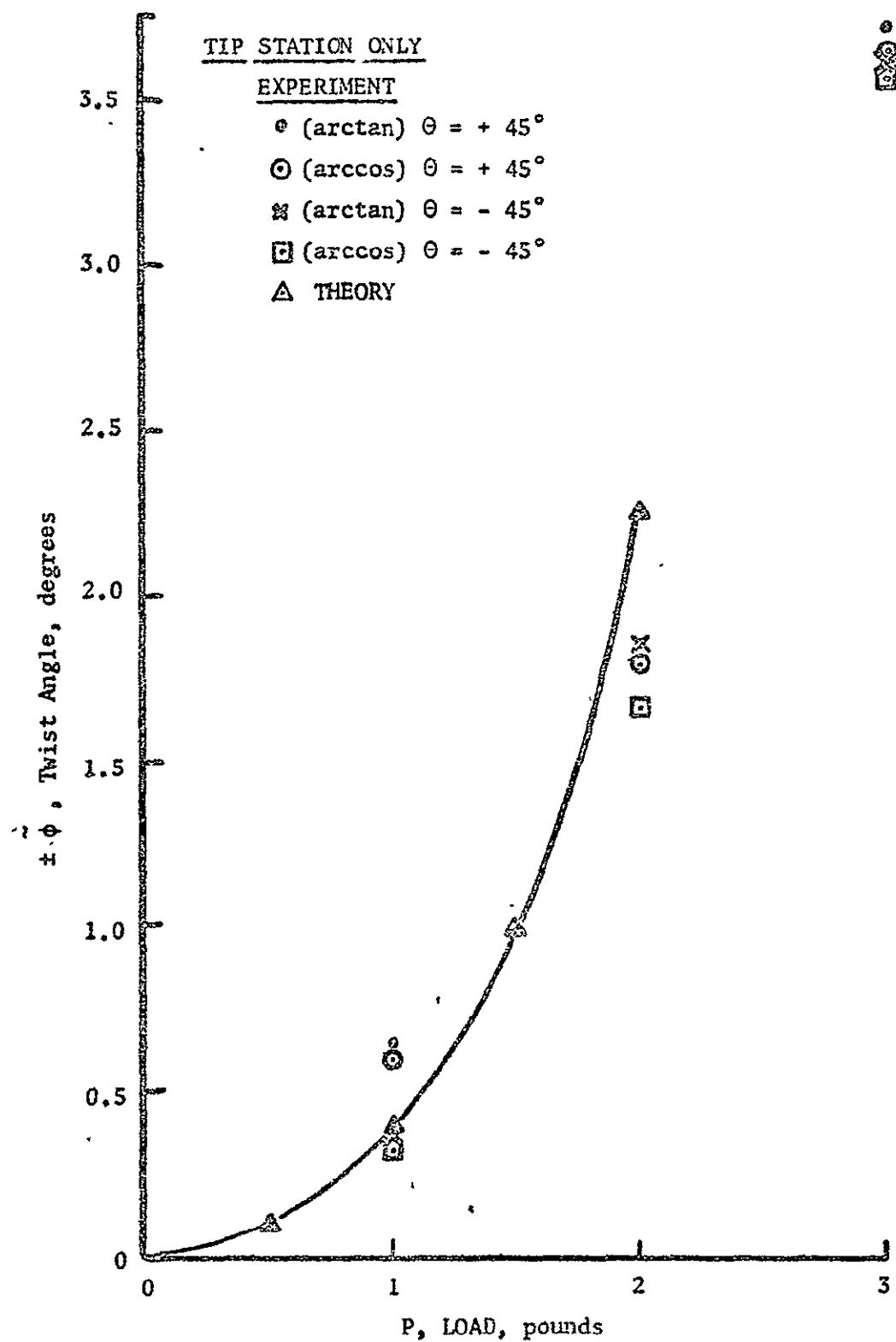


Figure 7-3. Twist Angle versus Load,  $\theta = \pm 45^\circ$

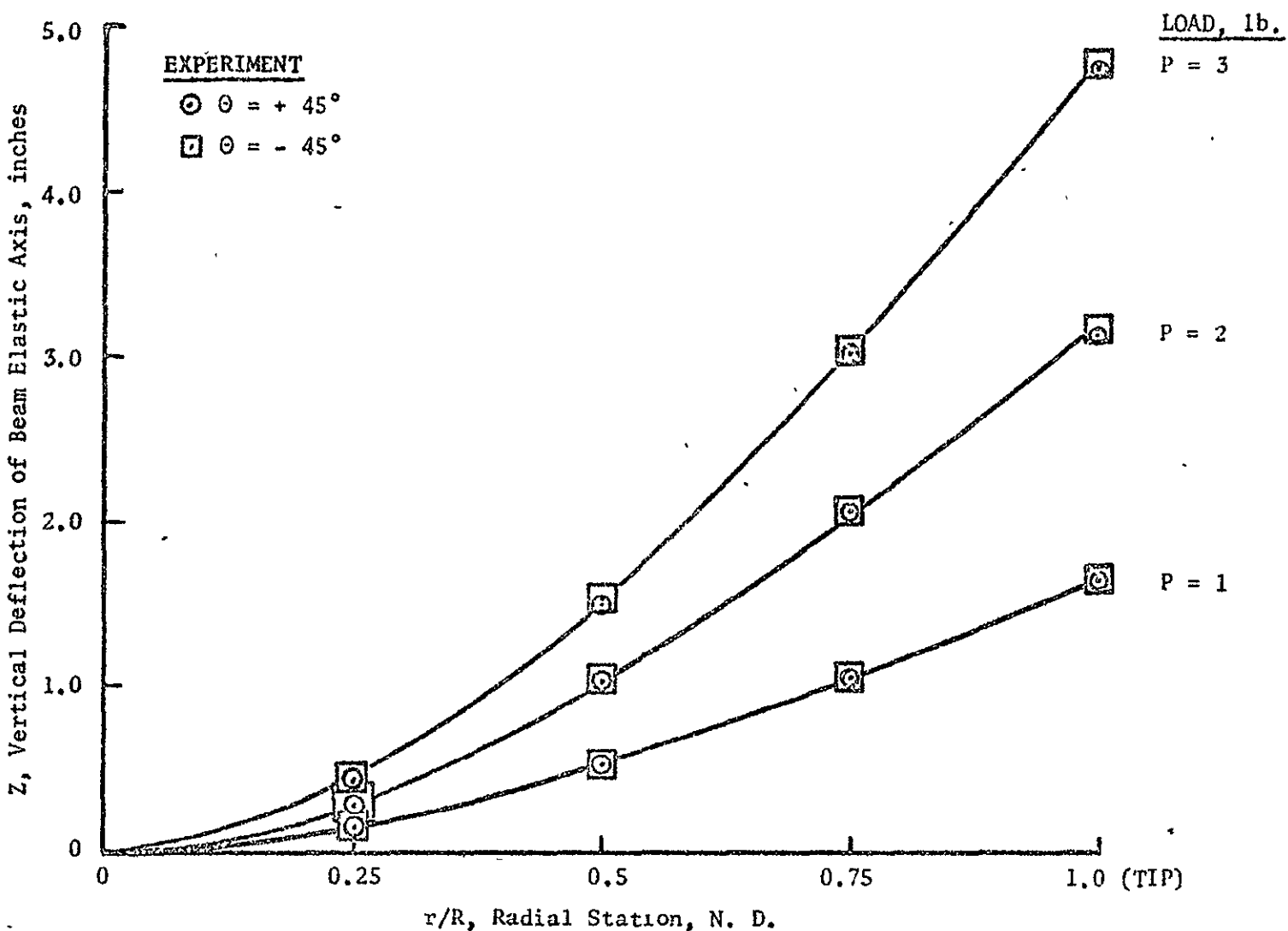


Figure 7-4. Vertical Deflection of Beam Elastic Axis versus Radial Station,  $\theta = \pm 45^\circ$

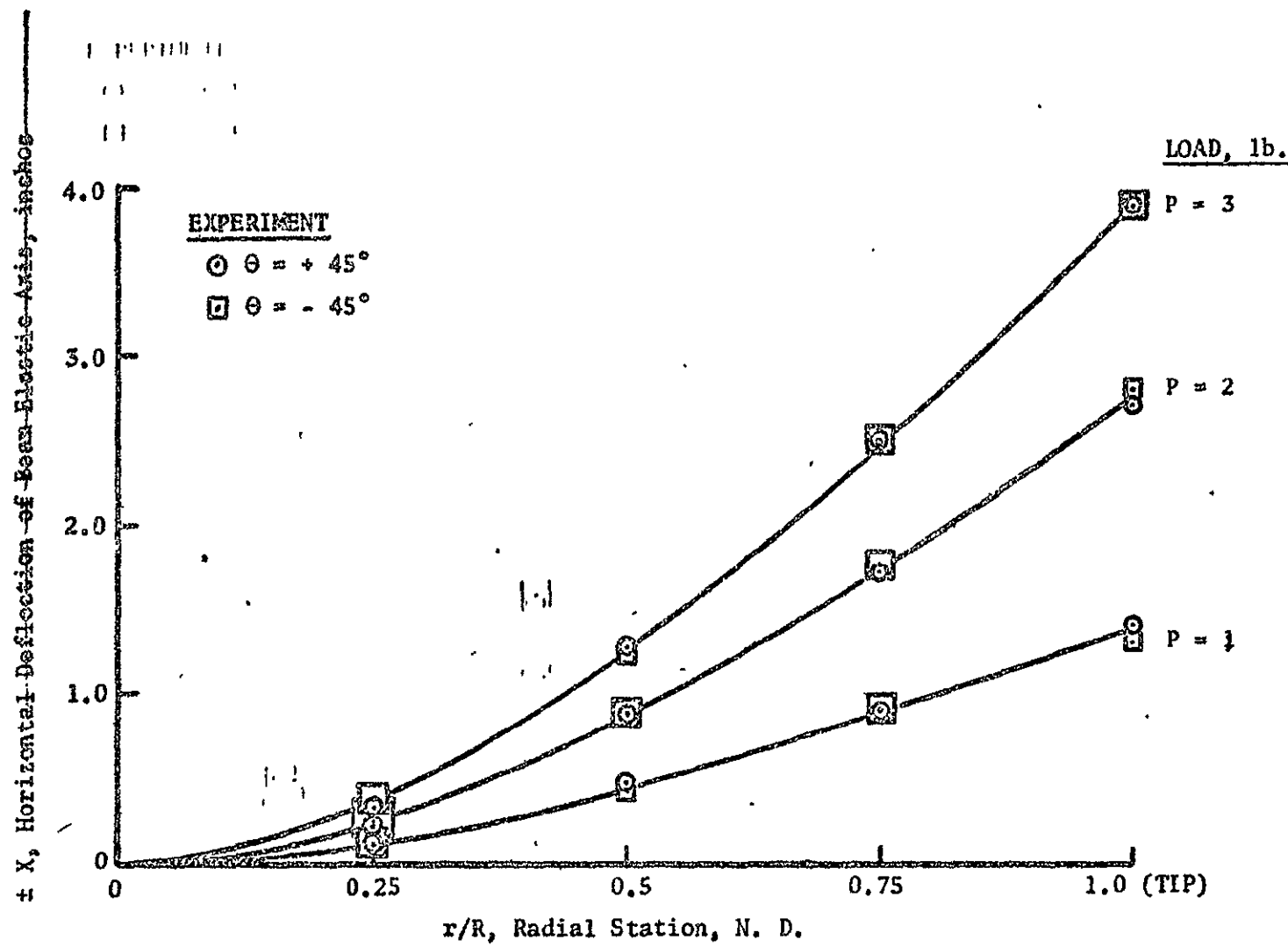


Figure 7-5. Horizontal Deflection of Beam Elastic Axis versus Radial Station,  $\theta = \pm 45^\circ$

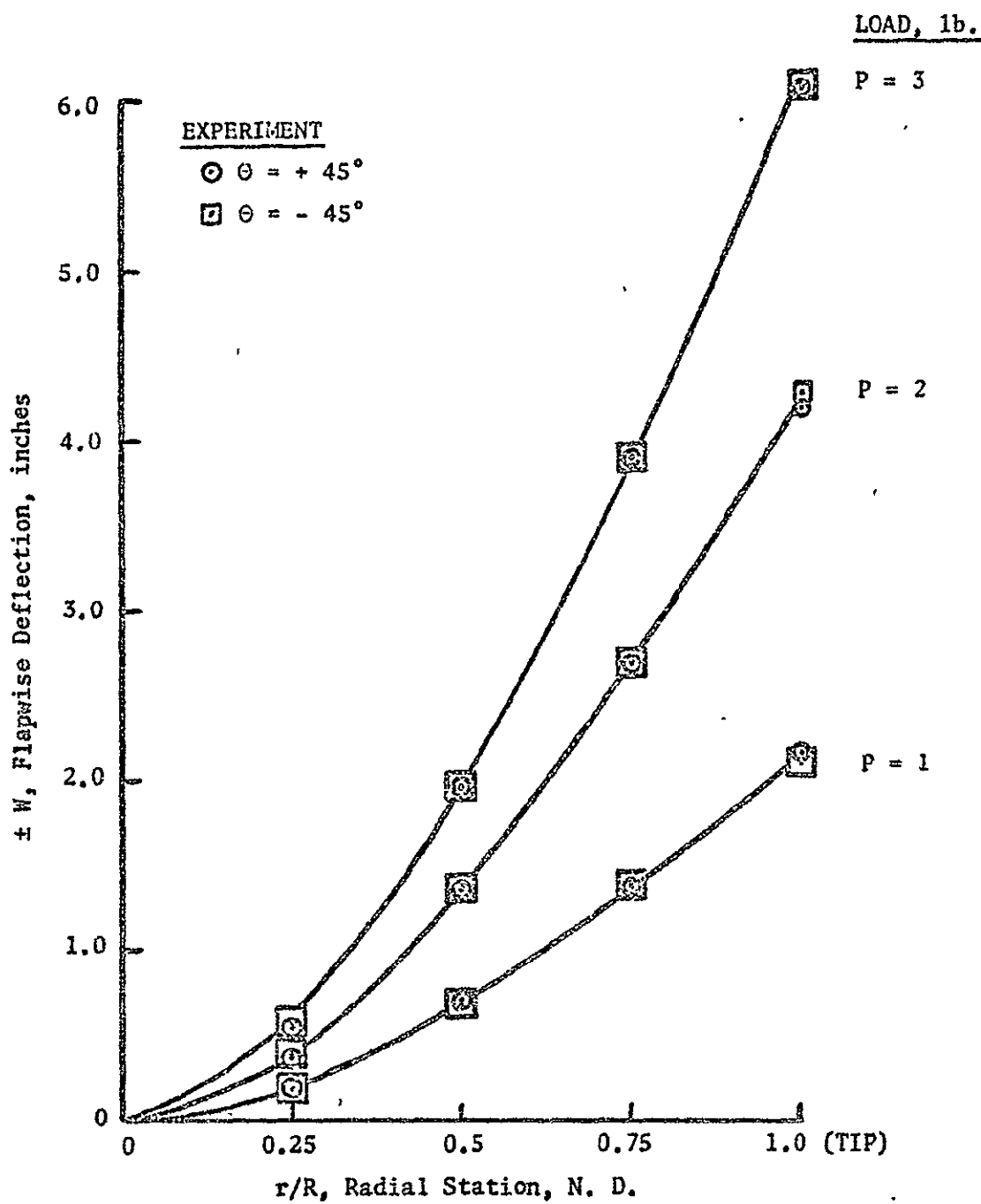


Figure 7-6. Flapwise Deflection versus  
Radial Station,  $\Theta = \pm 45^\circ$

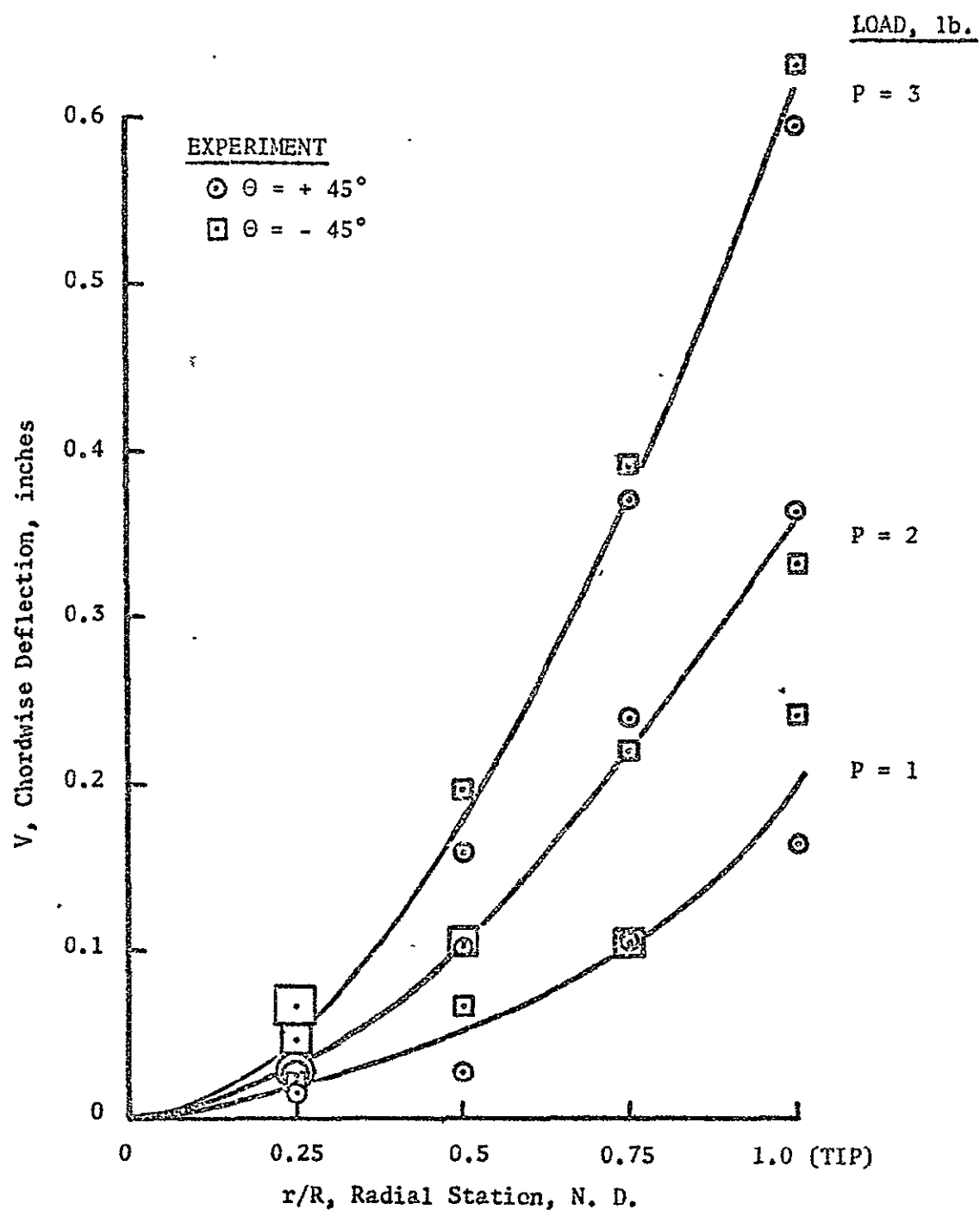


Figure 7-7. Chordwise Deflection versus Radial Station,  $\Theta = \pm 45^\circ$

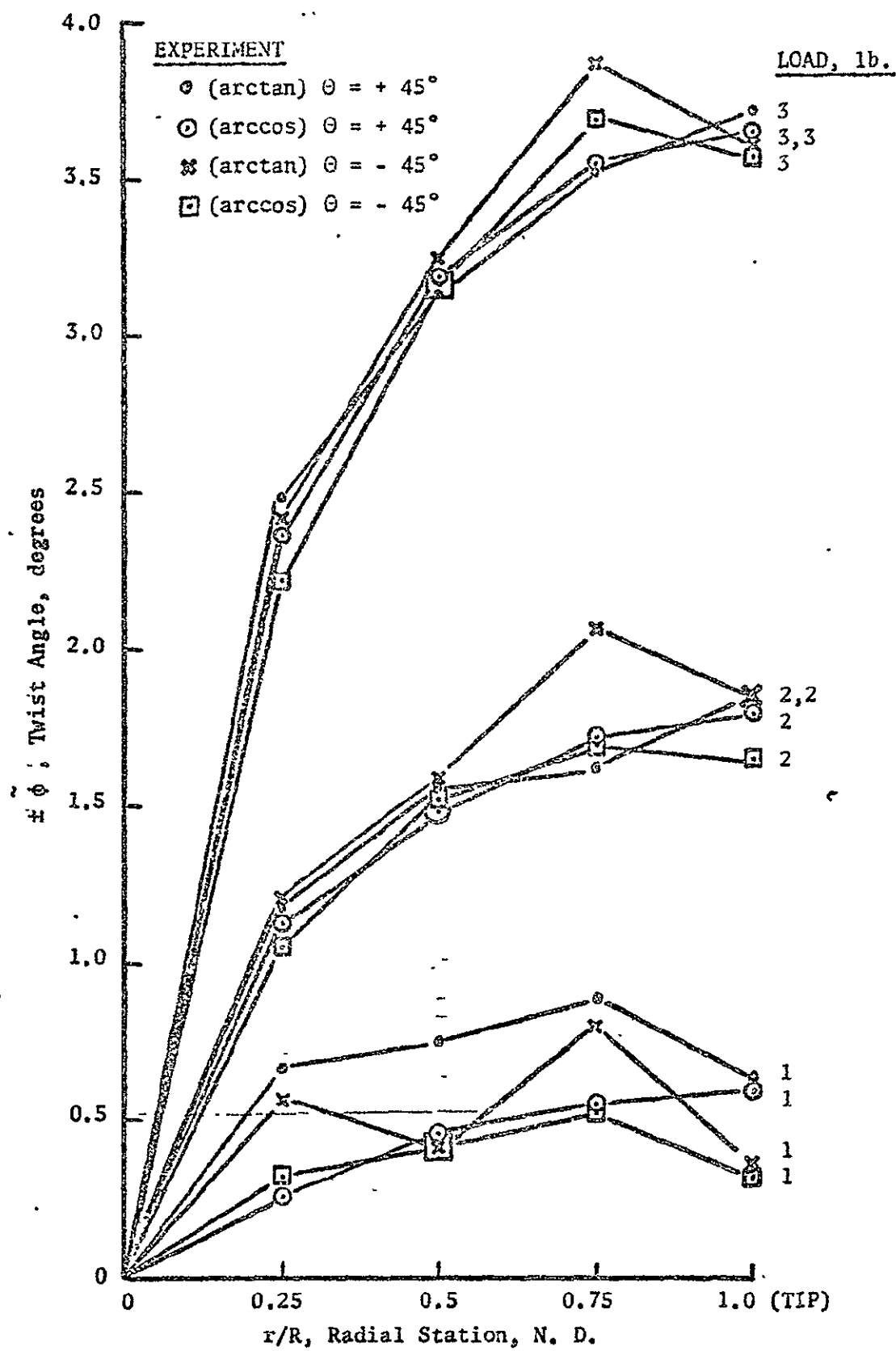


Figure 7-8. Blade Twist Angle versus Radial Station,  $\Theta \approx \pm 45^\circ$

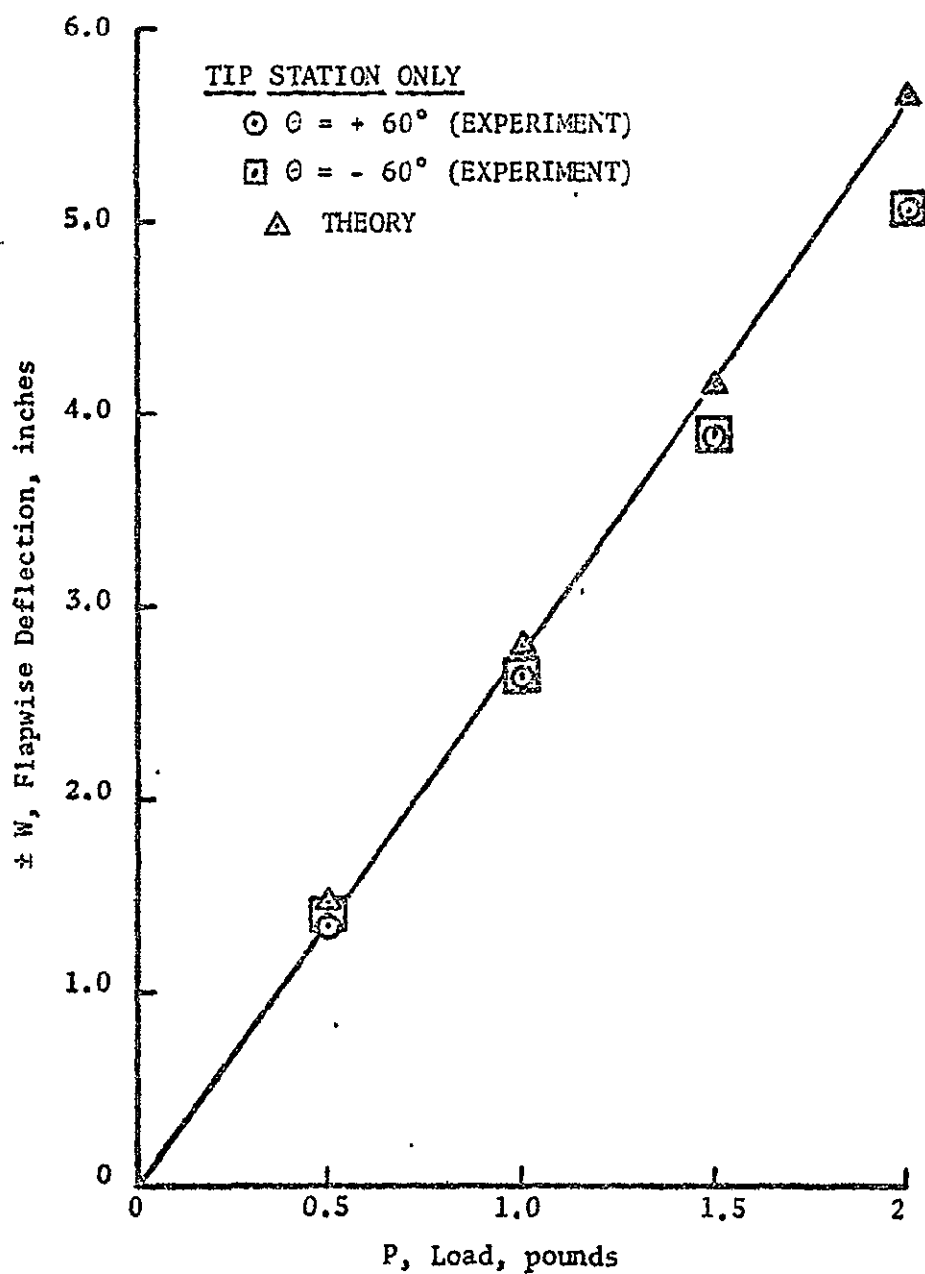


Figure 8-1. Flapwise Deflection versus Load,  
 $\theta = \pm 60^\circ$

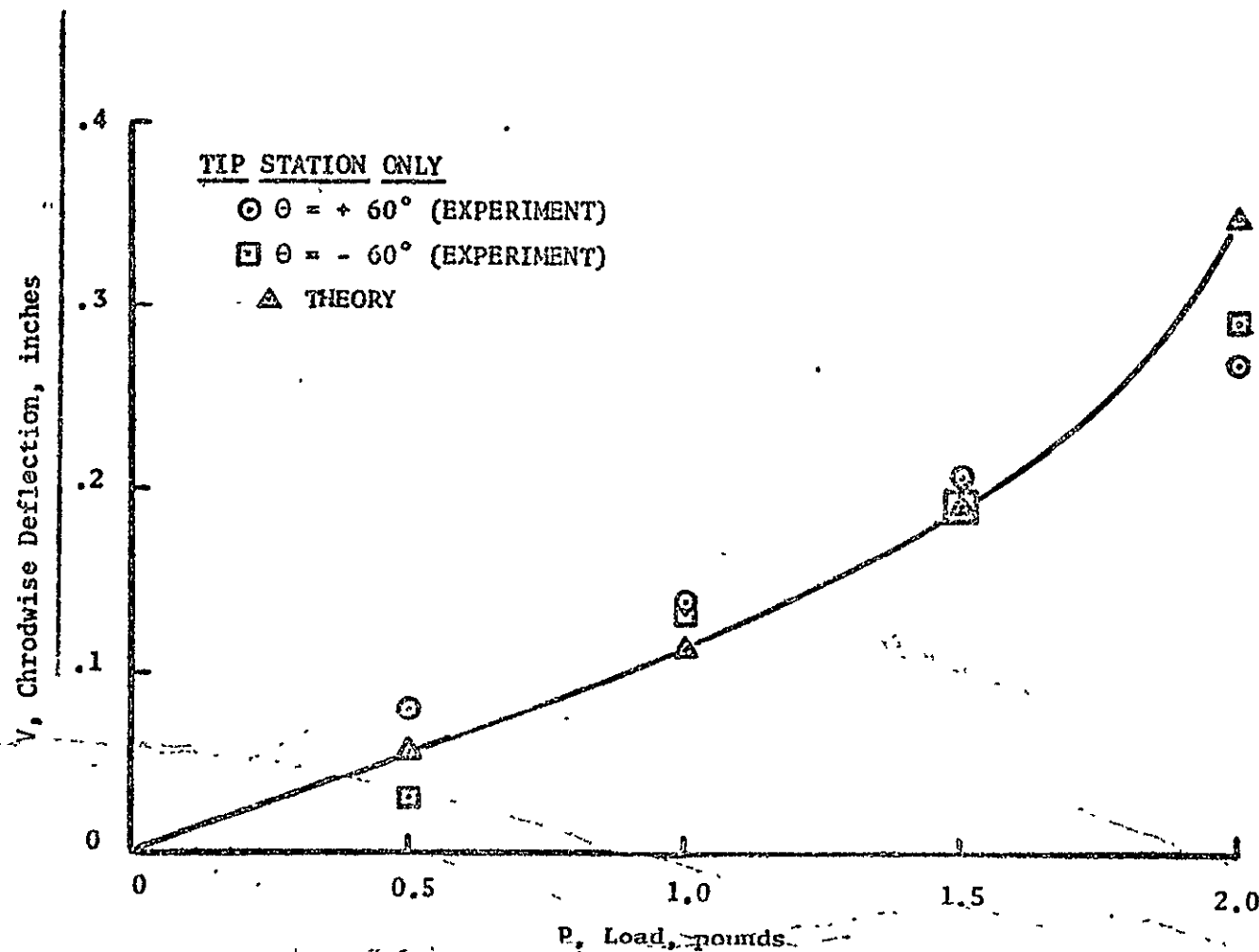


Figure 8-2. Chordwise Deflection versus Load,  $\theta = \pm 60^\circ$

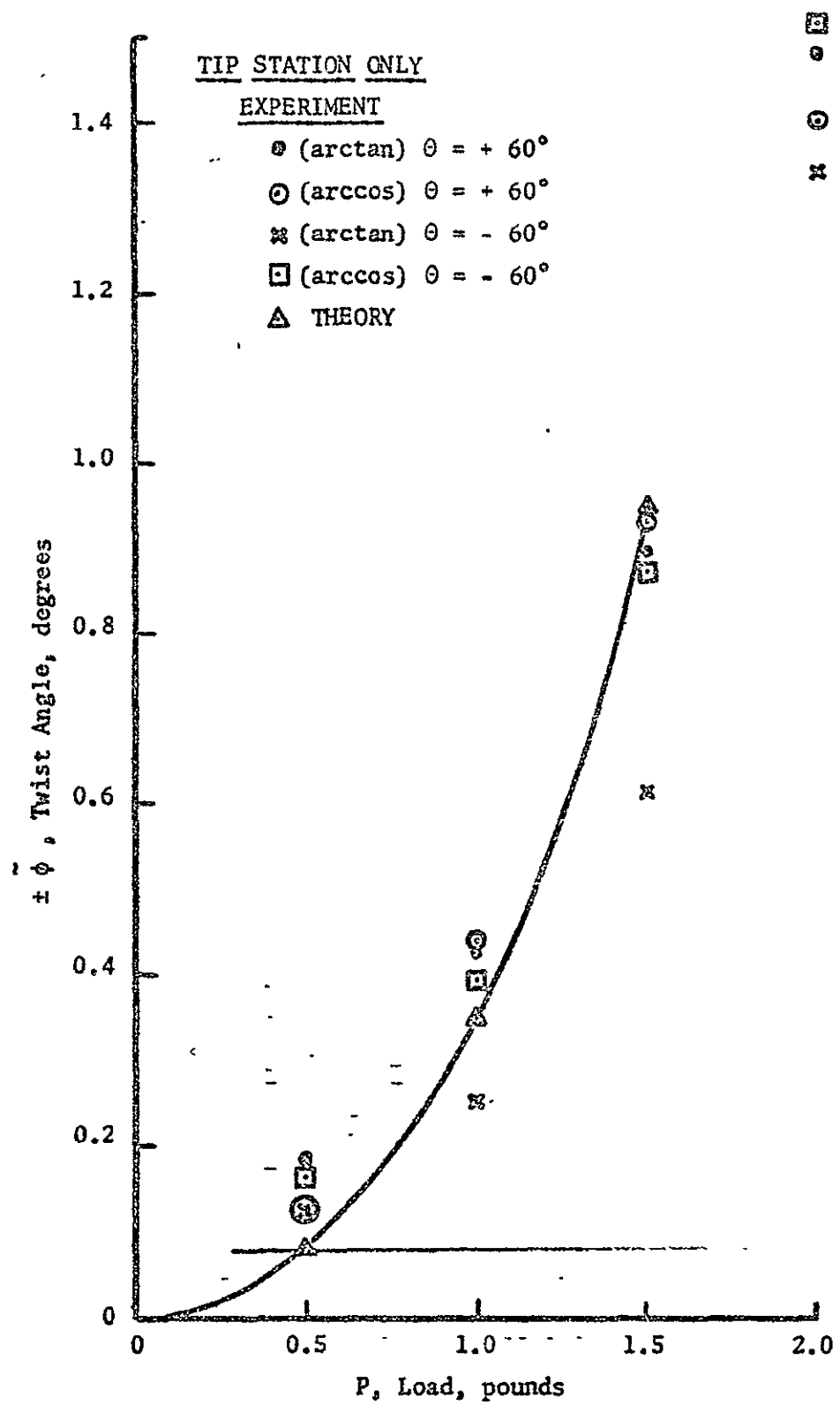


Figure 8-3. Twist Angle versus Load,  $\theta \approx \pm 60^\circ$

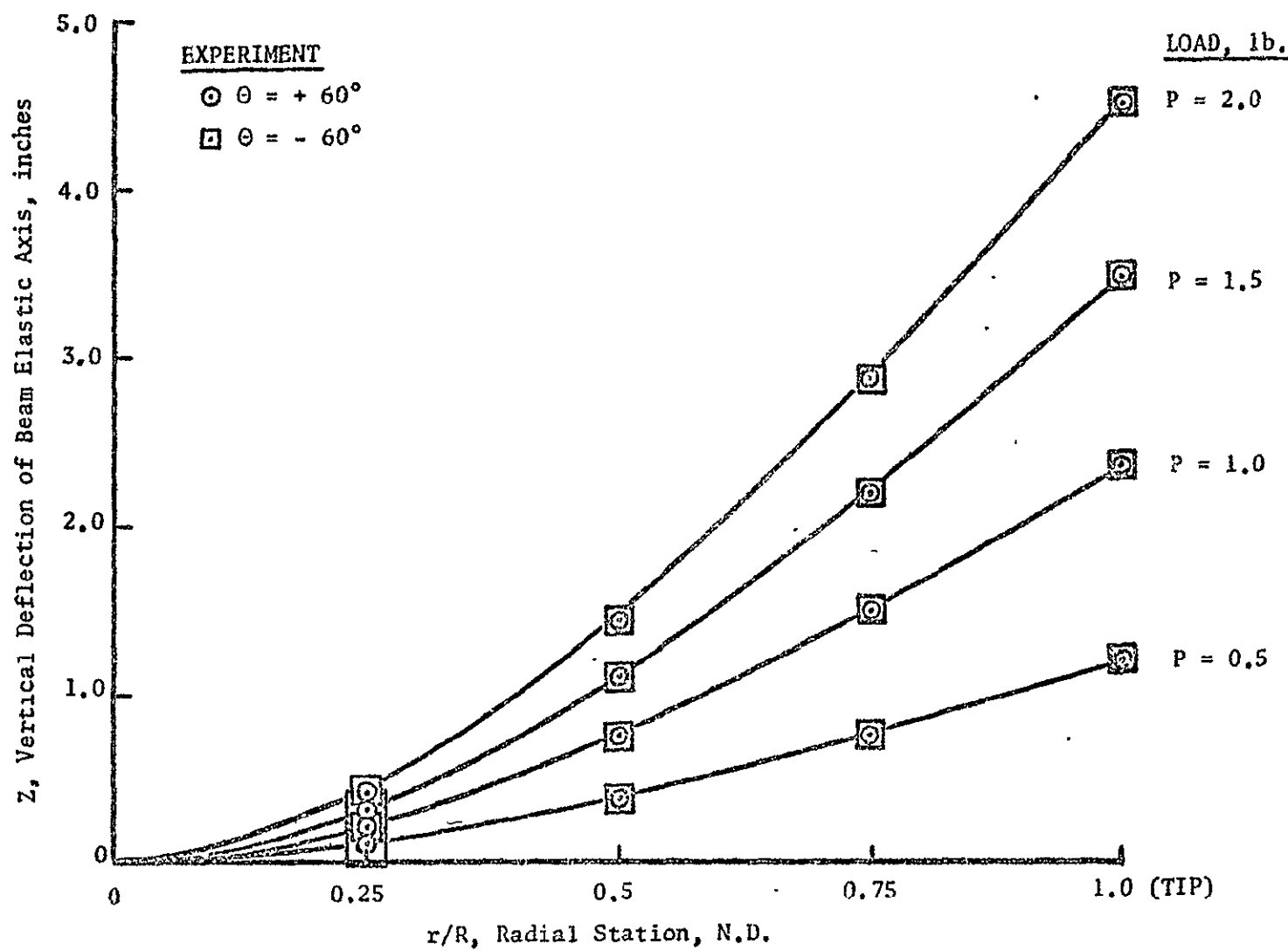


Figure 8-4. Vertical Deflection of Beam Elastic Axis versus Radial Station,  $\theta = \pm 60^\circ$

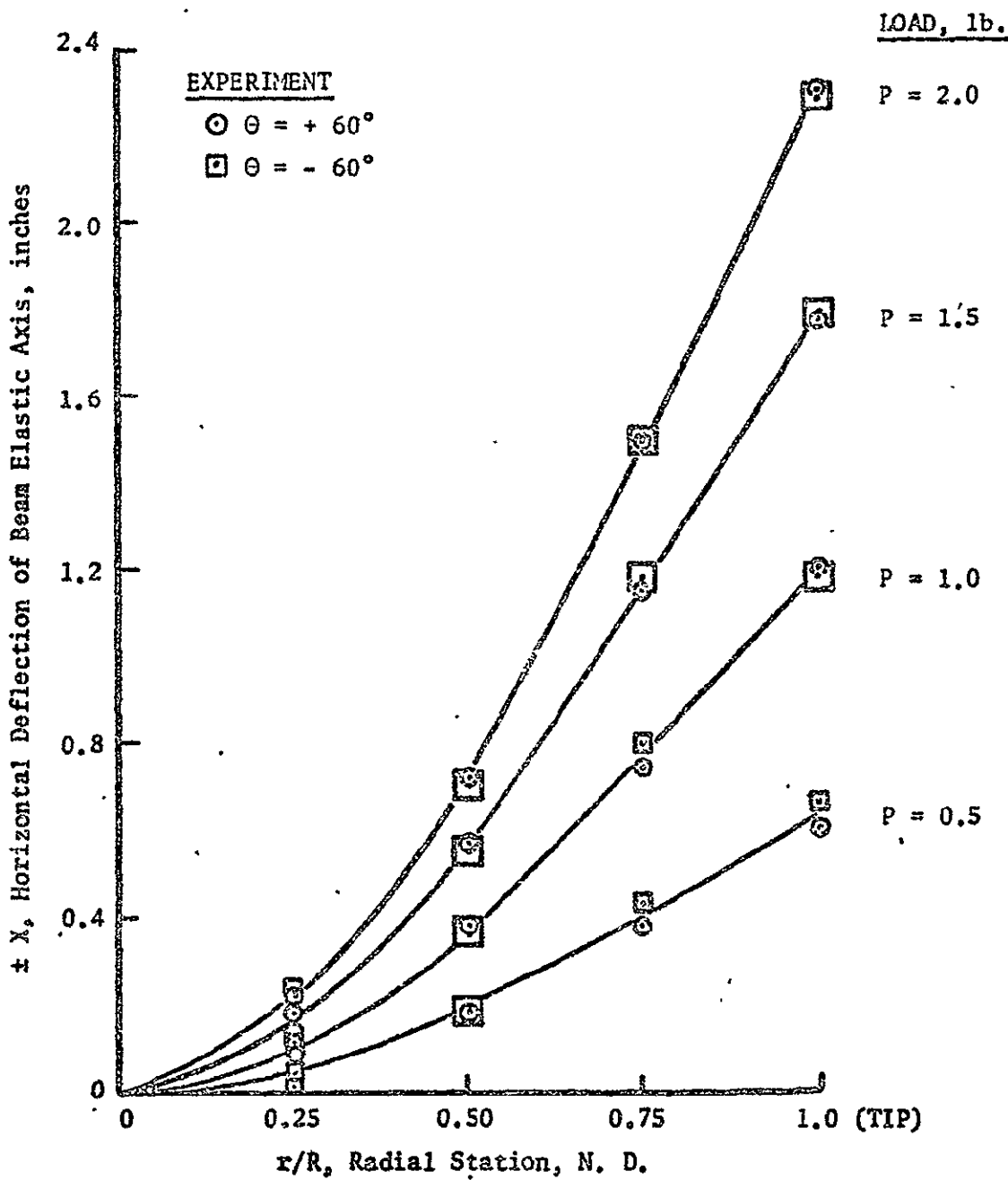


Figure 8-5. Horizontal Deflection of Beam Elastic Axis versus Radial Station,  $\theta = \pm 60^\circ$

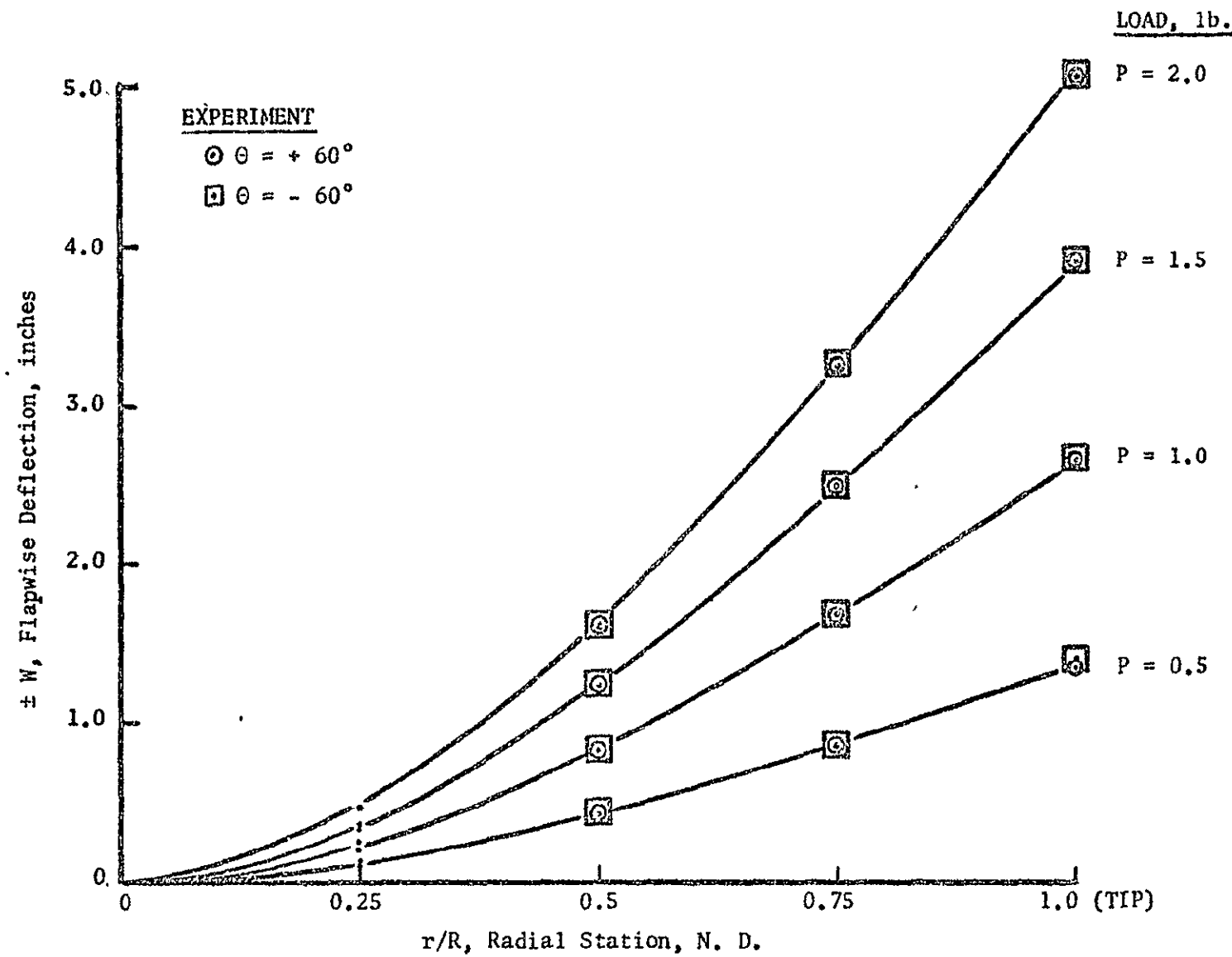


Figure 8-6. Flapwise Deflection versus Radial Station,  $\theta = \pm 60^\circ$

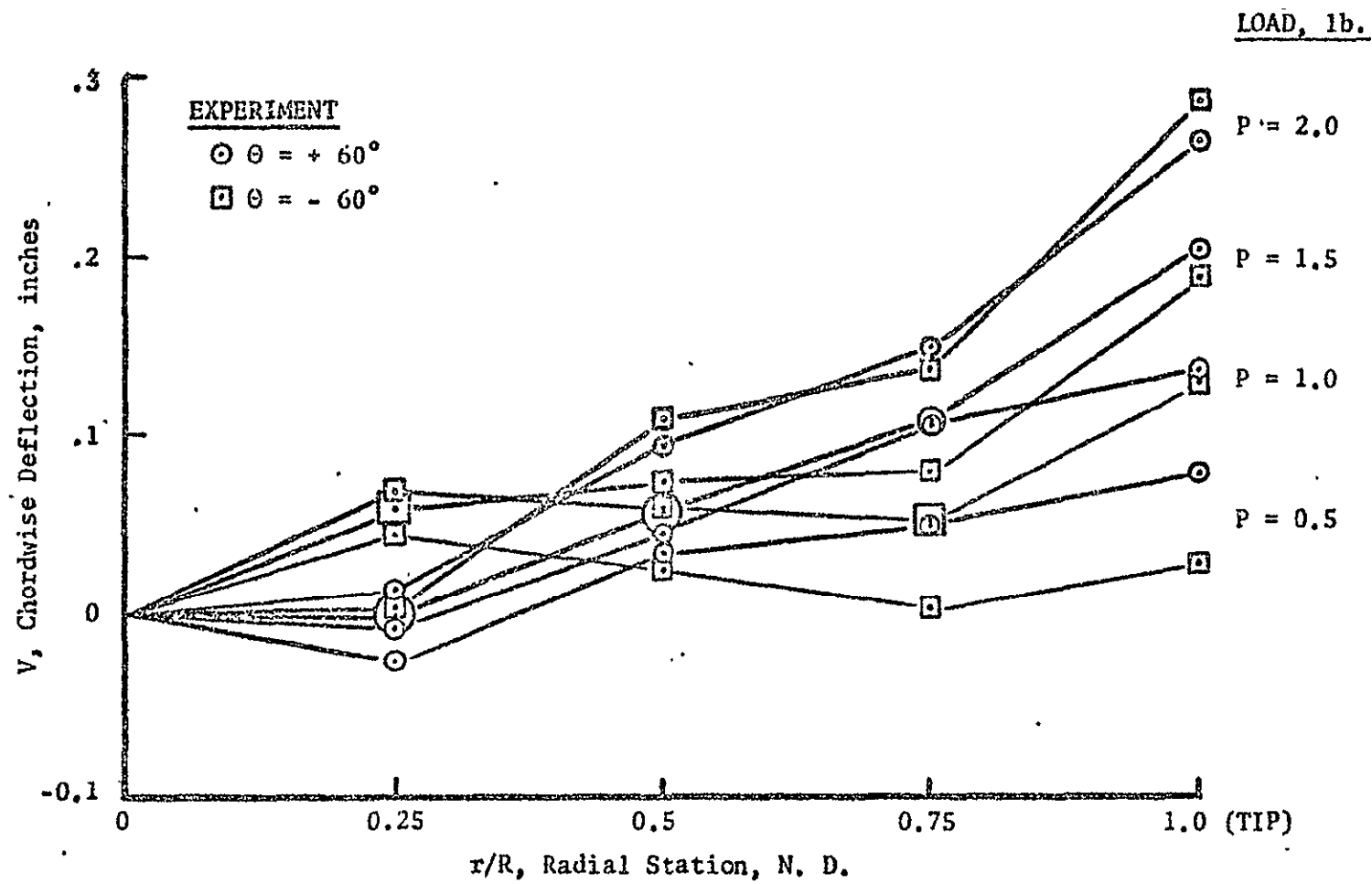


Figure 8-7. Chordwise Deflection versus Radial Station,  $\theta = \pm 60^\circ$

EXPERIMENT

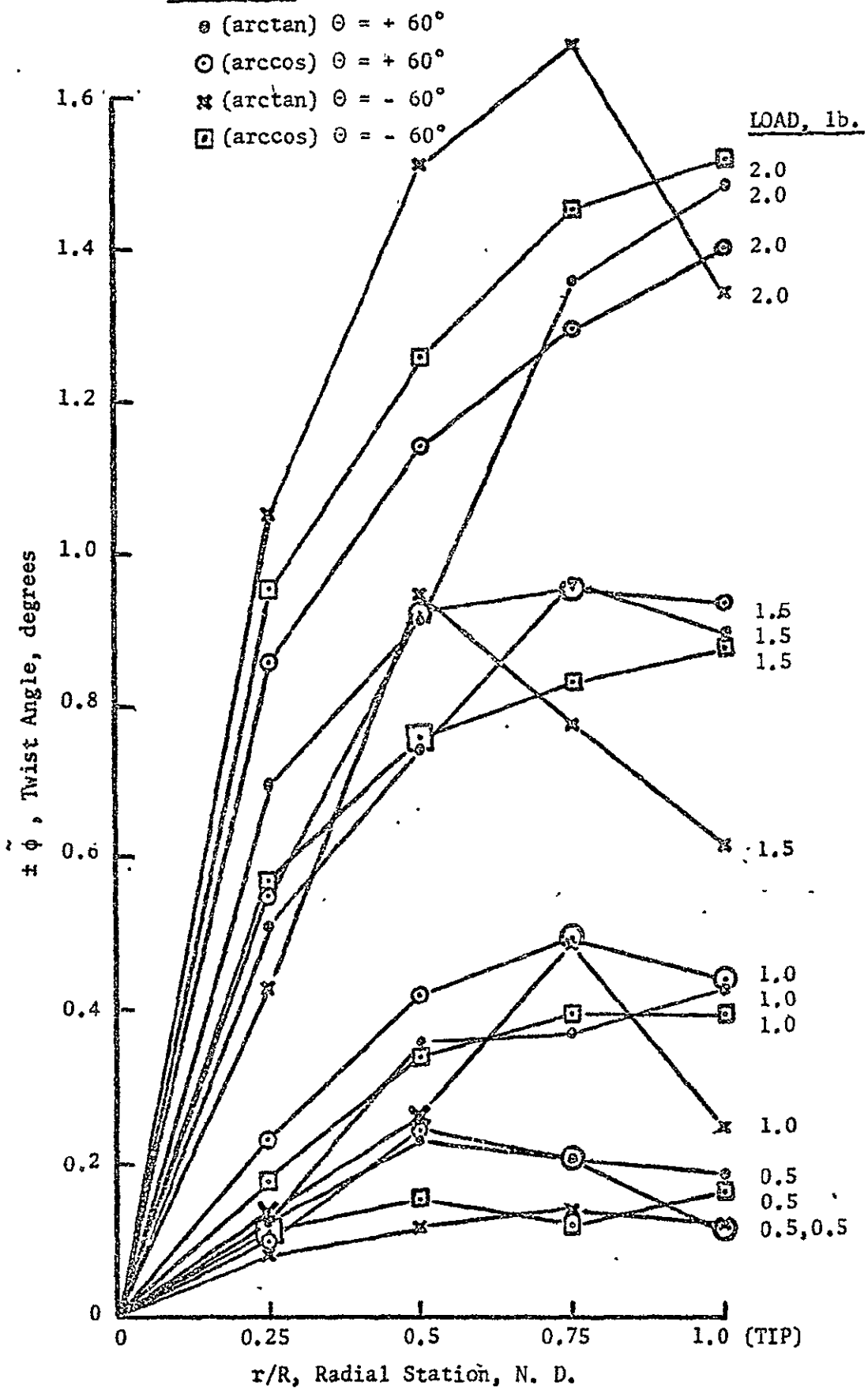


Figure 8-8. Blade Twist Angle versus Radial Station,  
 $\theta = \pm 60^\circ$

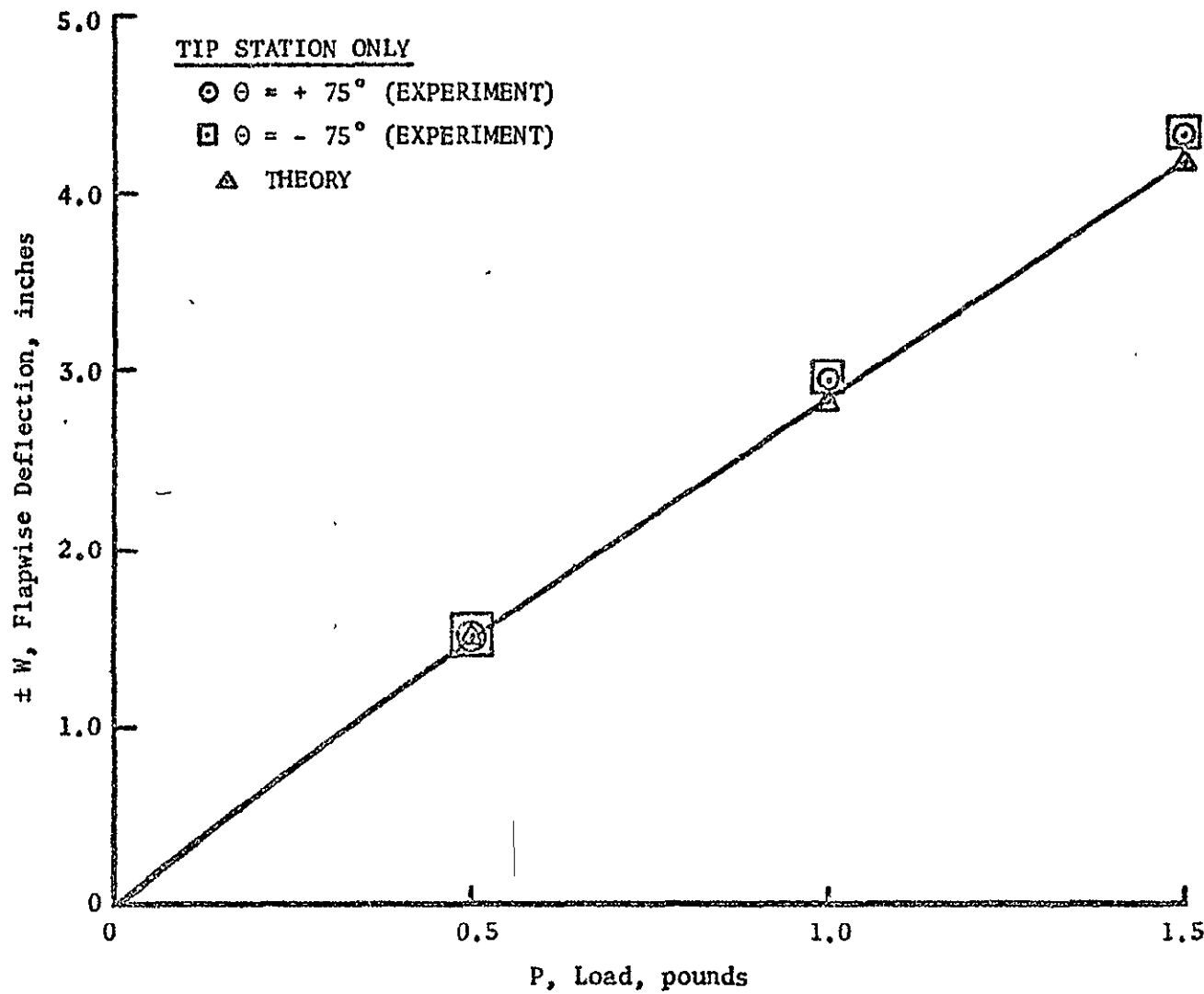


Figure 9-1. Flapwise Deflection versus Load,  $\theta = \pm 75^\circ$

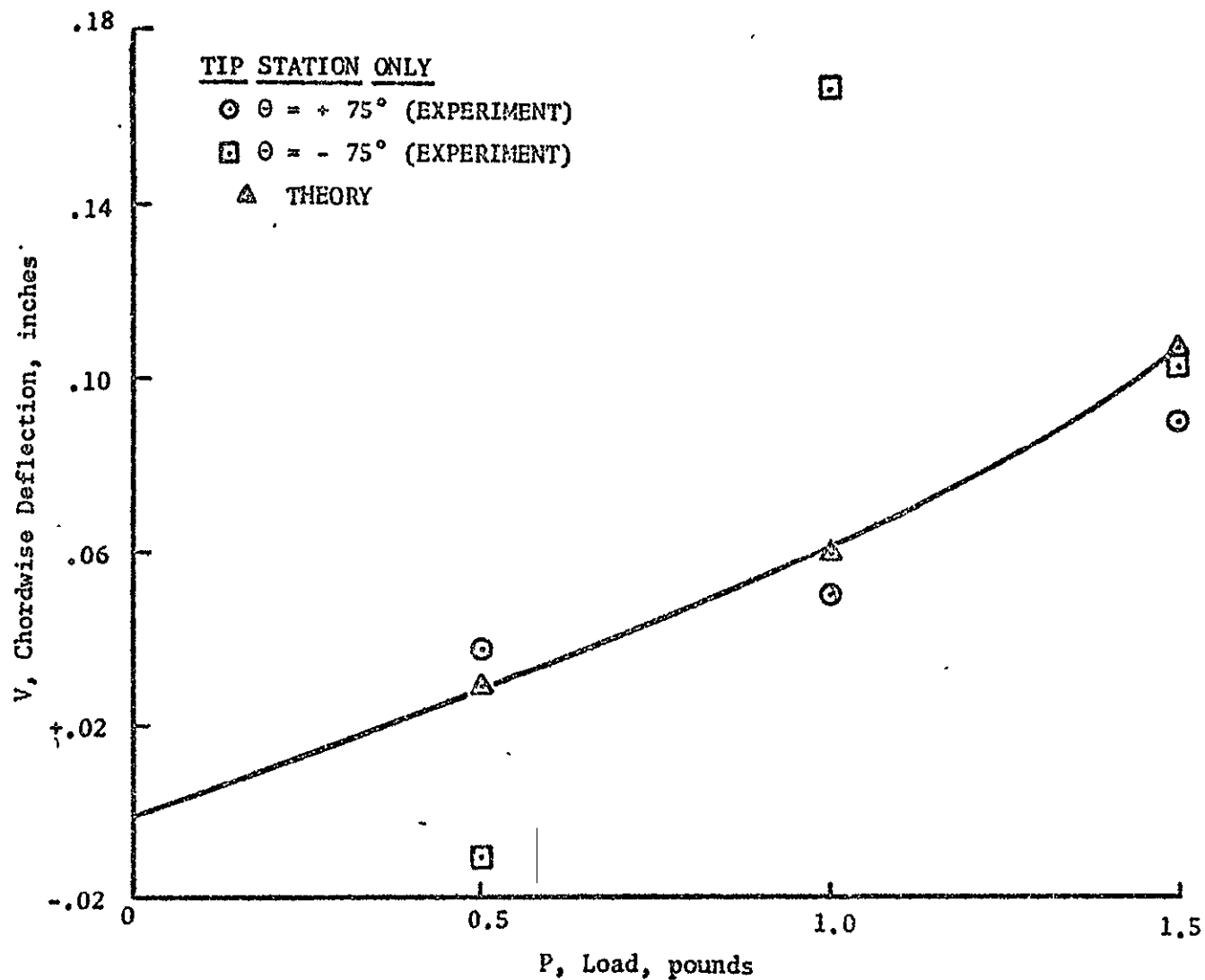


Figure 9-2. Chordwise Deflection versus Load,  $\theta = \pm 75^\circ$

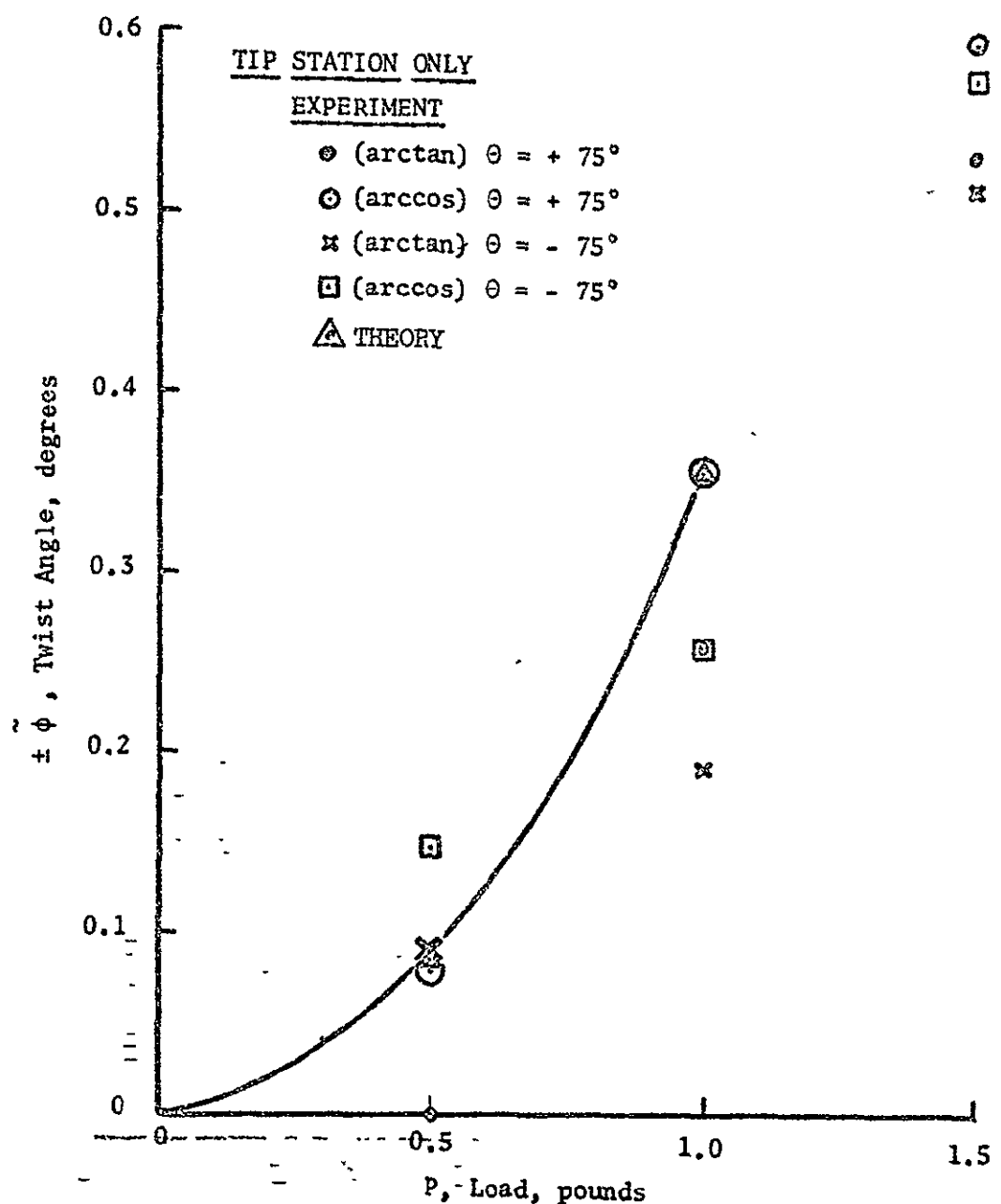


Figure 9-3. Twist Angle at Blade Tip versus Load,  $\theta = \pm 75^\circ$ .

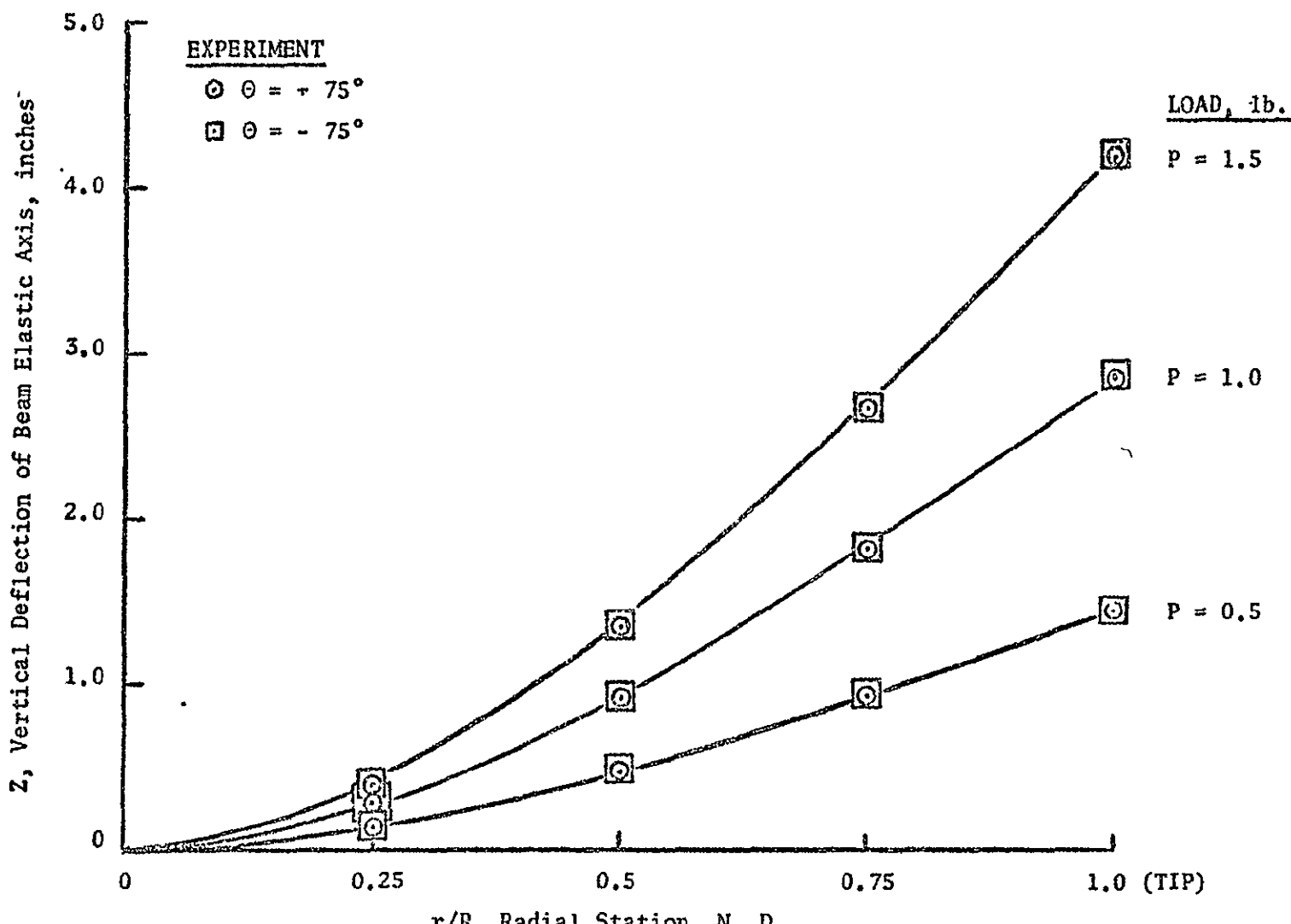


Figure 9-4. Vertical Deflection of Beam Elastic Axis versus Radial Station,  $\Theta = \pm 75^\circ$

- 22 -

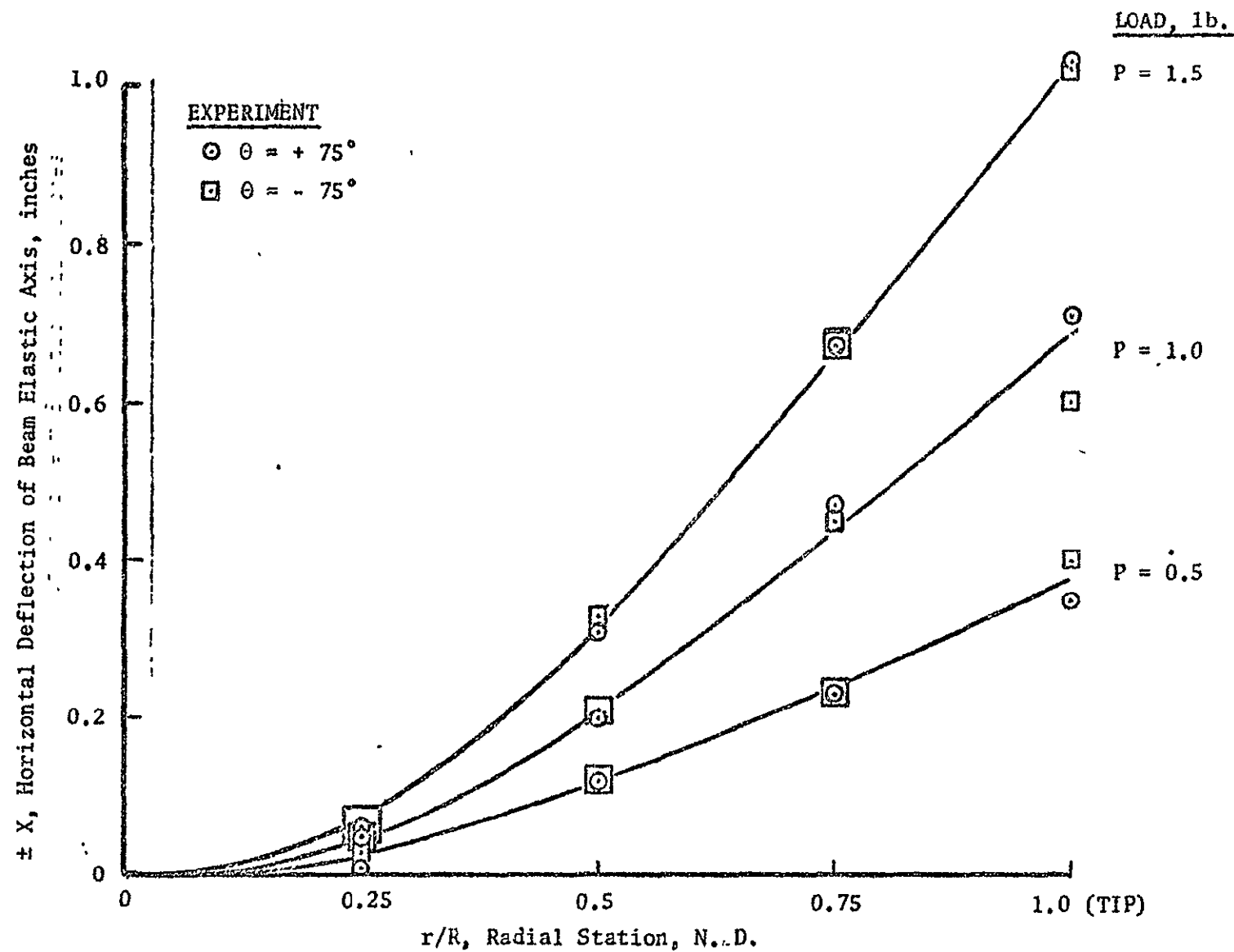


Figure 9-5. Horizontal Deflection of Beam Elastic Axis versus Radial Station,  $\theta = \pm 75^\circ$

- 15 -

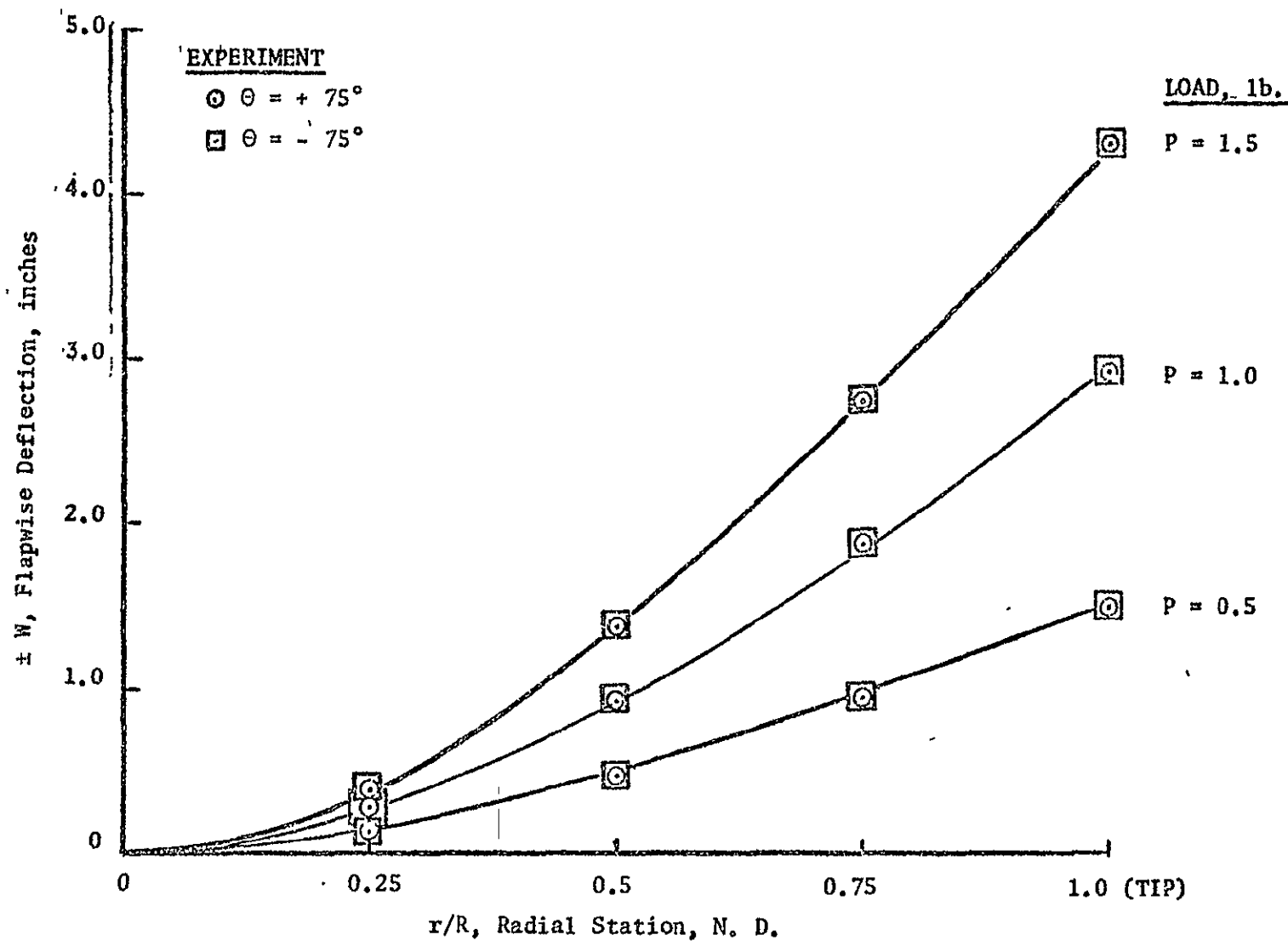


Figure 9-6. Flapwise Deflection versus Radial Station,  $\theta = \pm 75^\circ$

- 55 -

REPRODUCIBILITY OF THIS  
ORIGINAL PAGE IS POOR

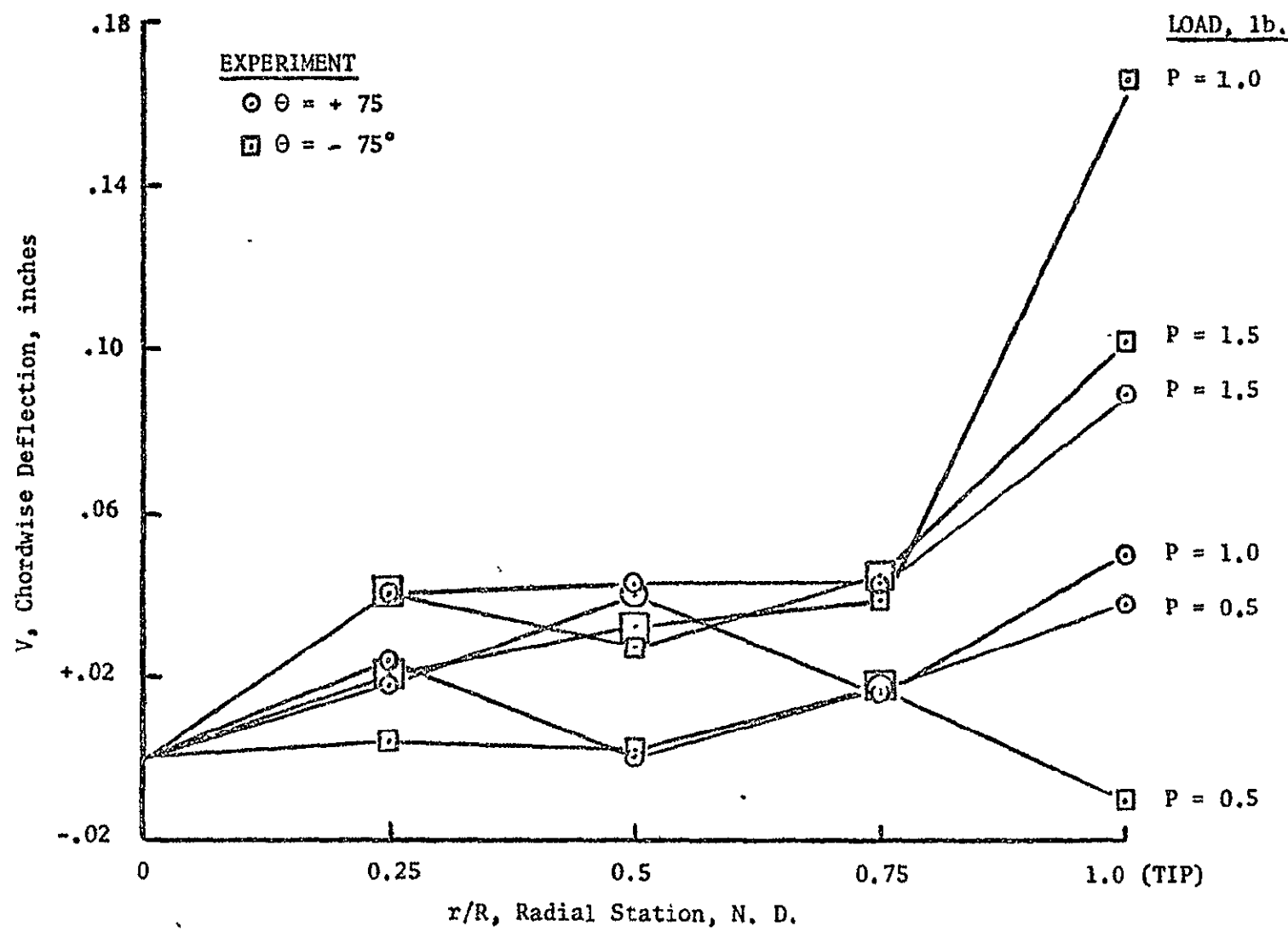


Figure 9-7. Chordwise Deflection versus Radial Station,  $\theta = \pm 75^\circ$

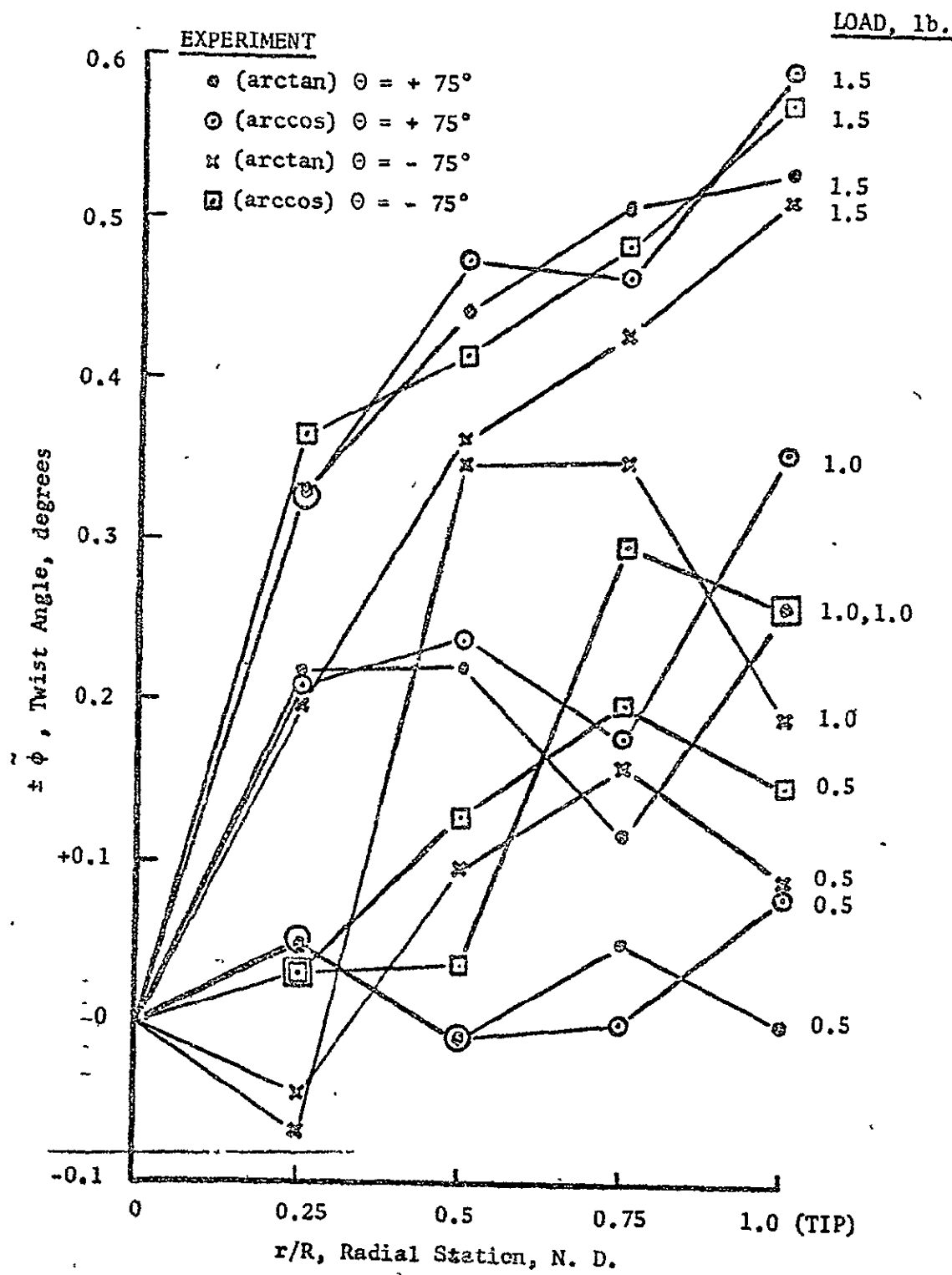


Figure 9-8. Blade Twist Angle versus Radial Station,  $\theta = \pm 75^\circ$

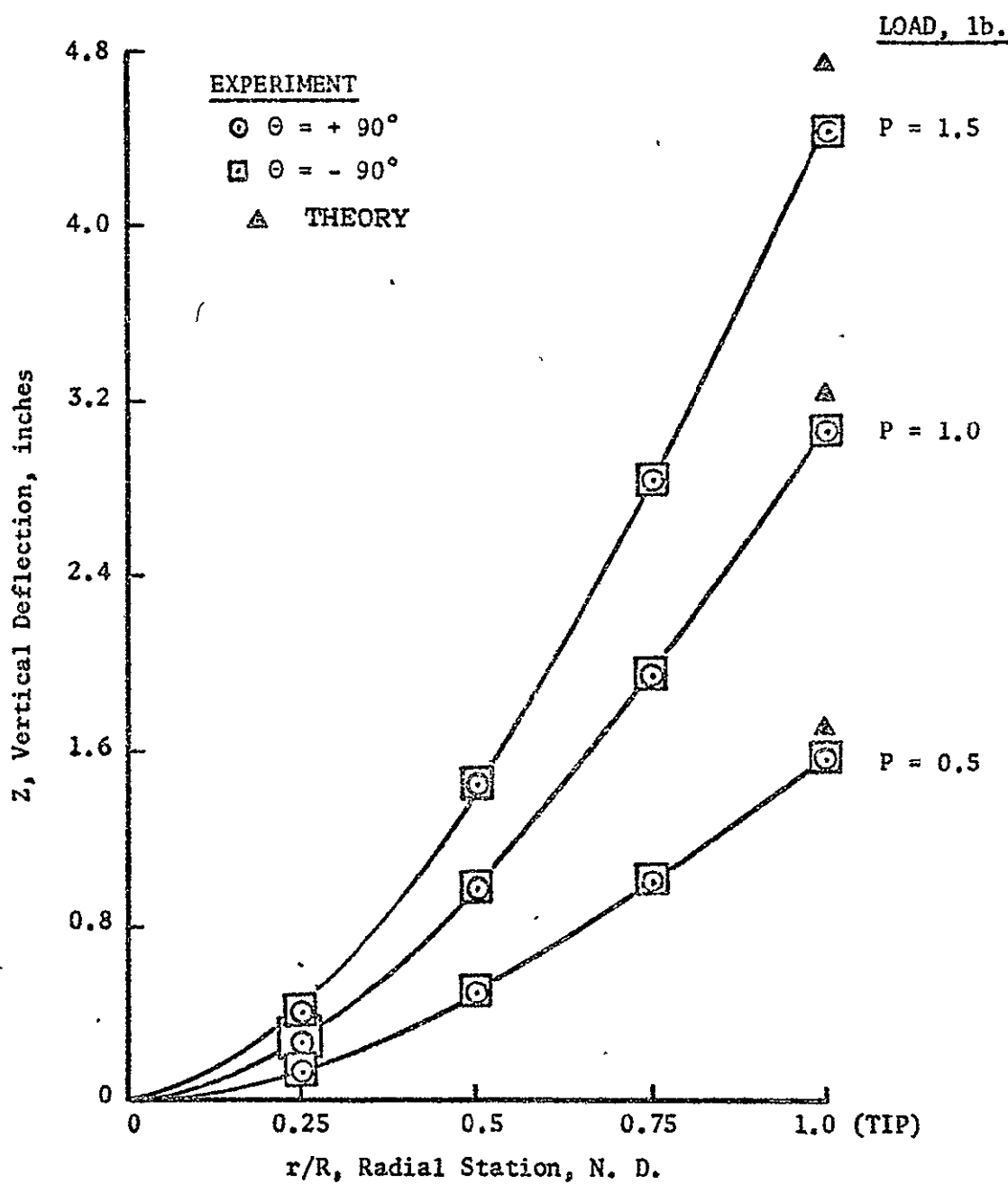


Figure 10. Vertical Deflection versus Radial Station,  $\theta = \pm 90^\circ$

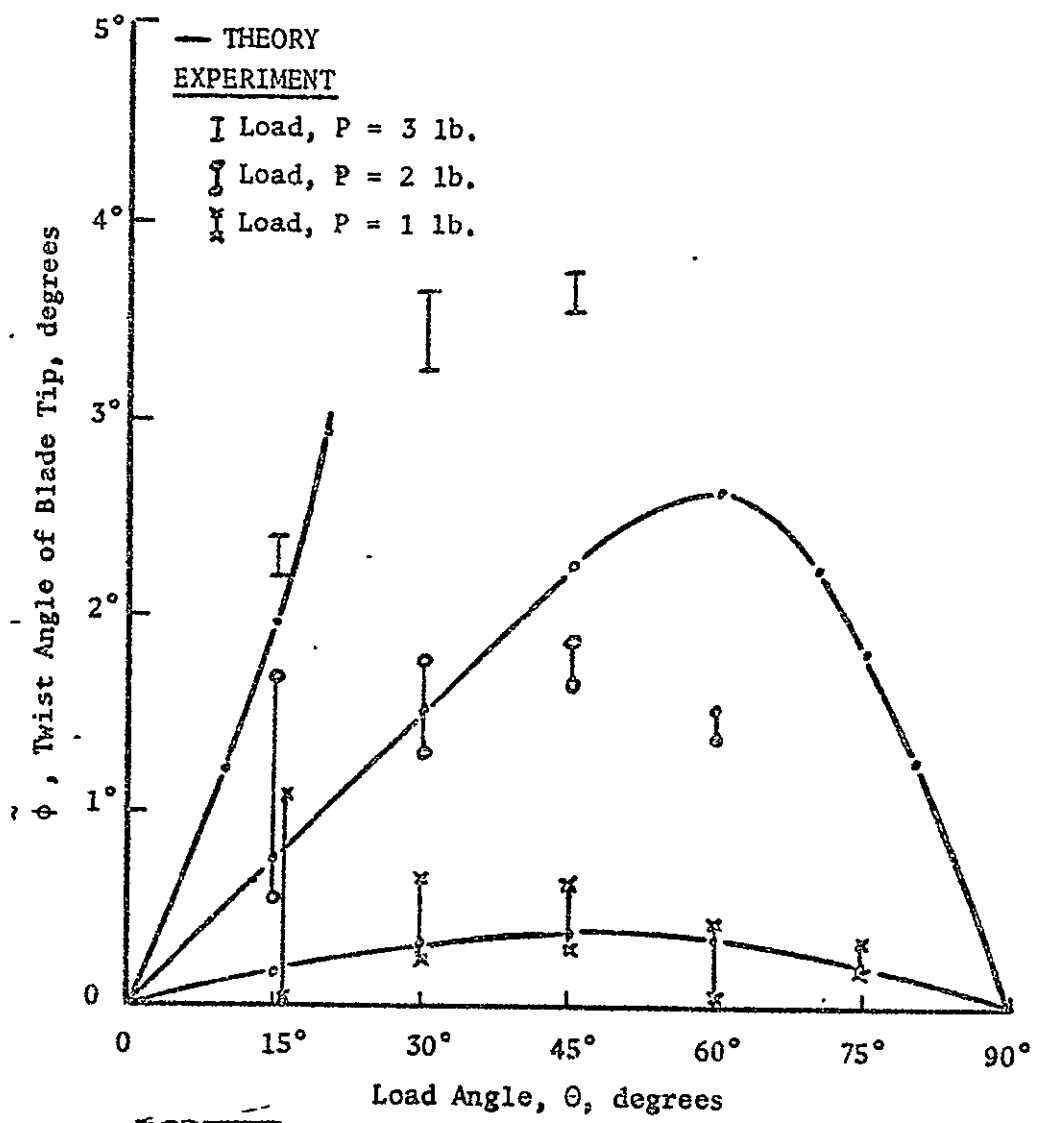


Figure 11. Twist Angle versus Load Angle.

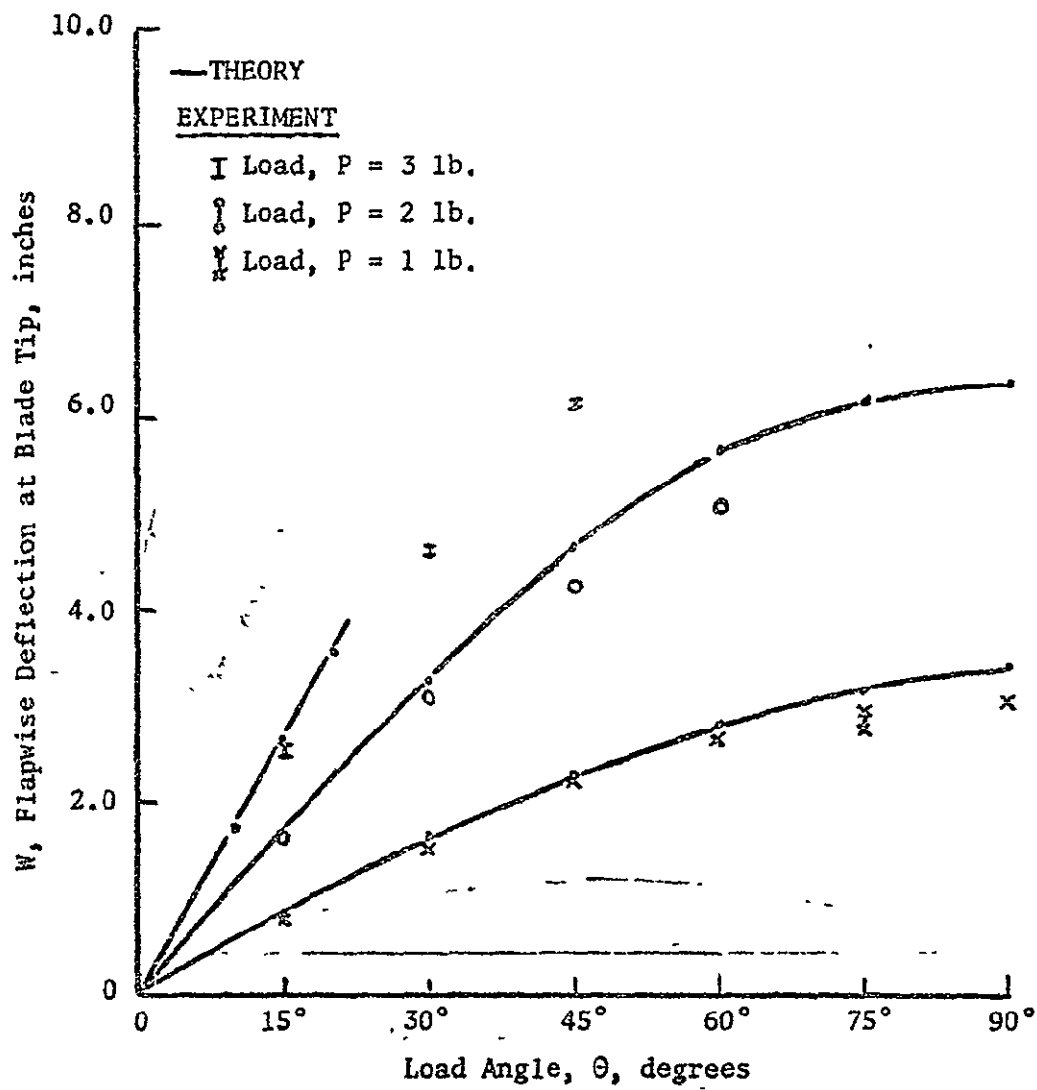


Figure 12. Flapwise Deflection versus Load Angle

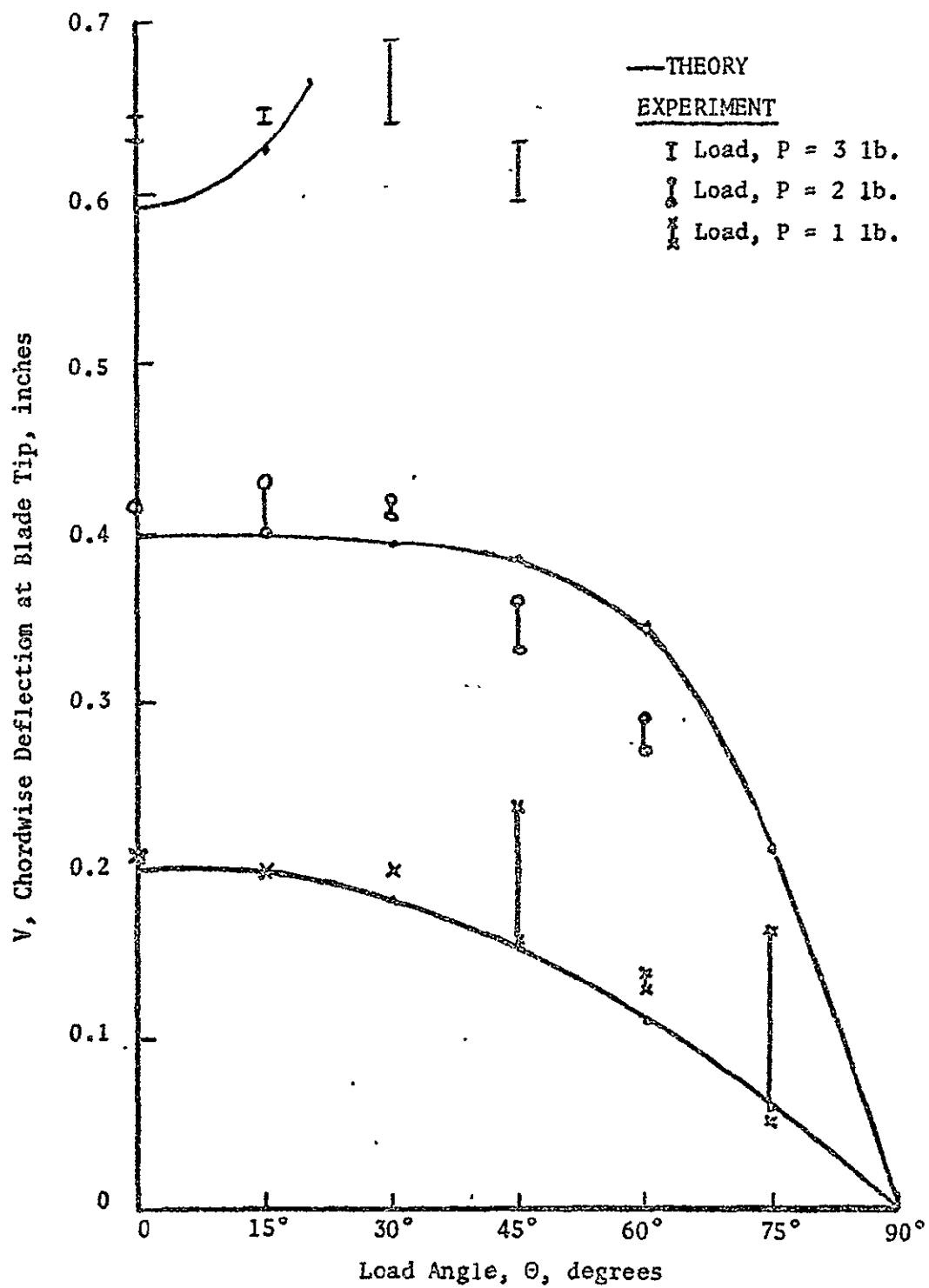


Figure 13. Chordwise Deflection versus Load Angle

## Large Deflection Loading Tests on Aluminum Beam

Initial Blade Pitch Angle Setting:  $\theta = 0^\circ$ 

Tip Load P, lb	Radial Station r/R, N.D.	Blade Elastic Axis Deflection				Blade Twist Angle	
		Space-Fixed Axes		Body-Fixed Axes		use arc-tan	use arc-cos
		X, inches	Z, inches	W, inches	V, inches	$\phi, t$ degrees	$\bar{\phi}, c$ degrees
0	1.00	-	0.0	-	0.0	-	-
0	0.75	-	0.0	-	0.0	-	-
0	0.50	-	0.0	-	0.0	-	-
0	0.25	-	0.0	-	0.0	-	-
1	1.00	-	0.211	-	0.211	-	-
1	0.75	-	0.131	-	0.131	-	-
1	0.50	-	0.069	-	0.069	-	-
1	0.25	-	0.023	-	0.023	-	-
2	1.00	-	0.418	-	0.418	-	-
2	0.75	-	0.266	-	0.266	-	-
2	0.50	-	0.135	-	0.135	-	-
2	0.25	-	0.044	-	0.044	-	-
3	1.00	-	0.631	-	0.631	-	-
3	0.75	-	0.403	-	0.403	-	-
3	0.50	-	0.207	-	0.207	-	-
3	0.25	-	0.060	-	0.060	-	-
4	1.00	-	0.841	-	0.841	-	-
4	0.75	-	0.541	-	0.541	-	-
4	0.50	-	0.284	-	0.284	-	-
4	0.25	-	0.089	-	0.089	-	-

Large Deflection Loading Tests on Aluminum Beam  
Initial Blade Pitch Angle Setting:  $\theta = + 15^\circ$

Tip Load P, lb	Radial Station r/R, N.D.	Blade Elastic Axis Deflection				Blade Twist Angle	
		Space-Fixed Axes		Body-Fixed Axes		use arc-tan $\phi, t$ degrees	use arc-cos $\phi, c$ degrees
X, inches	Z, inches	W, inches	V, inches				
0	1.00	0.0	0.0	0.0	0.0	0.0	0.0
0	0.75	0.0	0.0	0.0	0.0	0.0	0.0
0	0.50	0.0	0.0	0.0	0.0	0.0	0.0
0	0.25	0.0	0.0	0.0	0.0	0.0	0.0
1	1.00	0.71	0.409	0.789	0.203	0.1094	0.2582
1	0.75	0.46	0.252	0.509	0.124	0.8451	0.2200
1	0.50	0.21	0.131	0.236	0.722	0.5341	-0.2977
1	0.25	0.09	0.039	0.097	0.014	0.0780	-0.2216
2	1.00	1.50	0.817	1.660	0.400	1.6410	1.0780
2	0.75	0.95	0.523	1.052	0.259	1.6204	0.7921
2	0.50	0.45	0.250	0.499	0.125	0.9679	0.6495
2	0.25	0.18	0.076	0.193	0.027	0.7611	0.3266
3	1.00	2.24	1.259	2.489	0.636	2.3908	2.4137
3	0.75	1.42	0.796	1.570	0.401	2.2948	2.3346
3	0.50	0.68	0.394	0.763	0.203	2.0569	1.6773
3	0.25	0.27	0.113	0.290	0.039	1.1859	1.0979
4	1.00	3.13	1.754	3.477	0.884	3.9940	3.9542
4	0.75	1.93	1.102	2.149	0.564	4.1172	4.2239
4	0.50	0.95	0.546	1.058	0.281	3.7667	3.4477
4	0.25	0.31	0.152	0.338	0.066	2.4734	2.2562

Large Deflection Loading Tests on Aluminum Beam

Initial Blade Pitch Angle Setting:  $\theta = -15^\circ$

Tip Load P, lb	Radial Station r/R,N.D.	Blade Elastic Axis Deflection				Blade Twist Angle	
		Space-Fixed Axes		Body-Fixed Axes		use arc-tan $\phi, t$ degrees	use arc-cos $\phi, c$ degrees
		X, inches	Z, inches	W, inches	V, inches		
0	1.00	0.0	0.0	0.0	0.0	0.0	0.0
0	0.75	0.0	0.0	0.0	0.0	0.0	0.0
0	0.50	0.0	0.0	0.0	0.0	0.0	0.0
0	0.25	0.0	0.0	0.0	0.0	0.0	0.0
1	1.00	-0.72	0.406	-0.800	0.206	-0.0024	-0.0359
1	0.75	-0.49	0.263	-0.541	0.127	-0.0050	-0.0721
1	0.50	-0.20	0.131	-0.227	0.075	-0.0074	-0.1078
1	0.25	-0.05	0.041	-0.058	0.026	0.2666	-0.1453
2	1.00	-1.47	0.837	-1.636	0.428	-1.1446	-0.5657
2	0.75	-0.93	0.535	-1.036	0.276	-0.3197	-0.6031
2	0.50	-0.41	0.266	-0.464	0.150	-0.6912	-0.6365
2	0.25	-0.12	0.077	-0.135	0.043	-0.2171	-0.4674
3	1.00	-2.30	1.289	-2.555	0.649	-2.1968	-2.2199
3	0.75	-1.45	0.825	-1.614	0.421	-1.8252	-2.1653
3	0.50	-0.69	0.410	-0.772	0.217	-1.6144	-1.8407
3	0.25	-0.15	0.121	-0.176	0.078	-1.1421	-1.7289
4	1.00	-3.11	1.796	-3.469	0.930	-3.4526	-3.8808
4	0.75	-2.01	1.141	-2.236	0.581	-3.5529	-3.9819
4	0.50	-1.01	0.568	-1.122	0.287	-2.9438	-3.3591
4	0.25	-0.22	0.164	-0.255	0.101	-2.0559	-2.7504

## Large Deflection Loading Tests on Aluminum Beam

Initial Blade Pitch Angle Setting:  $\theta = +30^\circ$ 

Tip Load P, lb	Radial Station r/R, N.D.	Blade Elastic Axis Deflection				Blade Twist Angle	
		Space-Fixed Axes		Body-Fixed Axes		use arc-tan $\phi, t$ degrees	use arc-cos $\beta, c$ degrees
		X, inches	Z, inches	W, inches	V, inches		
0	1.00	0.0	0.0	0.0	0.0	0.0	0.0
0	0.75	0.0	0.0	0.0	0.0	0.0	0.0
0	0.50	0.0	0.0	0.0	0.0	0.0	0.0
0	0.25	0.0	0.0	0.0	0.0	0.0	0.0
1	1.00	1.22	0.936	1.495	0.201	0.4028	0.2865
1	0.75	0.75	0.594	0.946	0.139	0.1875	0.4208
1	0.50	0.36	0.293	0.458	0.073	- 0.0163	0.2684
1	0.25	0.12	0.084	0.146	0.013	- 0.1227	0.1728
2	1.00	2.43	1.893	3.050	0.424	1.6828	1.7203
2	0.75	1.58	1.198	1.967	0.247	1.0285	1.7443
2	0.50	0.72	0.596	0.921	0.156	0.7459	1.6161
2	0.25	0.23	0.168	0.283	0.030	0.5946	1.0423
3	1.00	3.68	2.862	4.618	0.638	3.6308	3.7075
3	0.75	2.31	1.814	2.907	0.416	3.4176	3.5628
3	0.50	1.13	0.893	1.425	0.208	3.0160	3.3009
3	0.25	0.38	0.248	0.453	0.024	2.1725	2.3427
4	1.00	4.73	3.853	6.022	0.971	5.8569	5.7273
4	0.75	3.01	2.443	3.828	0.611	5.8524	5.9900
4	0.50	1.50	1.207	1.902	0.295	5.0895	5.5956
4	0.25	0.43	0.331	0.538	0.072	3.7772	3.9780

Large Deflection Loading Tests on Aluminum Beam  
Initial Blade Pitch Angle Setting:  $\theta = -30^\circ$

Tip Load	Radial Station	Blade Elastic Axis Deflection				Blade Twist Angle	
		Space-Fixed Axes		Body-Fixed Axes		use arc-tan	use arc-cos
		X, inches	Z, inches	W, inches	V, inches	$\phi, t$ degrees	$\phi, c$ degrees
0	1.00	0.0	0.0	0.0	0.0	0.0	0.0
0	0.75	0.0	0.0	0.0	0.0	0.0	0.0
0	0.50	0.0	0.0	0.0	0.0	0.0	0.0
0	0.25	0.0	0.0	0.0	0.0	0.0	0.0
1	1.00	-1.26	0.951	-1.566	0.194	-0.2509	-0.6606
1	0.75	-0.81	0.608	-1.005	0.121	-0.0670	-0.2654
1	0.50	-0.40	0.310	-0.501	0.068	-0.1883	-0.4165
1	0.25	-0.13	0.083	-0.154	0.006	-0.0718	-0.2838
2	1.00	-2.48	1.909	-3.102	0.413	-1.2960	-1.4916
2	0.75	-1.59	1.213	-1.983	0.255	-1.4850	-1.5810
2	0.50	-0.77	0.609	-0.971	0.142	-1.2823	-1.4361
2	0.25	-0.23	0.168	-0.283	0.030	-0.2310	-0.8998
3	1.00	-3.64	2.902	-4.603	0.693	-3.2471	-3.4798
3	0.75	-2.31	1.837	-2.919	0.435	-3.2691	-3.5452
3	0.50	-1.12	0.921	-1.430	0.237	-3.1822	-3.2528
3	0.25	-0.32	0.252	-0.407	0.055	-1.6200	-2.3496
4	1.00	-4.71	3.900	-6.029	1.022	-5.6334	-6.1844
4	0.75	-2.98	2.480	-3.821	0.657	-5.5118	-6.0493
4	0.50	-1.51	1.229	-1.922	0.309	-5.1528	-5.4486
4	0.25	-0.41	0.341	-0.529	0.087	-3.6230	-3.6412

Large Deflection Loading Tests on Aluminum Beam  
Initial Blade Pitch Angle Setting:  $\theta = + 45^\circ$

Tip Load P, lb	Radial Station r/R,N.D.	Blade Elastic Axis Deflection				Blade Twist Angle	
		Space-Fixed Axes		Body-Fixed Axes		use arc-tan $\tilde{\theta}, t$ degrees	use arc-cos $\tilde{\theta}, c$ degrees
		X, inches	Z, inches	W, inches	V, inches		
0	1.00	0.0	0.0	0.0	0.0	0.0	0.0
0	0.75	0.0	0.0	0.0	0.0	0.0	0.0
0	0.50	0.0	0.0	0.0	0.0	0.0	0.0
0	0.25	0.0	0.0	0.0	0.0	0.0	0.0
1	1.00	1.42	1.652	2.172	0.164	0.6378	0.5924
1	0.75	0.90	1.049	1.378	0.105	0.8850	0.5519
1	0.50	0.48	0.520	0.707	0.028	0.7558	0.4310
1	0.25	0.12	0.143	0.185	0.016	0.6675	0.2565
2	1.00	2.72	3.234	4.210	0.363	1.8583	1.7859
2	0.75	1.73	2.068	2.685	0.239	1.6232	1.7195
2	0.50	0.88	1.027	1.348	0.103	1.5632	1.4818
2	0.25	0.22	0.288	0.359	0.048	1.1775	1.1256
3	1.00	3.89	4.731	6.095	0.594	3.7187	3.6484
3	0.75	2.50	3.024	3.906	0.370	3.5301	3.5448
3	0.50	1.28	1.505	1.969	0.159	3.1347	3.1851
3	0.25	0.33	0.427	0.535	0.068	2.4877	2.3604

## Large Deflection Loading Tests on Aluminum Beam

Initial Blade Pitch Angle Setting:  $\theta = -45^\circ$ 

Tip Load P, lb	Radial Station r/R, N.D.	Blade Elastic Axis Deflection				Blade Twist Angle	
		Space-Fixed Axes		Body-Fixed Axes		use arc-tan	use arc-cos
		X, inches	Z, inches	W, inches	V, inches	$\phi, t$ degrees	$\phi, c$ degrees
0	1.00	0.0	0.0	0.0	0.0	0.0	0.0
0	0.75	0.0	0.0	0.0	0.0	0.0	0.0
0	0.50	0.0	0.0	0.0	0.0	0.0	0.0
0	0.25	0.0	0.0	0.0	0.0	0.0	0.0
1	1.00	-1.32	1.661	-2.107	0.241	-0.3658	-0.3224
1	0.75	-0.91	1.058	-1.391	0.104	-0.8041	-0.5236
1	0.50	-0.43	0.527	-0.676	0.068	-0.4124	-0.4162
1	0.25	-0.11	0.143	-0.178	0.023	-0.5666	-0.3219
2	1.00	-2.80	3.270	-4.292	0.332	-1.8583	-1.6601
2	0.75	-1.77	2.082	-2.723	0.220	-2.0698	-1.6882
2	0.50	-0.89	1.039	-1.364	0.105	-1.5805	-1.5166
2	0.25	-0.25	0.286	-0.379	0.025	-1.2095	-1.0531
3	1.00	-3.88	4.773	-6.118	0.631	-3.6141	-3.5693
3	0.75	-2.49	3.043	-3.912	0.391	-3.8712	-3.6875
3	0.50	-1.24	1.520	-1.951	0.197	-3.2489	-3.1627
3	0.25	-0.39	0.427	-0.577	0.026	-2.4178	-2.2179

Large Deflection Loading Tests on Aluminum Beam  
Initial Blade Pitch Angle Setting:  $\theta = +60^\circ$

Tip Load P, lb	Radial Station r/R,N.D.	Blade Elastic Axis Deflection				Blade Twist Angle	
		Space-Fixed Axes		Body-Fixed Axes		use arc-tan $\phi, t$ degrees	use arc-cos $\phi, c$ degrees
X, inches	Z, inches	W, inches	V, inches				
0	1.00	0.0	0.0	0.0	0.0	0.0	0.0
0	0.75	0.0	0.0	0.0	0.0	0.0	0.0
0	0.50	0.0	0.0	0.0	0.0	0.0	0.0
0	0.25	0.0	0.0	0.0	0.0	0.0	0.0
0.5	1.00	0.60	1.201	1.340	0.080	0.1866	0.1214
0.5	0.75	0.38	0.764	0.851	0.052	0.2057	0.2095
0.5	0.50	0.18	0.382	0.420	0.035	0.2292	0.2428
0.5	0.25	0.09	0.103	0.134	-0.026	0.1221	0.0993
1.0	1.00	1.20	2.356	2.640	0.138	0.4267	0.4409
1.0	0.75	0.74	1.499	1.668	0.108	0.3740	0.4956
1.0	0.50	0.38	0.752	0.841	0.046	0.3616	0.4190
1.0	0.25	0.13	0.210	0.246	-0.007	0.1259	0.2315
1.5	1.00	1.77	3.474	3.893	0.204	0.8956	0.9346
1.5	0.75	1.15	2.210	2.488	0.109	0.9621	0.9561
1.5	0.50	0.57	1.104	1.241	0.058	0.7441	0.9239
1.5	0.25	0.18	0.307	0.355	-0.002	0.5094	0.5504
2.0	1.00	2.30	4.516	5.060	0.266	1.4864	1.4042
2.0	0.75	1.49	2.884	3.242	0.151	1.3614	1.2946
2.0	0.50	0.72	1.441	1.607	0.096	0.9114	1.1426
2.0	0.25	0.22	0.410	0.465	0.014	0.6956	0.8574

Large Deflection Loading Tests on Aluminum Beam

Initial Blade Pitch Angle Setting:  $\theta = -60^\circ$

Tip Load P, lb	Radial Station r/R,N,D	Blade Elastic Axis Deflection				Blade Twist Angle	
		Space-Fixed Axes		Body-Fixed Axes		use arc-tan	use arc-cos
X, inches	Z, inches	W, inches	V, inches	$\bar{\phi}, t$ degrees	$\bar{\phi}, c$ degrees		
0	1.00	0.0	0.0	0.0	0.0	0.0	0.0
0	0.75	0.0	0.0	0.0	0.0	0.0	0.0
0	0.50	0.0	0.0	0.0	0.0	0.0	0.0
0	0.25	0.0	0.0	0.0	0.0	0.0	0.0
0.5	1.00	-0.66	1.203	-1.395	0.029	-0.1241	-0.1651
0.5	0.75	-0.43	0.757	-0.870	0.006	-0.1390	-0.1210
0.5	0.50	-0.19	0.382	-0.425	0.026	-0.1159	-0.1541
0.5	0.25	-0.01	0.109	-0.099	0.045	-0.0829	-0.1100
1.0	1.00	-1.18	2.358	-2.647	0.131	-0.2512	-0.3959
1.0	0.75	-0.80	1.495	-1.694	0.054	-0.4888	-0.3957
1.0	0.50	-0.36	0.745	-0.825	0.060	-0.2572	-0.3409
1.0	0.25	-0.04	0.209	-0.200	0.069	-0.1327	-0.1759
1.5	1.00	-1.79	3.479	-3.907	0.189	-0.6188	-0.8777
1.5	0.75	-1.18	2.208	-2.502	0.082	-0.7756	-0.8337
1.5	0.50	-0.55	1.101	-1.228	0.074	-0.9466	-0.7573
1.5	0.25	-0.11	0.311	-0.324	0.060	-0.4327	-0.5708
2.0	1.00	-2.28	4.526	-5.059	0.288	-1.3466	-1.5202
2.0	0.75	-1.50	2.876	-3.240	0.138	-1.6671	-1.4546
2.0	0.50	-0.70	1.436	-1.593	0.111	-1.5114	-1.2590
2.0	0.25	-0.23	0.407	-0.467	0.004	-1.0508	-0.9533

Large Deflection Loading Tests on Aluminum Beam  
Initial Blade Pitch Angle Setting:  $\theta = + 75^\circ$

Tip Load P, lb	Radial Station r/R,N.D	Blade Elastic Axis Deflection				Blade Twist Angle	
		Space-Fixed Axes		Body-Fixed Axes		use arc-tan $\phi, t$ degrees	use arc-cos $\phi, c$ degrees
X, inches	Z, inches	W, inches	V, inches				
0	1.00	0.0	0.0	0.0	0.0	0.0	0.0
0	0.75	0.0	0.0	0.0	0.0	0.0	0.0
0	0.50	0.0	0.0	0.0	0.0	0.0	0.0
0	0.25	0.0	0.0	0.0	0.0	0.0	0.0
0.5	1.00	0.35	1.454	1.495	0.038	-0.0005	0.0791
0.5	0.75	0.23	0.927	0.954	0.017	0.0495	0.000
0.5	0.50	0.12	0.451	0.466	0.0008	-0.0092	-0.0098
0.5	0.25	0.01	0.132	0.130	0.024	0.0460	0.0494
1.0	1.00	0.71	2.846	2.932	0.050	0.2586	0.3557
1.0	0.75	0.47	1.817	1.876	0.016	0.1171	0.1778
1.0	0.50	0.20	0.901	0.922	0.040	0.2213	0.2372
1.0	0.25	0.05	0.257	0.261	0.018	0.2180	0.2075
1.5	1.00	1.03	4.190	4.313	0.089	0.5293	0.5925
1.5	0.75	0.67	2.668	2.750	0.043	0.5076	0.4641
1.5	0.50	0.31	1.340	1.375	0.042	0.4430	0.4741
1.5	0.25	0.06	0.382	0.384	0.040	0.3287	0.3260

Large Deflection Loading Tests on Aluminum Beam  
 Initial Blade Pitch Angle Setting:  $\theta = -75^\circ$

Tip Load P, lb	Radial Station r/R, N.D.	Blade Elastic Axis Deflection				Blade Twist Angle	
		Space-Fixed Axes		Body-Fixed Axes		use arc-tan	use arc-cos
		X, inches	Z, inches	W, inches	V, inches	$\phi, t$ degrees	$\phi, c$ degrees
0	1.00	0.0	0.0	0.0	0.0	0.0	0.0
0	0.75	0.0	0.0	0.0	0.0	0.0	0.0
0	0.50	0.0	0.0	0.0	0.0	0.0	0.0
0	0.25	0.0	0.0	0.0	0.0	0.0	0.0
0.5	1.00	-0.40	1.454	-1.507	-0.010	-0.0895	-0.1481
0.5	0.75	-0.23	0.927	-0.954	0.017	-0.1598	-0.1975
0.5	0.50	-0.12	0.458	-0.473	0.002	-0.0953	-0.1284
0.5	0.25	-0.03	0.130	-0.133	0.004	0.0449	-0.0296
1.0	1.00	-0.60	2.883	-2.940	0.166	-0.1913	-0.2567
1.0	0.75	-0.45	1.831	-1.885	0.039	-0.3479	-0.2963
1.0	0.50	-0.21	0.908	-0.931	0.032	-0.3467	-0.0345
1.0	0.25	-0.05	0.266	-0.269	0.020	0.0692	-0.0296
1.5	1.00	-1.02	4.204	-4.324	0.102	-0.5117	-0.5724
1.5	0.75	-0.67	2.676	-2.758	0.045	-0.4276	-0.4837
1.5	0.50	-0.33	1.339	-1.378	0.027	-0.3634	-0.4147
1.5	0.25	-0.06	0.380	-0.382	0.040	-0.1962	-0.3651

Large Deflection Loading Tests on Aluminum Beam  
Initial Blade Pitch Angle Setting:  $\theta = + 90^\circ$

Tip Load, P, lb	Radial Station r/R, N.D.	Blade Elastic Axis Deflection				Blade Twist Angle	
		Space-Fixed Axes		Body-Fixed Axes		use arc-tan	use arc-cos
X, inches	Z, inches	W, inches	V, inches	$\phi, t$ degrees	$\theta, c$ degrees		
0	1.00	-	0.0	0.0	-	-	-
0	0.75	-	0.0	0.0	-	-	-
0	0.50	-	0.0	0.0	-	-	-
0	0.25	-	0.0	0.0	-	-	-
0.5	1.00	-	1.560	1.560	-	-	-
0.5	0.75	-	0.984	0.984	-	-	-
0.5	0.50	-	0.497	0.497	-	-	-
0.5	0.25	-	0.136	0.136	-	-	-
1.0	1.00	-	3.048	3.048	-	-	-
1.0	0.75	-	1.938	1.938	-	-	-
1.0	0.50	-	0.973	0.973	-	-	-
1.0	0.25	-	0.275	0.275	-	-	-
1.5	1.00	-	4.453	4.453	-	-	-
1.5	0.75	-	2.841	2.841	-	-	-
1.5	0.50	-	1.428	1.428	-	-	-
1.5	0.25	-	0.404	0.404	-	-	-

Large Deflection Loading Tests on Aluminum Beam  
Initial Blade Pitch Angle Setting:  $\theta = -90^\circ$

Tip Load P, lb	Radial Station r/R, N.D.	Blade Elastic Axis Deflection				Blade Twist Angle	
		Space-Fixed Axes		Body-Fixed Axes		use arc-tan	use arc-cos
		X, inches	Z, inches	W, inches	V, inches	$\bar{\phi}, t$ degrees	$\bar{\phi}, c$ degrees
0	1.00	-	0.0	0.0	-	-	-
0	0.75	-	0.0	0.0	-	-	-
0	0.50	-	0.0	0.0	-	-	-
0	0.25	-	0.0	0.0	-	-	-
0.5	1.00	-	1.569	-1.569	-	-	-
0.5	0.75	-	0.996	-0.996	-	-	-
0.5	0.50	-	0.494	-0.494	-	-	-
0.5	0.25	-	0.137	-0.137	-	-	-
1.0	1.00	-	3.065	-3.065	-	-	-
1.0	0.75	-	1.954	-1.954	-	-	-
1.0	0.50	-	0.969	-0.969	-	-	-
1.0	0.25	-	0.277	-0.277	-	-	-
1.5	1.00	-	4.449	-4.449	-	-	-
1.5	0.75	-	2.838	-2.838	-	-	-
1.5	0.50	-	1.416	-1.416	-	-	-
1.5	0.25	-	0.400	-0.400	-	-	-

## Large Deflection Loading Tests on Aluminum Beam

Initial Blade Pitch Angle Setting:  $\theta = 180^\circ$ 

Tip Load, P, lb	Radial Station r/R,N.D.	Blade Elastic Axis Deflection				Blade Twist Angle	
		Space-Fixed Axes		Body-Fixed Axes		use arc-tan $\phi, t$ degrees	use arc-cos $\tilde{\phi}, \tilde{t}$ degrees
		X, inches	Z, inches	W, inches	V, inches		
0	1.00	-	0.0	-	0.0	-	-
0	0.75	-	0.0	-	0.0	-	-
0	0.50	-	0.0	-	0.0	-	-
0	0.25	-	0.0	-	0.0	-	-
3.0	1.00	-	0.646	-	-0.646	-	-
3.0	0.75	-	0.415	-	-0.415	-	-
3.0	0.50	-	0.206	-	-0.206	-	-
3.0	0.25	-	0.056	-	-0.056	-	-